8-2010

Simulation and fabrication of microhotplates for metal oxide gas sensors.

Kane Jonathan Miller 1987-
University of Louisville

SIMULATION AND FABRICATION OF MICROHOTPLATES FOR METAL OXIDE GAS SENSORS

By

Kane Jonathan Miller
B.S., University of Louisville, 2009

A Thesis
Submitted to the Faculty of the
University of Louisville
J. B. Speed School of Engineering
in Partial Fulfillment of the Requirements
for the Professional Degree

MASTER OF ENGINEERING

Department of Chemical Engineering

August 2010

SIMULATION AND FABRICATION OF MICROHOTPLATES FOR METAL OXIDE GAS SENSORS

Submitted by:_____
Kane Jonathan Miller

A Thesis Approved On

_____
(Date)

by the Following Reading and Examination Committee:

_____
Xiao-An Fu, Thesis Director

_____
James C. Watters

_____
Kevin M. Walsh

ACKNOWLEDGEMENTS

My thanks to Dr. Xiao-An Fu, my advisor, who gave me the opportunity to enter a new and interesting research area for the Department of Chemical Engineering at the University of Louisville.

I would also like to thank Dr. Julia Aebersold for training and assistance with infrared imaging, Mr. Tommy Roussel for assistance and support in design and analysis using computer software, along with Mr. Steve Williamson for general computer support.

I thank the University of Louisville cleanroom staff and users, especially Mr. Mark Crain, Mr. Joseph Lake, Mr. Don Yeager, Ms. Caitlin Grothaus, Ms. Vanessa Velasco, and Mr. Hiren Trada, for equipment training and support and for their time. In addition, I thank Mr. Curt McKenna, who prepared the photomasks used in this research.

Special thanks to Dr. James Watters, Dr. Kevin Walsh, and Mr. Michael Martin for suggestions and improvements.

ABSTRACT

Microhotplates for metal oxide gas sensors are fabricated using platinum microheaters and tested. Power consumption is monitored and temperature distributions are observed using infrared microscopy. Temperature line traces are extracted from the resulting thermal images and compared with simulations of the microhotplates in CoventorWare 2008. Methodology for creating simulations in this software is presented. Both unreleased and thermally isolated microhotplates are fabricated and simulated. It is shown that unreleased microhotplates are ineffective in heating the microhotplate membrane, while thermally isolated microhotplates require an order of magnitude less power than unreleased devices to bring to operating temperature (300°C) for a gas sensor.

Further, CoventorWare is used to simulate microhotplates using nitrogen-doped silicon carbide microheaters, which require smaller volumes than platinum microheaters due to having higher electrical resistivity than platinum. The effects of microheater resistance and microhotplate geometry are discussed, and "coplanar" and "stacked" configurations of microhotplates resulting in uniform temperature distributions are simulated and presented. For microhotplates using a constant sensor area of 100 µm by 100 µm, the "stacked" configuration is found to be desirable because of the ability to thermally isolate a microhotplate with a smaller area, increasing the temperature attained.

TABLE OF CONTENTS

NOMENCLATURE

A	Cross-sectional area	m^2
I	Current	A
k	Thermal conductivity	W/m/K
L	Length	m
P	Power	W
Q	Volumetric heat generation	W/m^3
R	Resistance	Ω
T	Temperature	K
$T_{experimental}$	Temperature of point read from fabricated device	K
$T_{simulation}$	Temperature of point obtained from simulation	K
t	Thickness	m
V	Voltage	V
Vol	Volume	m^3
w	Width	m
x	Distance along microheater length	m
ρ	Electrical resistivity	Ω·m
∇	Gradient operator	m^{-1}
%E	Percent error	%

LIST OF TABLES

LIST OF FIGURES

I. INTRODUCTION

Gas sensors see use in many applications and in varying environments. From detecting traces of volatile, explosive chemicals to monitoring emissions of toxic substances and air pollutants, gas sensors play a large role in the development and enforcement of standards and regulations.

Microfabricated gas sensors have become an active research interest in recent years. Along with the advantage of small physical size, these devices require low power consumption to operate and maintain [1], and can easily be incorporated into sensor arrays for detecting concentrations of multiple gases [2].

The type of microfabricated gas sensor of interest in this work is the metal oxide chemiresistor gas sensor. Gas sensors of this type commonly rely on the ability to detect a change in electrical properties of a metal oxide sensing material when exposed to a gas mixture. The adsorption or reaction of a gas on a sensing film of a particular metal oxide introduces a measurable change in the resistance of the film [3]. The change in resistance can be correlated to the concentration of the gas, allowing the film to be calibrated as a gas sensor. A dramatic resistance change when one particular sensor, fabricated by Triantafyllopoulou and Tsamis [3], is exposed to carbon monoxide is shown in Figure 1.1.

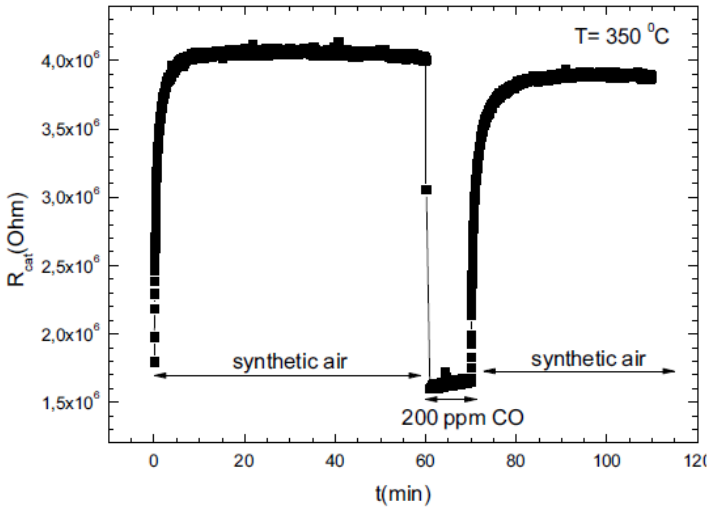

FIGURE 1.1 – Sensor response for detection of 200 ppm CO at a constant temperature of 350°C [3]

Several metal oxides with varying nanostructures and fabrication methods, and the resulting sensitivities to target gases, are reported in literature. Tin oxide is commonly used in the form of nanowires or nanorods [4-8], and sensitivities to various gases are reported using tin oxide alone or doped with other materials, including copper [9] and antimony [10].

Zinc oxide is another common metal oxide in use, whether alone [11-14], combined with tin oxide as a backbone-coating composite structure [15-18], or doped with silver [19, 20]. Work is also reported using oxides of other metals, including copper oxide [21-23] and tungsten oxide [24-26]. Many references and gas sensor papers have been compiled and reviewed by Fine [27] et al.

Metal oxide chemiresistor sensors are capable of detecting wide ranges of multiple gases. Carbon monoxide detection is a common goal for personal safety and pollution monitoring, and can be accomplished with tin oxide [3, 6], though some research has investigated the use of titanium oxide and cerium oxide [27]. Nitrogen oxides can be

detected using tungsten oxide [25, 26] or indium oxide [27] films. Other target gases include ammonia [28] and hydrogen sulfide [9] for personal safety, hydrogen [23, 29] and ethanol [18] for fuel sensing applications, and acetone [24] in human breath as a means to monitor the onset of diabetes.

In most of these sensors, the sensing material requires heating to an operating temperature. Typical operating temperatures for tin oxide-based chemiresistors reach or exceed 300°C [3, 8]. Zinc oxide chemiresistors are maintained at 300°C as well [16], while tungsten oxide chemiresistors operate at temperatures up to 500°C [24]. See Table 1.1.

TABLE 1.1

PUBLISHED OPERATING TEMPERATURES OF SELECTED METAL OXIDES COMMONLY USED IN GAS SENSORS

Common Metal Oxides	**Operating Temperatures**
Tin oxide (SnO_2)	300°C or above
Zinc oxide (ZnO)	300°C
Tungsten oxide (WO_3)	Up to 500°C
Indium tin oxide (ITO)	300°C
Titanium oxide (TiO_2)	250°C
Cerium oxide (CeO_2)	400°C

This operating temperature requirement exists because temperature affects the base properties of the sensing film, as well as the reaction rates of adsorption and desorption of target gases. Thus, it is desirable to control and evenly distribute the temperature throughout the sensors. Microhotplate platforms supporting the sensing films provide one method of bringing these devices to operating temperature [1].

Microhotplate platforms normally incorporate at least three layers: a suspended membrane of an electrically insulating material, a resistor that acts as a heating element,

and a set of electrode structures that make electrical contact when the sensing film is placed over them [1, 30] as shown in Figure 1.2. This figure also shows a "thermometer plate," or temperature distributor layer intended to help evenly heat the metal oxide.

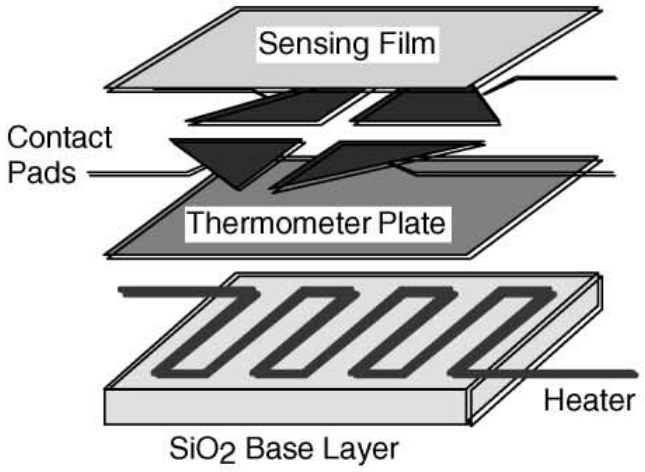

FIGURE 1.2 – Layers of a Microhotplate Fabricated by Semancik [1] et al.

Initially, microhotplates were based on doped polysilicon or metal resistors [31]. However, these devices cannot operate at temperatures much higher than the 300°C necessary for tin oxide gas sensors, nor can metal and silicon-based devices withstand harsh environments such as those encountered in aerospace applications [32].

Silicon carbide (SiC) has been studied as a replacement material for both the heating elements and the suspended membrane platform [30, 33] as well as in pressure sensors and infrared emitters [34]. Interest in this material is a result of a number of desirable properties, including chemical inertness, resistance to mechanical wear, and high thermal conductivity [30, 35].

The process of fabricating and testing multiple iterations of these devices is time-consuming and expensive. Finite element analysis software packages, such as COMSOL,

CoventorWare, and ANSYS, have been used to optimize the design of microhotplates for low power consumption and even temperature distribution prior to fabrication [36-38].

In this work, results of CoventorWare simulations of microhotplates using two sizes of platinum microheaters are compared to experimentally-determined results using microhotplates of the same design. The purpose of this is to test the accuracy and legitimacy of the simulations. Subsequently, simulations are used to design and optimize a microhotplate using silicon carbide microheaters in place of the platinum microheaters.

II. FABRICATION AND TESTING OF MICROHOTPLATES USING PLATINUM MICROHEATERS

The design of simple "coplanar-configured" platinum-based microhotplates for the purpose of comparison to simulation results involves a two-photomask process and basic microfabrication techniques. Coplanar-configured microhotplates, such as the one fabricated by Wiche [30] et al., in which the microhotplate microheaters and gas sensor are deposited on the same plane, are much easier and less time-consuming to fabricate compared with "stacked" microhotplate gas sensors, as reported in reference [1].

The fabrication includes the following steps. First, material intended to form the suspended membrane is deposited or formed on the substrate. A layer of photoresist is patterned to form electrodes and microheater structures. Then, metal is deposited and a liftoff process utilized to remove unwanted material, leaving the sensing electrodes and microheaters. Finally, the membrane is patterned and the substrate is undercut to suspend and thermally isolate the microhotplate.

Fabrication

A process flow diagram delineating these steps is shown in Figure 2.1 on the following page. The detailed fabrication processes are described in the following paragraphs.

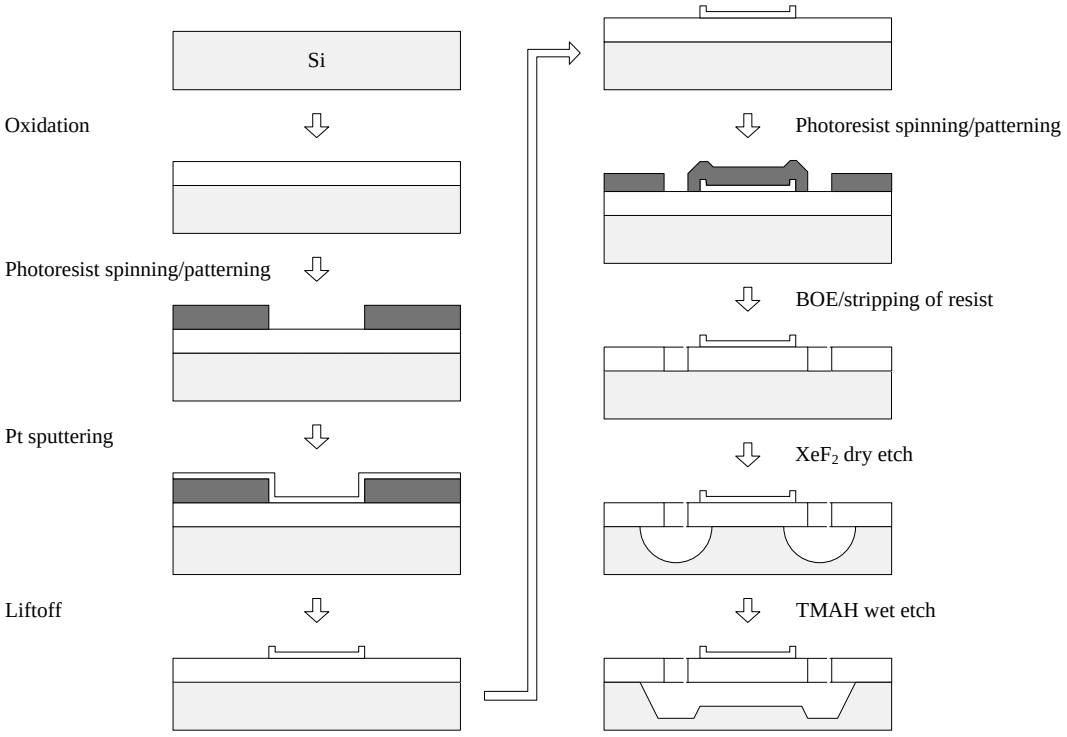

FIGURE 2.1 – Process Flow Diagram For Fabricating a Coplanar-configured Microhotplate with Platinum Microheaters

A (100)-oriented n-doped silicon wafer is used as the substrate for these devices. The microhotplate requires a layer of electrically insulating material to be deposited on the wafer surface; thermal oxide can also be used. For this research, wafers thermally oxidized at 1000°C to form a 500 nm layer of wet oxide were used, as commonly made available by cleanroom staff.

On the oxidized wafer, photoresist is spin-coated in preparation for the liftoff process. A layer of Lift-Off Resist (LOR) type 3A spun at 3000 rpm and baked at 150°C for five minutes, followed by a layer of Shipley 1827 positive photoresist spun at 4000 rpm and soft baked at 115°C for one minute, forms a re-entrant profile desired to leave photoresist sidewalls exposed. This allows the liftoff solvent to remove unwanted metal more easily. For the intended thickness of platinum (up to 200 nm), LOR 3A was chosen

as a safer and simpler alternative to other liftoff preparation methods, including the use of the aromatic compounds toluene or chlorobenzene.

Development of the 1827 photoresist requires exposure to ultraviolet light for 14.5 seconds in a Suss photomask aligner, followed by immersion in Microposit MF-319 developing solution for 75 seconds.

Deposition of the metal layer follows the resist patterning. Sputtering is the deposition process of choice for thin films of platinum metal. A 10-nm layer of titanium is deposited first, to promote platinum adhesion to the oxide; in this process, electron beam evaporation is used to form the titanium adhesion layer, after which platinum is deposited using radio frequency (RF) sputtering. In the KJL evaporation/sputtering system utilized, sputtering at a power of 200 W for eight minutes resulted in a metal layer thickness of 150 nm.

After the platinum deposition, the wafer is soaked in an *n*-methylpyrrolidone (NMP) bath to dissolve the photoresist and remove the excess metal. The liftoff process required soaking and agitation of the NMP for about two hours. Figure 2.2 below is an image of the microheater and electrode structures after liftoff, taken from a Zeiss Axioskop microscope. The microheater line width is 5 µm, while the width of the electrode "fingers" is 10 µm in this figure. Additional devices with "finger" widths ranging from 5 µm to 20 µm were fabricated, though all microheaters are 5 µm wide.

At this point in the fabrication process, some devices were retained, diced, and tested to determine the exact effect of not thermally isolating the microhotplate oxide membrane. The results of the testing of these "unreleased" microhotplates and a comparison to devices that continued to be processed are in the next section.

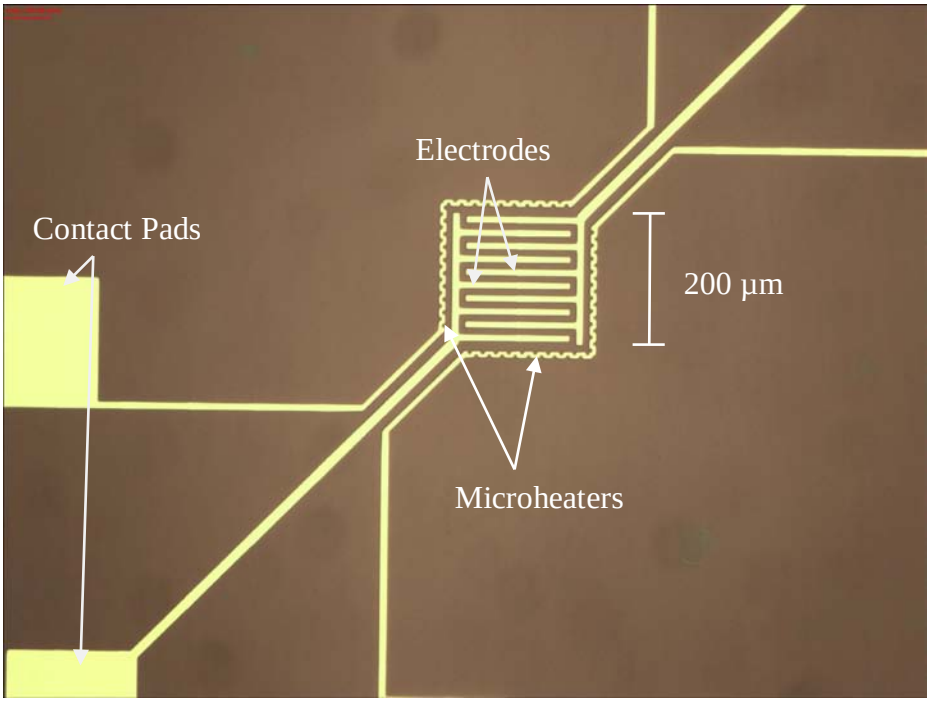

FIGURE 2.2 – Optical Micrograph of 200 µm Microhotplate After Liftoff In NMP, 50x Magnification

The remainder of the fabrication process involves etching the membrane shape in the oxide and thermally isolating the microhotplate by undercutting into the silicon below the devices using a combination of wet and dry etch techniques.

Liquid-phase hexamethyldisilazane (HMDS) is first used as an adhesion agent for photoresist on the oxide. Shipley 1813 photoresist is spin-coated after the HMDS and patterned to form etch windows around the microheaters. An exposure time of 6.5 seconds in the Suss mask aligner, followed by 45 seconds of immersion in MF-319, is adequate to develop the 1813 photoresist.

After exposure, the back side of the oxidized wafer must be protected with HMDS and photoresist as well to prevent etching of the oxide on the back surface, which may otherwise result in destruction of the wafer during bulk etching of the silicon.

The exposed oxide is etched in buffered oxide etch (BOE), a 6:1 solution of aqueous ammonium fluoride and hydrofluoric acid. Typical etch rates of oxide in this solution vary from 1000 to 1200 angstroms per minute with fluctuations in concentration and ambient temperature. A slight amount of overetching is desired to ensure that the silicon underneath is exposed. For a 500 nm layer of oxide, immersion in BOE for six minutes is acceptable to form etch windows in the oxide without endangering nearby features.

After etching the windows in the oxide layer, the Shipley 1813 photoresist may be stripped using acetone and methanol, as the silicon dioxide acts as the masking layer for all of the silicon etching steps.

To initiate the undercutting of the membrane, the wafer is exposed to xenon difluoride in a Xactix Xetch e1 series etching system. Gas-phase xenon difluoride is a dry, isotropic etchant for silicon with selectivity to silicon over silicon dioxide being reported to be greater than 1000:1 [39]. The isotropic etching properties of this etchant are desirable to expand the etching of the silicon beyond the <111> oriented crystal planes that would otherwise restrict an anisotropic etchant.

Etching with xenon difluoride takes place in a sealed vacuum chamber. The wafer is placed in the chamber and exposed to 20 cycles of xenon difluoride at a pressure of 1.5 Torr for 30 seconds per cycle. Multiple cycles are necessary as the etchant is mostly consumed in each cycle. Figure 2.3 shows a device after 20 cycles of isotropic etching using xenon difluoride, taken from a Zeiss Axio Imager microscope.

After the isotropic etch, the wafer is submerged in a beaker of tetramethylammonium hydroxide (TMAH) at 70°C for two hours. TMAH is chosen over potassium hydroxide as an anisotropic etchant for higher etch rate and greater selectivity

to silicon over silicon dioxide. A reflux condenser is attached to the beaker, and the TMAH is continuously stirred with a magnetic stir bar for the duration of the etch.

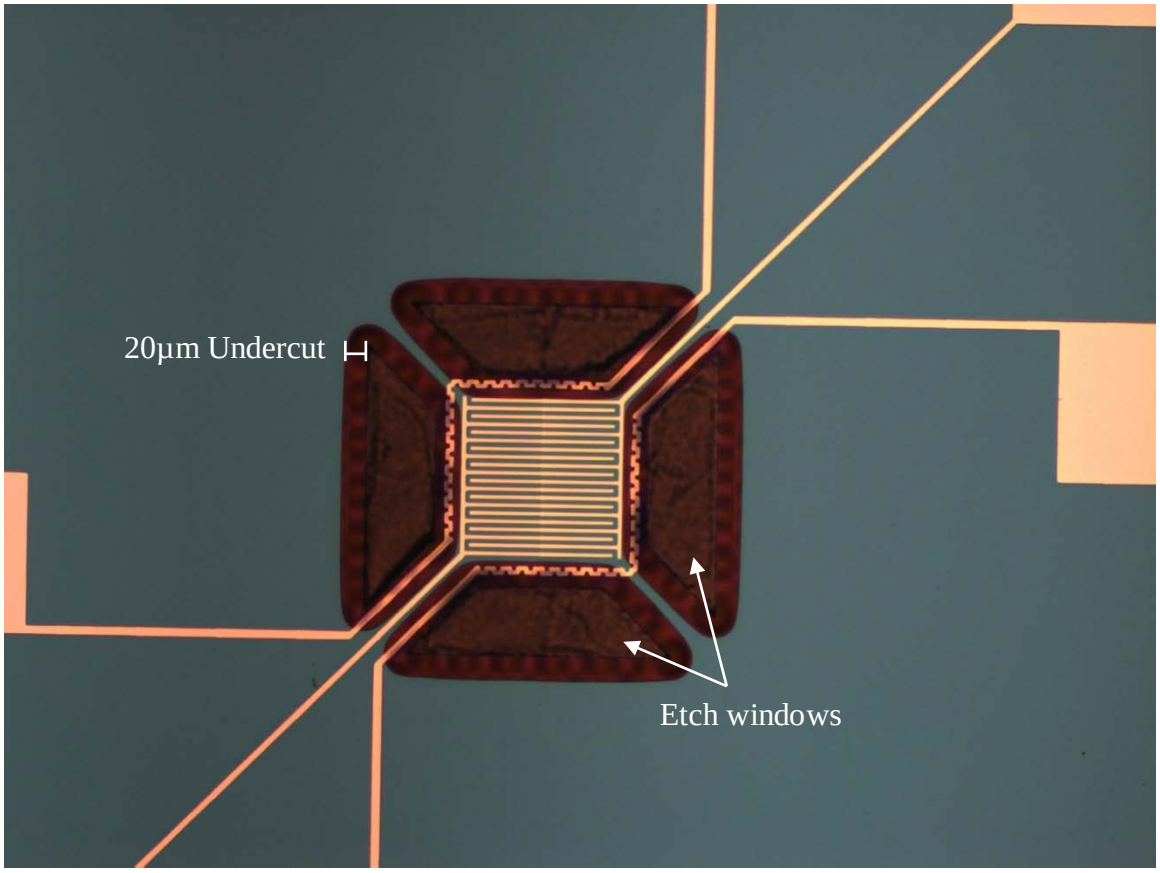

FIGURE 2.3 – Optical Micrograph of 200 µm Microhotplate After 20 30-second Cycles of XeF_2 Etching at 1.5 Torr, 50x Magnification

The wafer is then processed for an additional 20 cycles in xenon difluoride to complete the release of the silicon dioxide membrane from the underlying silicon.

Testing Results and Discussion

In order to test the performance of the microhotplates, a QFI InfraScope mid-wave infrared (MWIR) microscope system is employed. This system has a heated stage that can be used as a probe station and is capable of both visible and infrared microscopy with

up to 12x magnification in infrared. Figure 2.4 shows an image of a microhotplate device prior to testing one platinum microheater.

The probes are connected to a source meter, such as the Keithley Series 2400 SourceMeter used in this experiment. The source meter is able to measure the resistance of the microheaters, along with supplying a source voltage or source current, which passes through the microheater while the infrared microscope system records temperature data on the microhotplate.

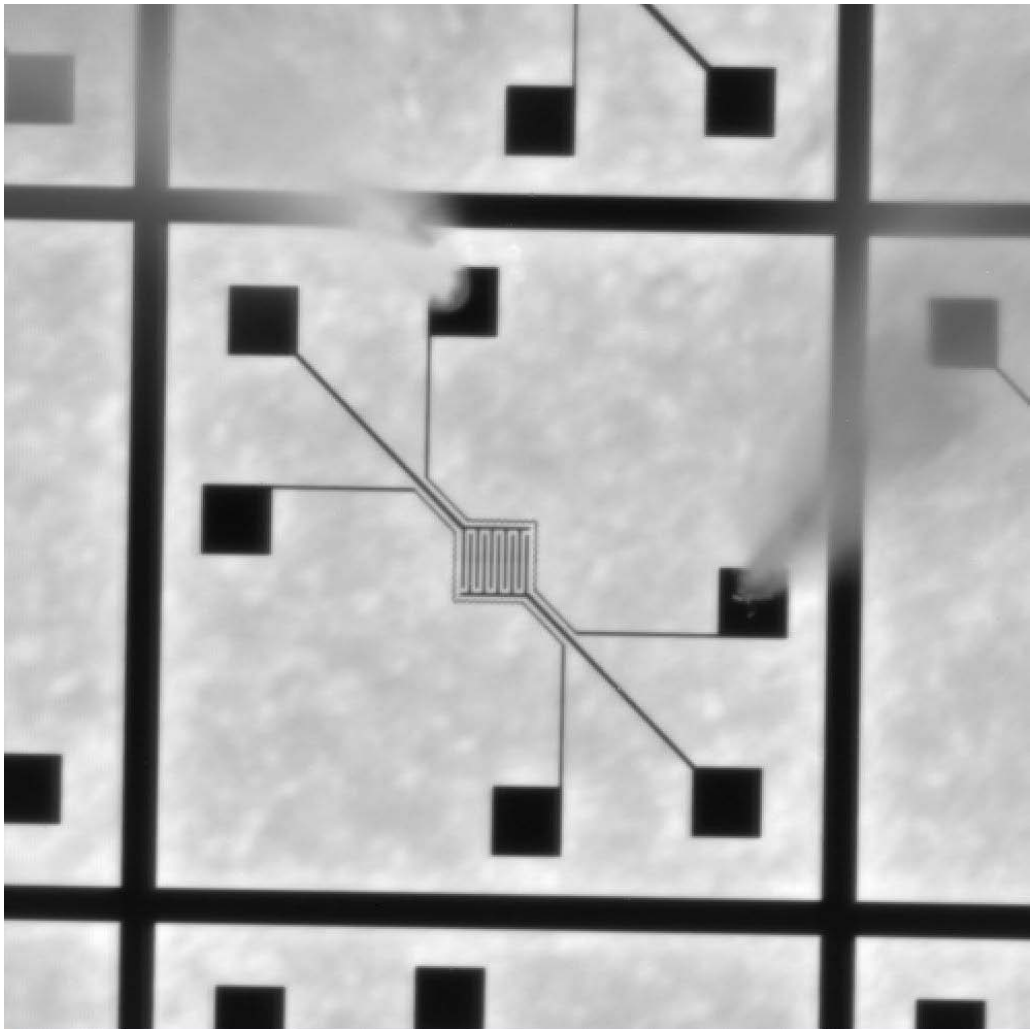

FIGURE 2.4 – MWIR Micrograph of 200 µm Unreleased Microhotplate with Probes Attached, 4x Magnification

Two sizes of microhotplates were tested. The smaller platform has an electrode area of 100 µm by 100 µm, while the larger platform has an electrode area of 200 µm by 200 µm. In each case, the pairs of microheaters, all with 5 µm line widths, surround the electrode area. 10 µm gaps separate the electrode area and the microheaters. For microhotplates that have been thermally isolated, another 10 µm gap separates the microheater from the etch window; thus, the square areas of the smaller and larger thermally isolated microhotplates, including the etch windows, are 240 µm by 240 µm and 440 µm by 440 µm, respectively.

The system is kept cool by liquid nitrogen, which is poured into the MWIR camera housing. Samples are placed on an adjustable heated stage. The stage is heated to 60°C to improve background readings for the MWIR microscope objectives. Visible light wavelength microscope objectives are first used to position the sample, the camera, and the probes. When the sample setup is complete, the MWIR camera and objectives are put in place. The camera must first perform a background radiation reading before it can be focused. Focusing results in an image such as in Figure 2.4.

With the MWIR camera in place and focused, a reference photograph is taken to provide a basis for temperature measurement. Then, current is applied through the microheater, and the camera is used to measure the achieved temperature with respect to the reference photograph. The voltage across the microheater is also recorded in order to calculate the resistance of the microheater and the power consumption. These data for all three microheaters tested are displayed in Table 2.1: current applied (I), voltage readings (V), resistance (R) calculations, and power consumption (P).

TABLE 2.1

CURRENT-VOLTAGE MEASUREMENTS AND RESISTANCE AND POWER CALCULATIONS FOR FABRICATED PLATINUM MICROHEATERS TESTED

Resistor	**I (mA) Meas.**	**V (V) Meas.**	**R (ohm) R = V/I**	**P (mW) $P = I^2R$**
100 μm unreleased	10	3.04	304	30.4
	20	6.15	308	123
	30	9.38	313	281.4
	40	12.8	320	512
	50	16.4	328	820
	60	20.3	338	1218
	70	24.4	349	1708
	80	29.0	363	2320
	90	33.3	370	2997
	100	38.8	388	3880
	110	45.8	416	5038
200 μm unreleased	10	4.08	408	40.8
	20	8.26	413	165.2
	30	12.6	420	378
	40	17.3	433	692
	50	22.4	448	1120
	60	27.9	465	1674
	70	33.7	481	2359
	80	40.0	500	3200
	90	46.7	519	4203
	100	56.1	561	5610
100 μm isolated	1	0.261	261	0.261
	2	0.525	263	1.05
	3	0.795	265	2.385
	4	1.08	270	4.32
	5	1.38	276	6.9
	6	1.74	290	10.44
	7	2.12	303	14.84
	8	2.50	313	20
	9	3.00	333	27
	10	3.55	355	35.5

Temperature measurements appear similar to that in Figure 2.5, in which a current of 60 mA is passing through a 411-Ω microheater of a 200 µm microhotplate. The camera software, ThermalMap, allows an image to be captured of the active microheater. A pixel-thick line trace is drawn on the image and temperature data is extracted.

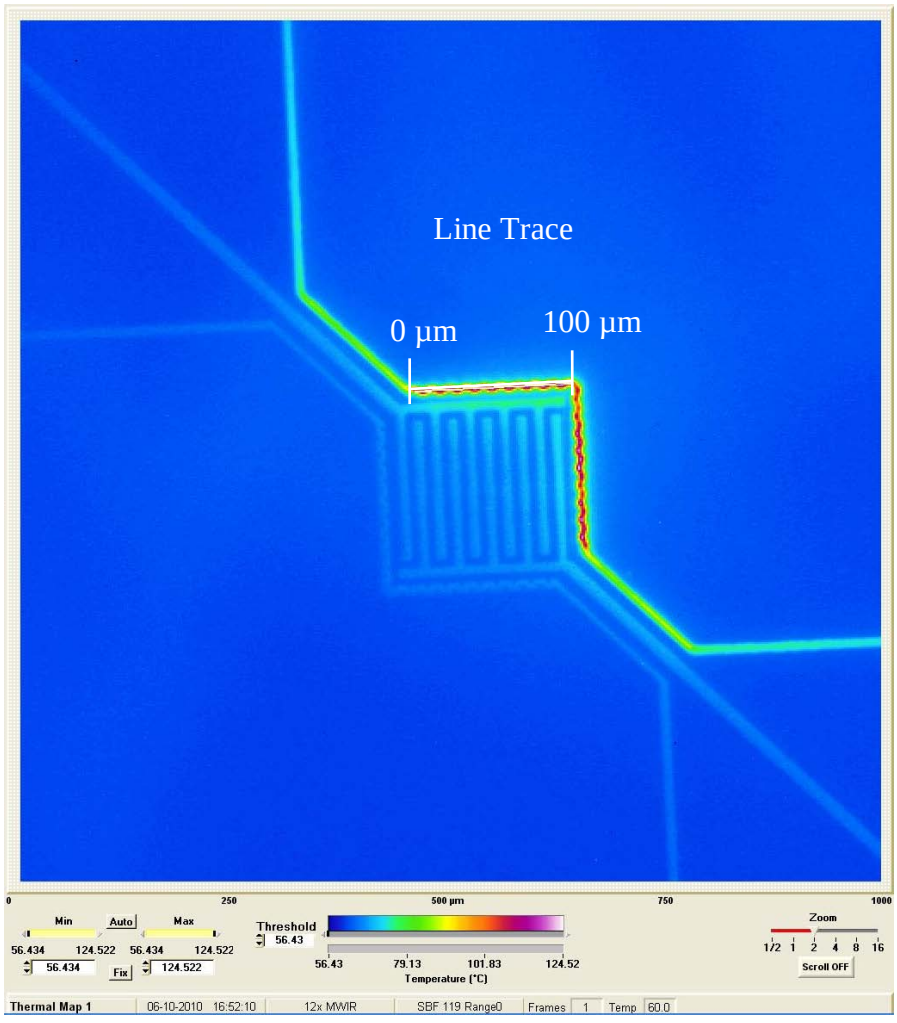

FIGURE 2.5 – MWIR Thermal Micrograph of Unreleased 200 µm Microhotplate with 60 mA of Current through One Microheater, 12x Magnification

For the unreleased microhotplates, temperature data is extracted from the surface of the microheaters due to lack of sufficiently measurable heating of the membrane; for

thermally isolated microhotplates, temperature data is extracted in a line starting from the corner of the microheater and crossing the isolated membrane, as shown in Figure 2.6.

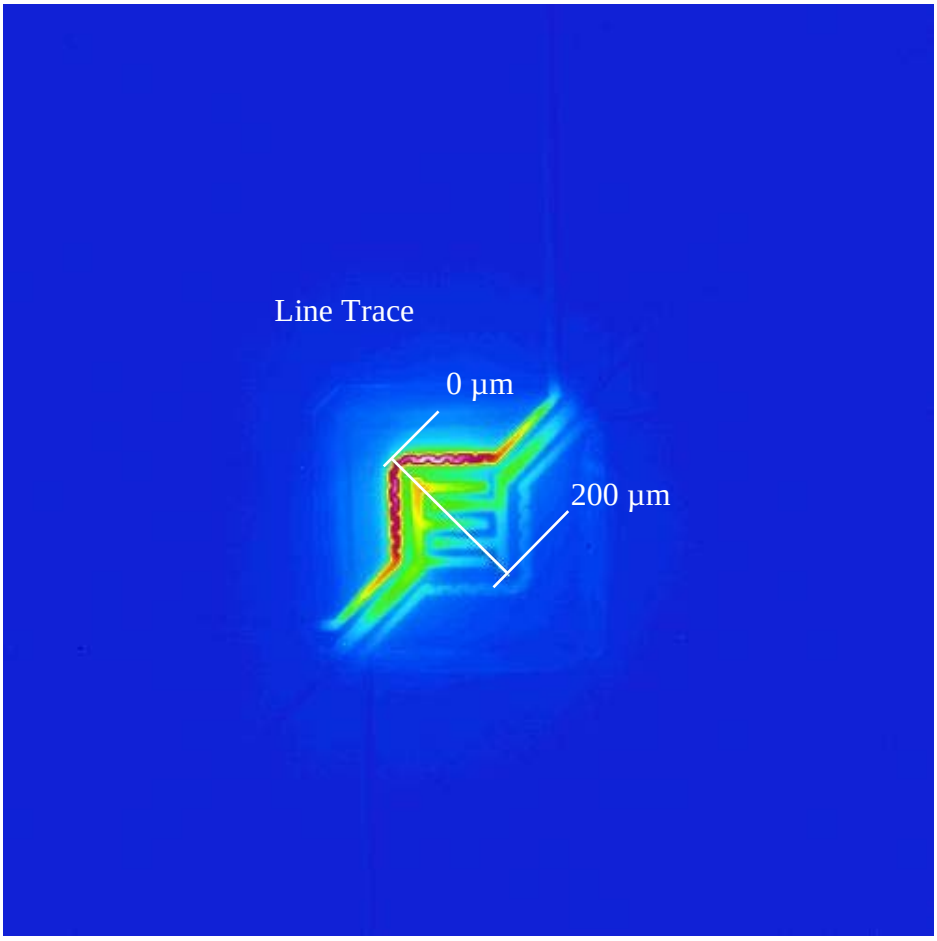

FIGURE 2.6 – MWIR Thermal Micrograph of Thermally Isolated 100 µm Microhotplate with 5 mA of Current through One Microheater, 12x Magnification

The following figures show collections of line traces extracted from infrared images of three microhotplates when constant current is applied through one microheater. Figure 2.7 represents data collected from the surface of a microheater on a 100 µm microhotplate, while Figure 2.8 shows data collected from the microheater of a 200 µm microhotplate. For these two data sets, temperature line traces from the microheaters, as in Figure 2.5, were collected at constant-current intervals of 20 mA.

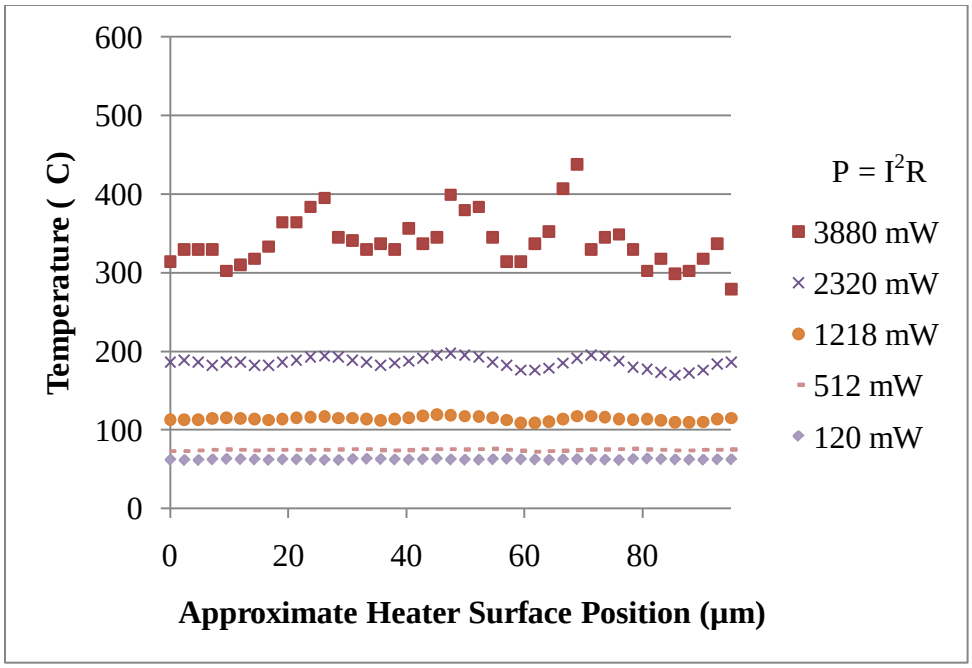

FIGURE 2.7 – Temperature Line Traces Extracted from an Unreleased 100 µm Microhotplate Microheater under Constant Current Conditions from 20 mA to 100 mA

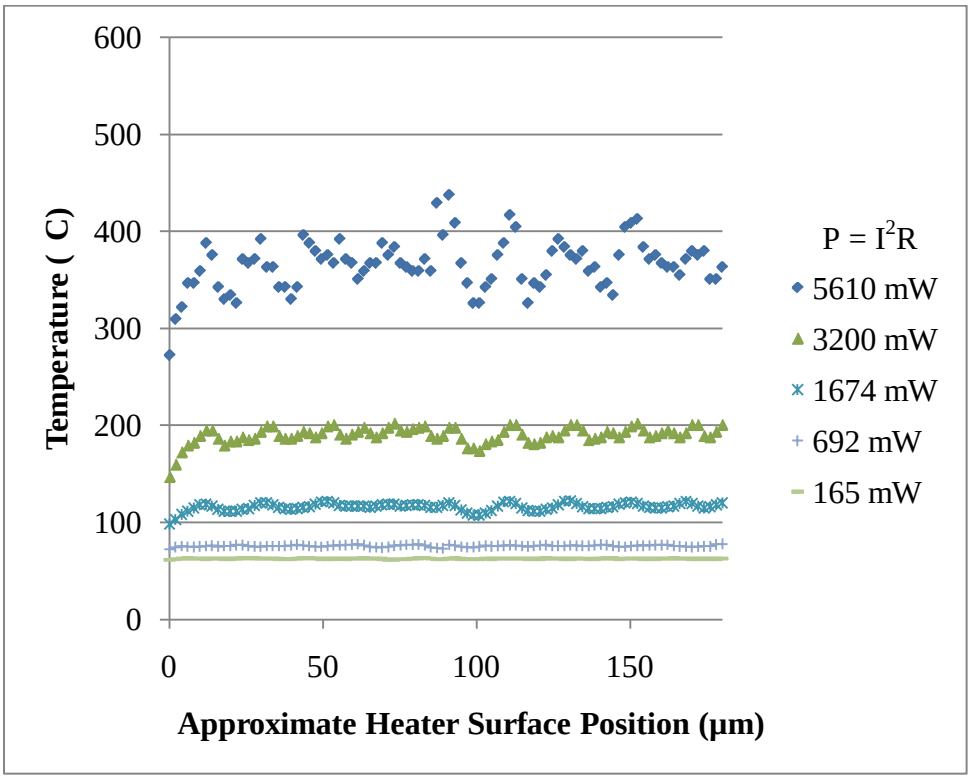

FIGURE 2.8 – Temperature Line Traces Extracted from an Unreleased 200 µm Microhotplate Microheater under Constant Current Conditions from 20 mA to 100 mA

In Figure 2.7, it can be seen that the microheater of the unreleased 100 µm microhotplate requires an appreciable 1.2 W of power, or 60 mA of current, before reaching even 100°C when the stage temperature is set to 60°C. As the current increased, greater variations in temperature across the microheater surface become visible due to small variations in geometry, and therefore current density, as a result of the sputtering and liftoff processes. At 100 mA, or 3.9 W, the microheater reaches an average temperature of 340°C, though the heating of the surrounding oxide remained minimal due to the lack of thermal isolation from the underlying silicon.

Figure 2.8 shows a similar trend expressed by the microheater of the 200 µm unreleased microhotplate, with a 60 mA current required to reach 100°C on the microheater surface. At 100 mA of current, or 5.6 W, the microheater reaches a slightly higher average temperature of 360°C. Again, however, heating of the surrounding oxide remains minimal for the unreleased microhotplates. This effect can be seen in the temperature map in Figure 2.5.

Comparing the results of these unreleased microhotplates (Figures 2.7, 2.8) to the temperature data of the thermally isolated microhotplate membrane shown in Figure 2.9, it becomes immediately apparent that the effect of the thermal isolation of the microhotplate membrane is significant. The current required to heat the microheater, as well as areas of the membrane in proximity to the microheater, is an order of magnitude less for the thermally isolated microhotplate than for the unreleased microhotplates. At only 35.5 mW, or 10 mA, the microheater reaches temperatures exceeding 400°C in localized points, and the membrane within 100 µm of the microheater heats to temperatures above 250°C.

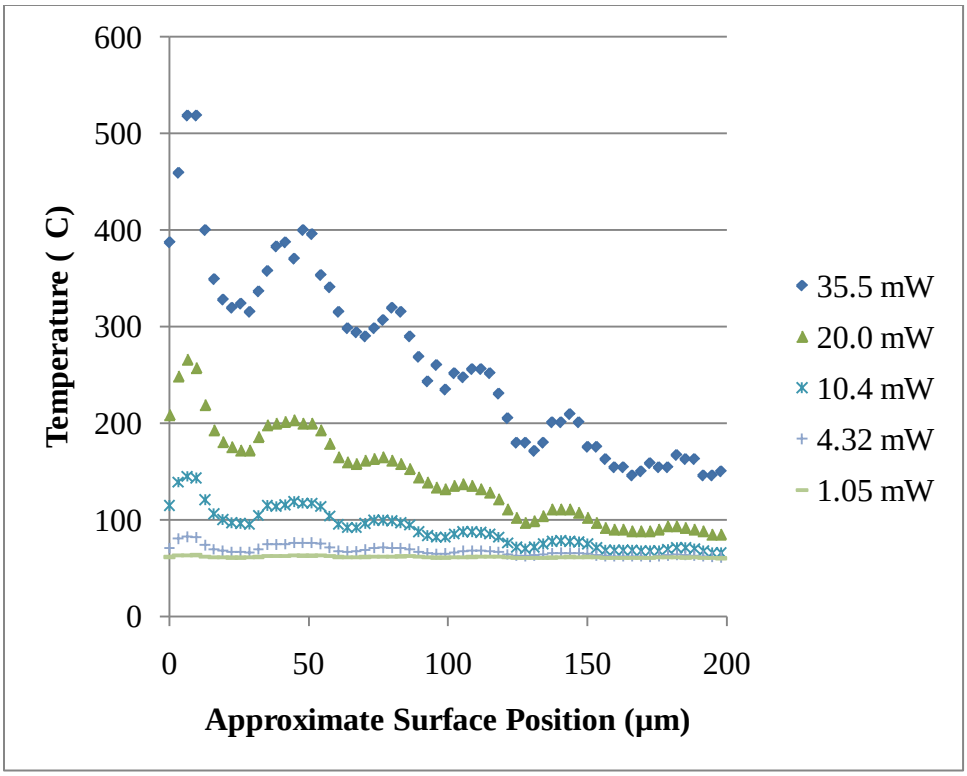

FIGURE 2.9 – Temperature Line Traces Extracted from a Thermally Isolated 100 µm Microhotplate Membrane under Constant Current Conditions from 2 mA to 10 mA

The intuitive explanation for this difference is simply that the thin, isolated silicon dioxide has a much lower thermal conductivity than the silicon wafer. According to Incropera and DeWitt [40], the thermal conductivity of silicon at room temperature is 148 Watts per meter per Kelvin, while that of silicon dioxide is on the order of 10 Watts per meter per Kelvin and that of air is approximately 0.03 Watts per meter per Kelvin. Both solid materials are seen to decrease slightly in thermal conductivity with increasing temperature.

In the case of the unreleased microhotplates, heat generated from the current flowing through the microheater flows by conduction through the thin oxide layer into the bulk silicon, where it is readily dispersed, resulting in little temperature increase. When the microhotplates are released, heat generated on the silicon dioxide membrane cannot

travel immediately by conduction into the bulk silicon, but rather dissipates through the support struts of the membrane and through the highly conductive platinum electrode traces, the latter effect of which results in heating of the platinum near the microheater as seen in Figure 2.6.

Summary of Test Results

Temperature line traces were extracted from the microheater surfaces of the unreleased microhotplates, and from the microhotplate membrane of the thermally isolated microhotplate. The 100 µm unreleased microhotplate microheater reached an average temperature of 340°C at a power consumption of 3.9 W, while the 200 µm unreleased microhotplate microheater reached an average temperature of 360°C at 5.6 W. Variations in microheater resistance and temperature along the microheater profiles arose due to the geometry of the microheaters. Neither unreleased microhotplate showed significant heating of the sensor area. The thermally isolated 100 µm microhotplate, however, reached over 250°C in the sensor area within 100 µm of the microheater at a power consumption of 35.5 mW.

III. SIMULATION OF MICROHOTPLATES USING PLATINUM MICROHEATERS

CoventorWare 2008 is the finite element analysis software package used to simulate the microhotplates. This software package includes tools to design and analyze microelectromechanical systems and microfluidics systems involving coupled electrical, mechanical, and thermal physics.

Summarizing the procedure of developing a general simulation, the first step is to create a project, which will retain all files and settings associated with the simulation. Each simulation must make use of a material properties database (MPD) file, which contains information about key physical properties of all materials used in the simulation. A fabrication process is then defined using materials available in the database. Further, the user draws the device layout, builds and meshes a three-dimensional model of the device, applies boundary and initial conditions, and finally analyzes the meshed model. Based on the type of solver chosen and the applicable physics, the software presents a visualization of the results and allows the user to extract relevant data from precise points or to run queries for information from or between surfaces and volumes.

Figure 3.1 shows a process flow diagram illustrating the general method of creating a simulation. Main steps, as delineated above, are categorized in boxes, with details and

important notes appearing to the right. The components of the software used, Designer and Analyzer, are listed on the left with applicable steps encircled.

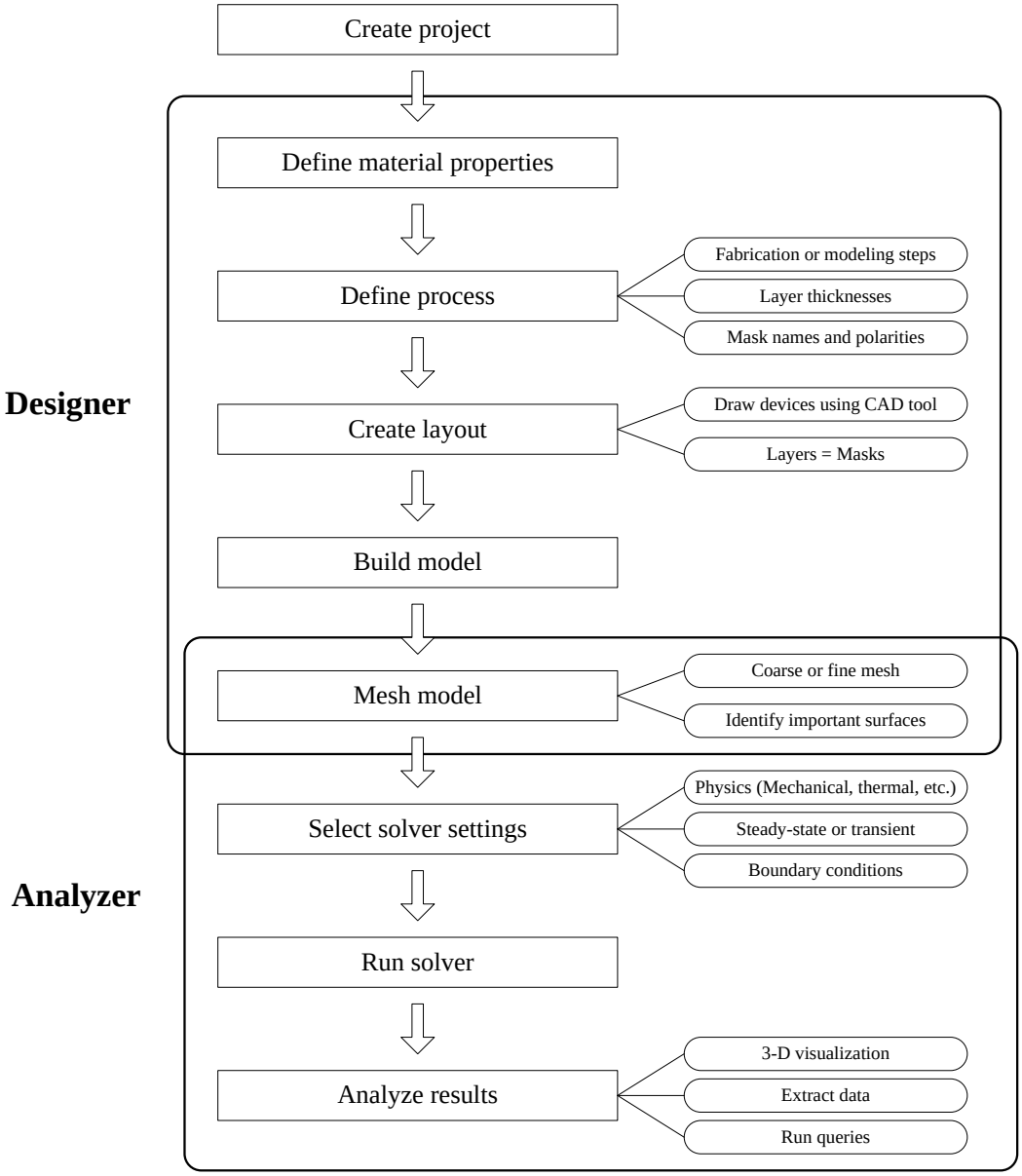

FIGURE 3.1 – General Process Flow Diagram for Creating Simulations in CoventorWare

After opening a project, the software is controlled through the use of a main window called the Function Manager, shown in Figure 3.2. The Designer tab is used first, to

design the simulation. Following the order of options from top to bottom, the Designer is used to change the material properties applied, to define the process, to draw the layout, and to build the model.

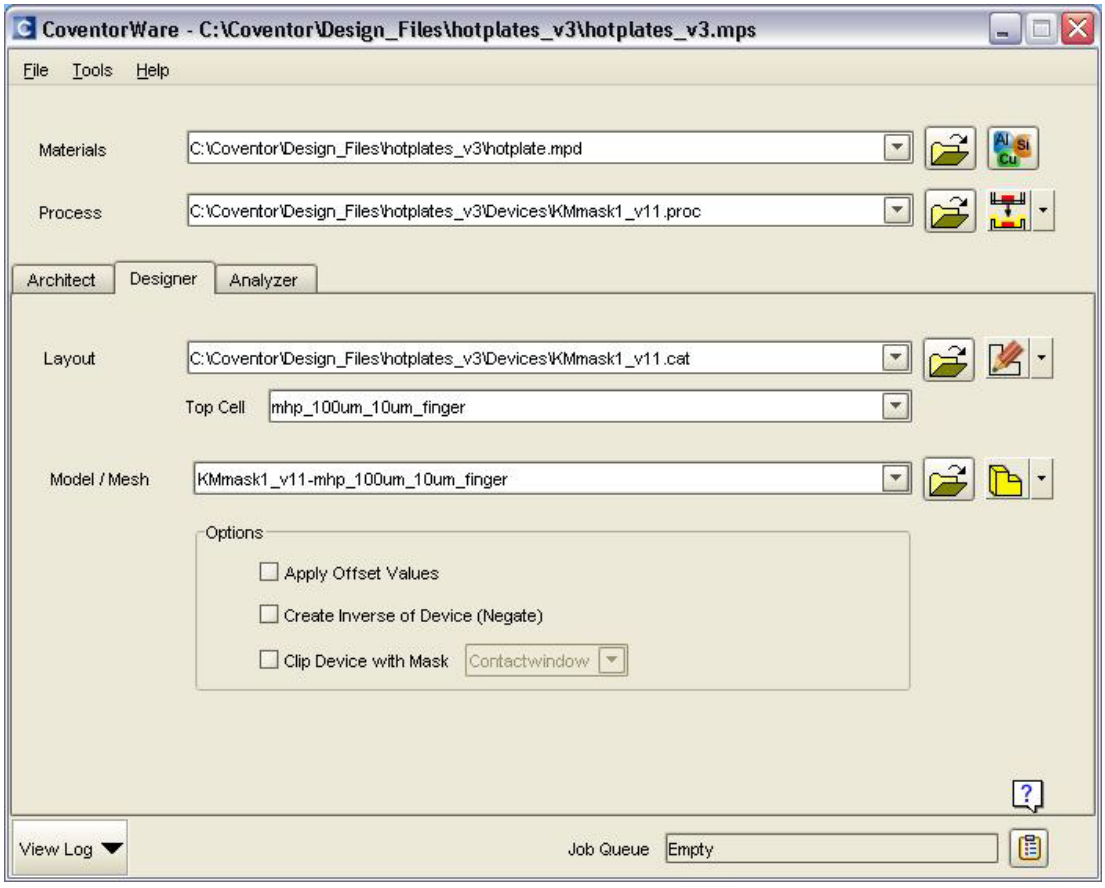

FIGURE 3.2 – CoventorWare Function Manager (Designer)

Material properties for the materials used in the simulation must be carefully monitored in order to assure the accuracy of simulation results. The properties most relevant to this study are electrical conductivity, thermal conductivity, and specific heat capacity, each of which can be specified as constant or as variable with respect to temperature, though care must be taken to provide property values with the correct units.

Thermal property data are taken from Incropera and DeWitt [40]. The temperature-dependent electrical conductivity of platinum is calculated using current-voltage data in Table 2.1, obtained during testing of the fabricated microhotplates. This information is entered into the material properties database, which appears as in Figure 3.3.

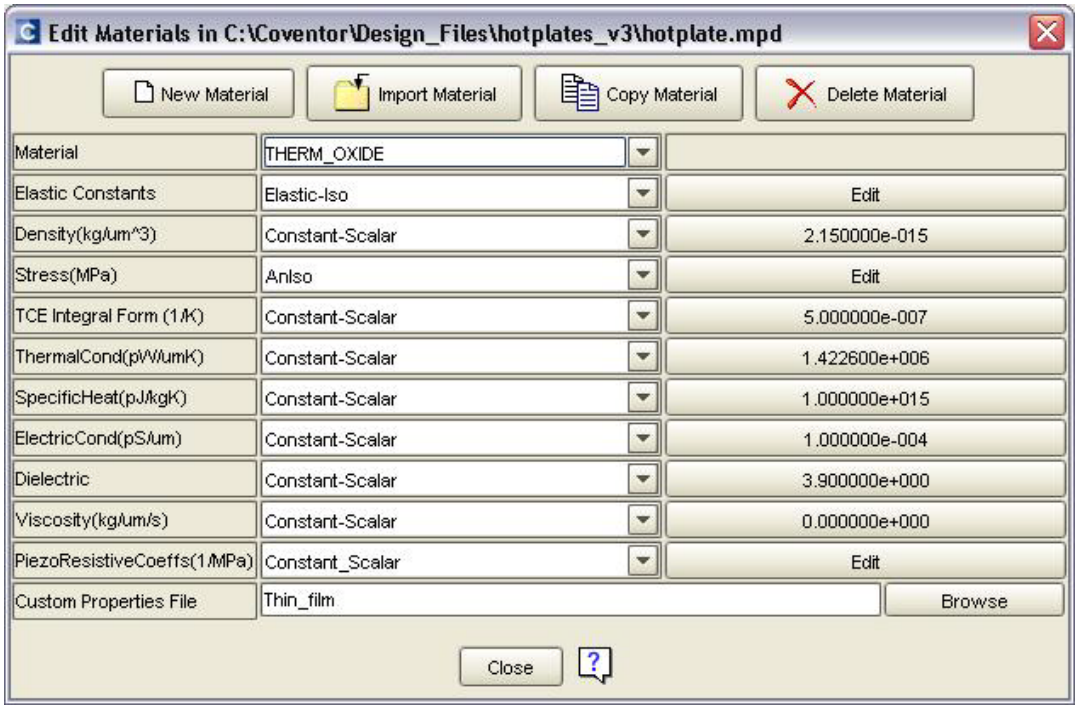

FIGURE 3.3 – Material Properties Database

Resistance calculations are used to determine the experimental resistivity of the platinum, which is converted to electrical conductivity. For a conductor, resistivity may be determined from the definition

– (3-1)

where electrical resistivity ρ is the reciprocal of electrical conductivity. The length to cross-sectional area ratio L/A is constant, and is most easily found using initial simulation results.

The temperature-dependent resistivity required to simulate microheaters with equivalent resistance to the fabricated microheaters is calculated and applied in the simulation. The resistance, rather than the perfect geometry of the microhotplate, is simulated because, for Ohmic heating, the amount of heat generated per unit of volume is equal to the power, P, dissipated in the resistor per unit volume, Vol, and therefore proportional to the current applied, I, and the resistance, R, of the microheater [40]:

— — (3-2)

The heat generated per unit volume, Q, is considered in an energy balance. The surroundings are considered to be gas-phase, consisting of air and possibly concentrations of other gases, at near-ambient temperature and atmospheric pressure; thus, heat loss by convection is initially assumed to be negligible, and radiation heat effects are ignored. This leaves only a set of conduction heat transport equations in the form of equation 3-3

(3-3)

where k is the thermal conductivity of a material and T is temperature. [40]

In the definition of the microfabrication process, the user specifies the order, method, material, and thickness of each deposition and etching step in sequence. The process definition used in the simulation of the experimentally fabricated microhotplate design is in Table 3.1.

From this process definition, it can be seen that the building of the model followed a sequence with some deviation from the fabrication process. The thermal oxide is etched prior to deposition of the platinum, and the platinum is “etched” as well. These steps are organized as such for the purpose of convenience and reflect that the simulation software

only requires a modeling process to follow, irrespective of the true applicability of the process to experimental fabrication.

TABLE 3.1

SIMULATION PROCESS DEFINITION FOR A MICROHOTPLATE WITH PLATINUM TRACES

Step Name	**Material**	**Thickness (μm)**	**Mask Name**	**Photoresist type**
Substrate	Si	50	SubstrateMask	
Thermal Oxidation	SiO_2	0.5		
Wet Etch		Last layer	Etchpit	-
Sputtering	Pt	0.15		
"Etch" (Liftoff)		Last layer	IDE	+
Anisotropic Wet Etch – Frontside*	Si only	50	BulkEtch	-

*Not present in simulation of unreleased microhotplates.

The process information is entered into the Process Editor, which is shown in Figure 3.4. Different fabrication steps from those used in this study appear in the list on the right side.

The second component required to create a model is the photomask layout. The layout is either drawn directly in the CoventorWare Catapult interface, or imported from other computer-aided design software such as AutoCAD or L-EDIT. In any design software used, it is possible to draw shapes on separate layers, which must correspond to the mask names used in the process definition.

The layout used to create simulations of microhotplates using platinum microheaters was identical to the design used for the experimental photomasks, and is shown in Figure 3.5. The BulkEtch layer lies underneath the other layers and is not shown.

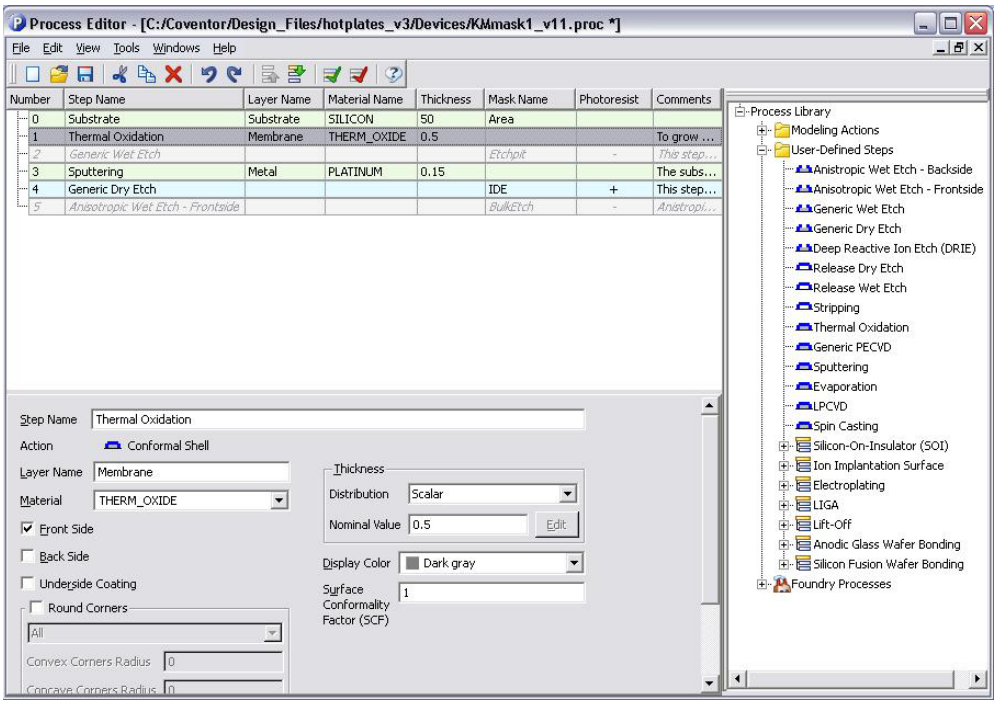

FIGURE 3.4 – CoventorWare Process Editor

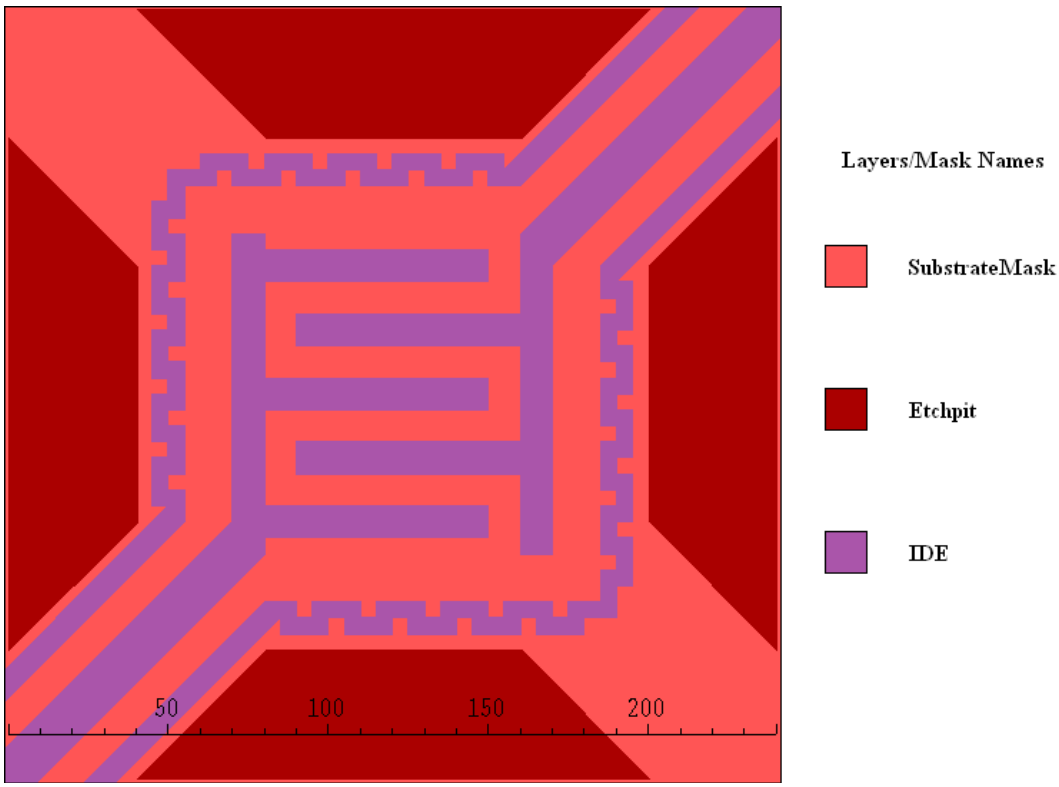

FIGURE 3.5 – Partial Layout of a 100 µm Isolated Microhotplate with Platinum Traces

When both a process definition and a layout containing layers corresponding to mask names in the process definition are specified, the simulation software can create a three-dimensional model; using the specified process and layout results in the model shown in Figure 3.6. The model is meshed, or divided into finite elements for numerical analysis, according to the precision and calculation time desired; finer meshes require longer times for the software to evaluate governing equations, but are more precise than coarse meshes.

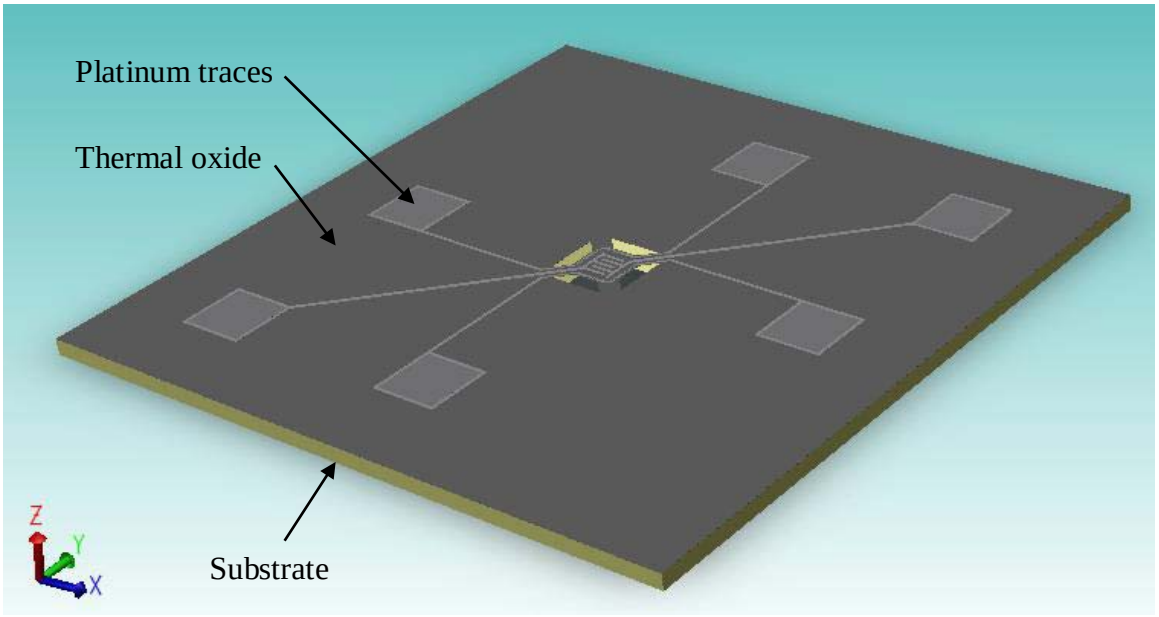

FIGURE 3.6 – Three-dimensional Model of a 100 µm Isolated Microhotplate

Within the meshed model, surfaces or volumes are selected and named, which allows the selected surfaces and volumes to have boundary conditions applied at those positions. In order to be consistent with the fabricated microhotplates, the surfaces selected for boundary conditions include the contact pad areas of one microheater and the external surfaces of the silicon substrate region, as illustrated in the final mesh in Figure 3.7.

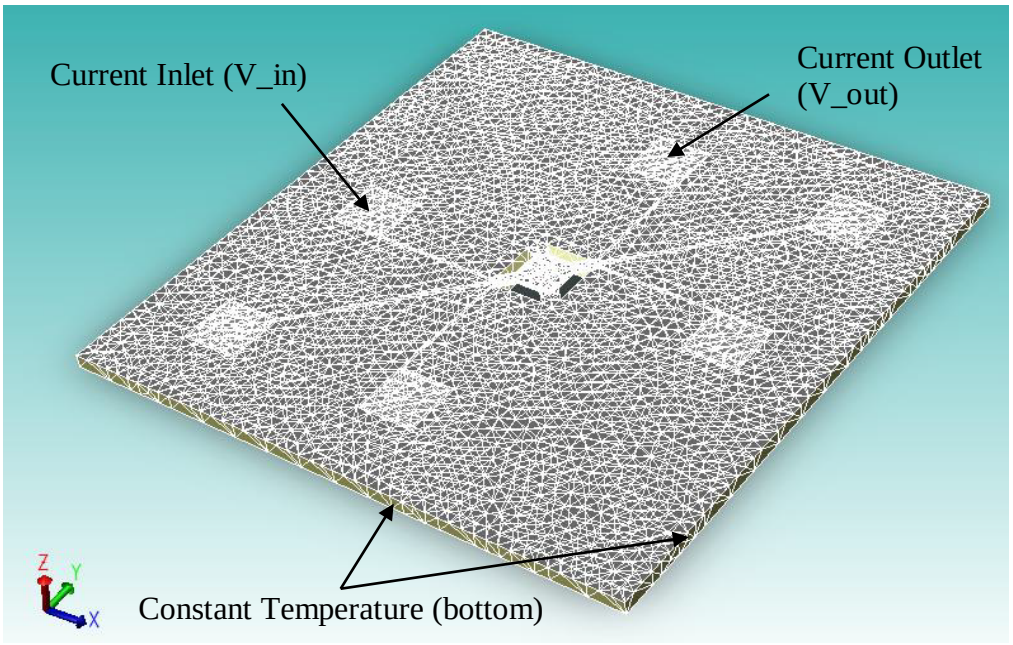

FIGURE 3.7 – Meshed Model of a 100 µm Isolated Microhotplate

CoventorWare contains multiple solver packages for various types of simulations. The solver MemMech is capable of electrothermal simulations, and is the solver of choice for this application. This solver is also capable of determining stress and mechanical effects, but these effects were ignored in this study.

The contact pad areas serve as input and output regions for electrical current, which must be specified as a density relative to the cross-sectional area of the surface of entry. Each contact pad is a 180 µm by 180 µm square having a resulting cross-sectional area of 32,400 μm^2. Thus, to match the current used in device testing, the amount of current used (10 mA, 20 mA, etc.) is divided by 32,400 and converted to the required units of $pA/\mu m^2$.

The two contact pads must be specified separately; one acts as a current inlet, while the other acts as a current outlet. An equal magnitude of the calculated current density,

such as 3.086 x 10^5 pA/µm^2, which corresponds to 10 mA, is specified at each contact pad. At the inlet, the current density value is negative, representing current entering the system; at the outlet, the current density is positive.

The silicon surfaces are held at a constant temperature of 60°C. Though the entire silicon region is not modeled in each simulation, the heat dissipative effects of the silicon are such that the substrate is essentially at constant temperature everywhere. This is evidenced by the fact that the results of the simulation are not affected whether the entire substrate is fixed at constant temperature or only the external surfaces of the substrate are held at constant temperature.

Figure 3.8 shows the surface boundary condition window in which each of the listed boundary conditions is applied.

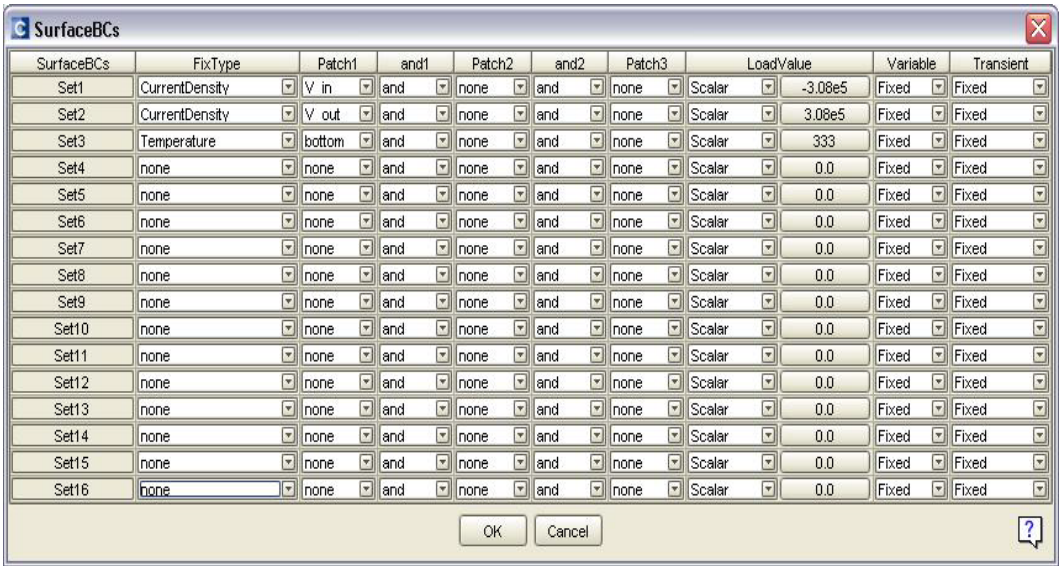

FIGURE 3.8 – CoventorWare Surface Boundary Conditions

When sufficient boundary conditions are applied, the solver calculates results using the finite elements in the mesh and presents the results for analysis. Electrical quantities

including current density, potential, resistance, and impedance can be obtained, along with thermal data such as heat flux and temperature for a simulation of this type. The latter is of primary interest to this study, as the temperature profile for each microhotplate and set of boundary conditions is desired for comparison to experimentally tested devices.

Figures 3.9 and 3.10 show simulated temperature profile results of 100 µm and 200 µm unreleased microhotplates, respectively, extracted from the surfaces of the microheaters as with the experimental testing. With a constant current of 100 mA, the simulated microheaters of the 100 µm and 200 µm microhotplates reach average temperatures of 130°C and 210°C, or 40% and 60% of those of the tested devices.

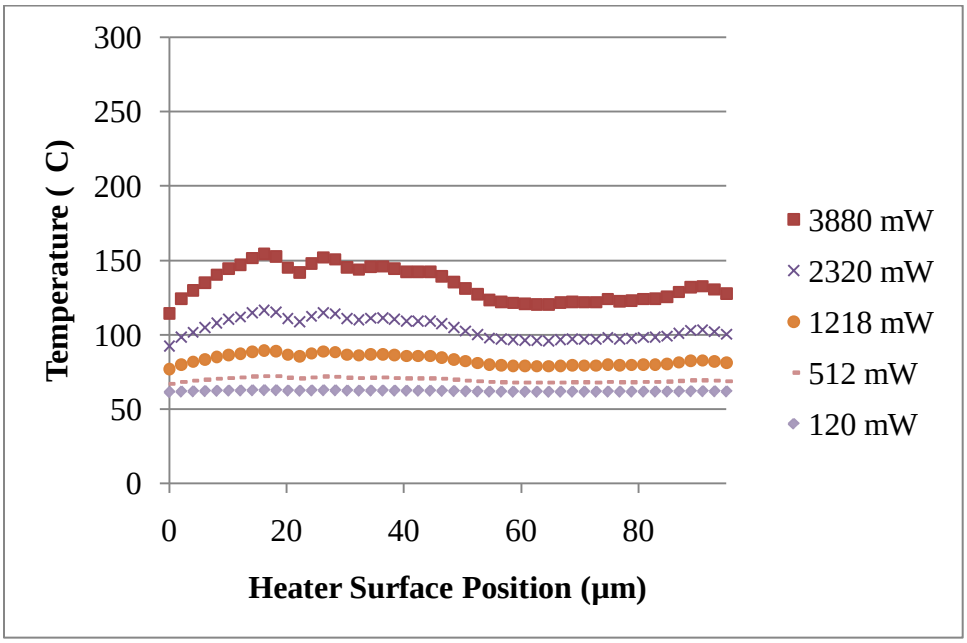

FIGURE 3.9 – Temperature Line Traces Extracted from an Unreleased 100 µm Microhotplate Simulation under Constant Current Conditions from 20 mA to 100 mA

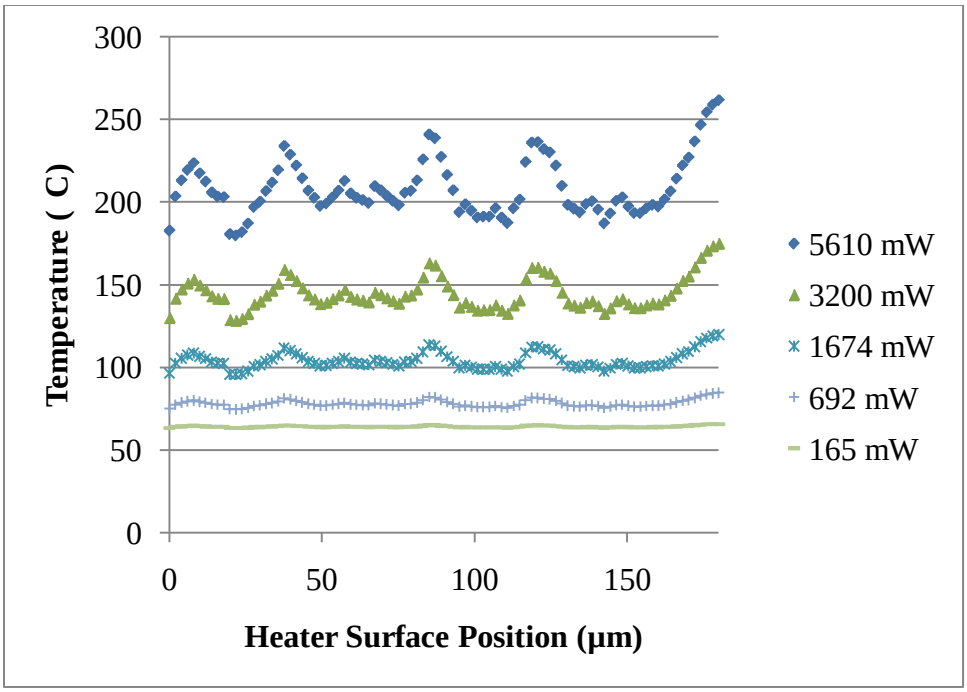

FIGURE 3.10 – Temperature Line Traces Extracted from an Unreleased 200 µm Microhotplate Simulation under Constant Current Conditions from 20 mA to 100 mA

Figure 3.11 shows the distribution of temperature across the microhotplate simulation. Compare the simulated temperature distribution for a 200 µm unreleased microhotplate, shown in Figure 3.11, to the infrared microscope image in Figure 2.5, both at 60 mA of current. The simulation accurately models the poor heat distributing qualities of the unreleased microhotplates, showing a concentration of maximum temperature along the center of the microheater with minimal heating of the oxide.

The reason for the differences in temperature values is most likely that the mesh used to cover the entire device area was not fine enough to allow the software to precisely calculate the geometry of the microheaters. The result is that current appears to be lost in triangular formations around the microheaters, outlining the tetrahedral finite elements of the mesh. This current loss is supported by the software results in that the current

entering the model at the current inlet “V_in” is reported as being over an order of magnitude larger than the current leaving the model at the current outlet “V_out”.

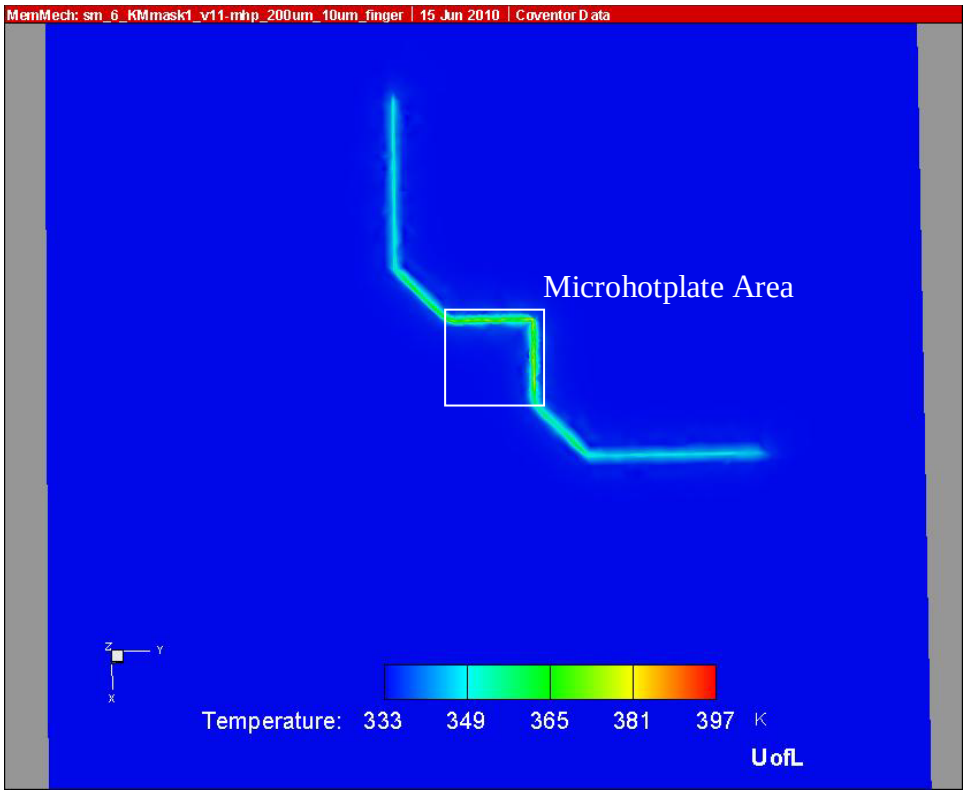

FIGURE 3.11 – Temperature Plot of a Simulated Unreleased 200 µm Microhotplate with 60 mA of Current through One Microheater

Notwithstanding the apparent discrepancy between simulated and observed temperature ranges, the temperature distributions in the simulations mimic those experimentally observed. As expected from equation (3-2), the longer microheaters of the 200 µm microhotplates, possessing greater resistance than the microheaters of the 100 µm microhotplates, dissipated more power, in turn exhibiting a higher temperature on average in both experimentally observed and simulated results. Interestingly, the simulation software also accurately modeled local temperature fluctuations across the microheater for the 200 µm microhotplate; compare Figures 2.8 and 3.10.

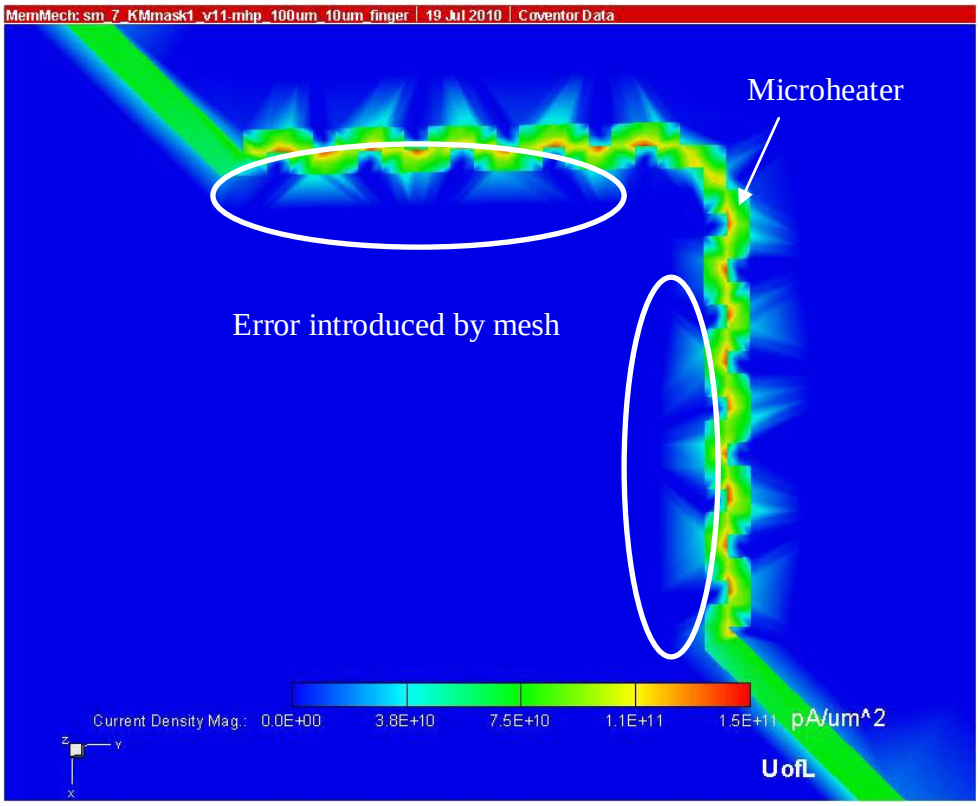

FIGURE 3.12 – Current Density Plot of a Simulated Unreleased 100 µm Microhotplate with 70 mA of Current through One Microheater

To simulate the thermally isolated microhotplate, an anisotropic wet etch through the underlying silicon is modeled, rather than attempting to model the isotropic and anisotropic etches used in fabrication. Since only heat transfer by conduction is considered and the temperature distribution away from the microhotplate area is not useful, it is only important to ensure that the silicon is separated from the thermal oxide underneath the microhotplate area.

Figure 3.13 compiles the temperature data extracted when current density equivalent to passing 2 to 10 mA of current is applied across one microheater. At 10 mA of current, or 35.5 mW of power, the simulation results show a temperature peak reaching nearly

1400°C on the surface of the microheater, with the temperature decreasing gradually across the surface of the microhotplate.

Though this result is much higher than that of the experimentally tested device, the main value of this simulation is that a significant difference between the unreleased and isolated microhotplate results is to be expected; this is reflected in the experimental results.

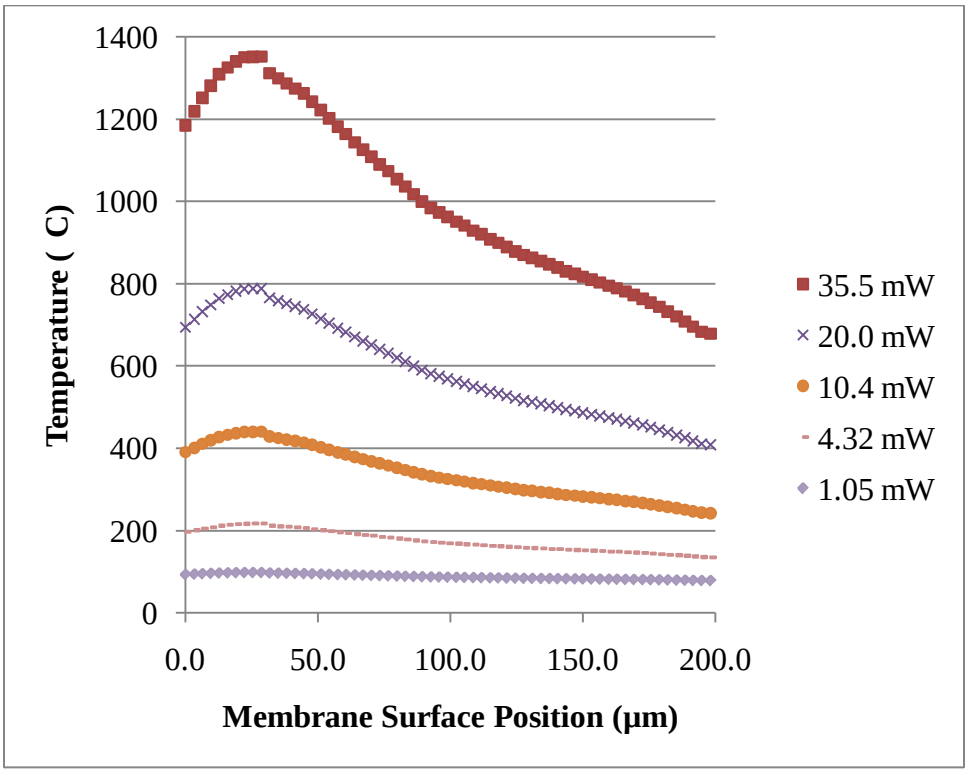

FIGURE 3.13 – Temperature Line Traces Extracted from a Thermally Isolated 100 µm Microhotplate Simulation under Constant Current Conditions from 2 mA to 10 mA

As seen in the temperature visualization in Figure 3.14, the simulation models a hot area inside the corner of the microheater, similar to how the hot portion of the electrode is shown in Figure 2.5. The simulation does not, however, distinguish that the platinum

traces become hotter than the underlying oxide, nor is there an indication of conductive heat loss specifically through the platinum on the supporting legs of the membrane.

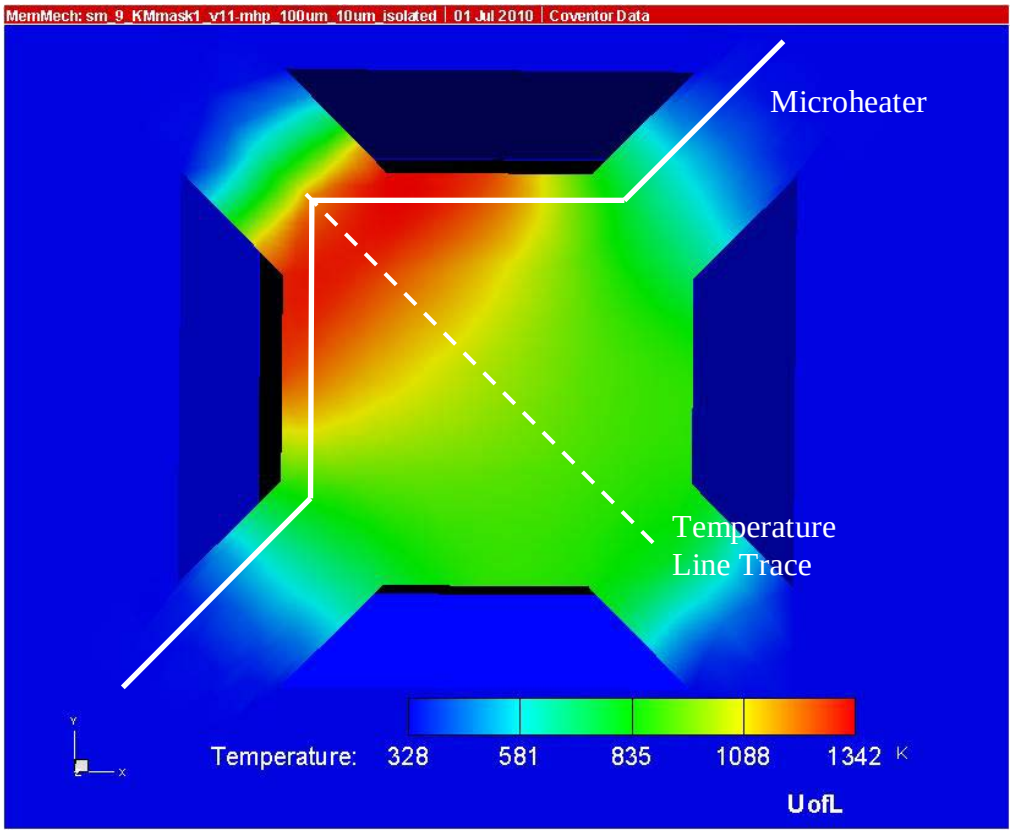

FIGURE 3.14 – Temperature Plot of a Simulated Thermally Isolated 100 µm Microhotplate with 9 mA of Current through One Microheater

There are two most probable factors contributing to the attainment of excessively high temperatures in the simulation. These factors include the range of applicability of the temperature-dependent platinum resistivity used and lack of consideration of mechanisms for heat loss.

Resistivity of platinum is a function of temperature, as shown in the measured resistance from Table 3.1. However, the temperature functionality is only certain for the range of temperatures experimentally obtained on the tested devices. Because the

simulation exceeds these temperatures, the applicability of the platinum electrical resistivity, among other material properties, including thermal conductivity and specific heat capacity, is nullified. The simulations not exceeding these temperatures, such as those using six milliamperes of current and below, demonstrate more believable, though still high, temperature results.

As mentioned previously, heat loss by convection and radiation were ignored in this study. However, an in-depth scale analysis of the significance of various mechanisms for heat loss was not performed. In addition to convection and radiation effects, the physical state of the oxide and platinum must be considered; at high temperatures, the sputtered platinum atoms may begin to reorganize. The properties of the platinum film may change as a result.

The rationale for neglecting convection effects stems from the suggested range of gas-phase convection heat transfer coefficients listed by Incropera and DeWitt [40] as 2 to 25 $W/m^2/K$. Under these conditions, the effect of convection on the temperatures of the microheaters in the simulations was found to be no more than a few degrees. However, according to the static analysis by Solzbacher [42] et al., characteristic heat transfer coefficients for a microhotplate in room-temperature air can reach over 500 $W/m^2/K$.

When a maximum convection heat transfer coefficient case suggested by Solzbacher [42] et al. of 550 $W/m^2/K$ is applied to a thermally isolated 100 μm microhotplate simulation, with 298 K air removing heat from both the top and bottom surfaces of the microhotplate, the temperature effect is significant, as seen in Figure 3.15.

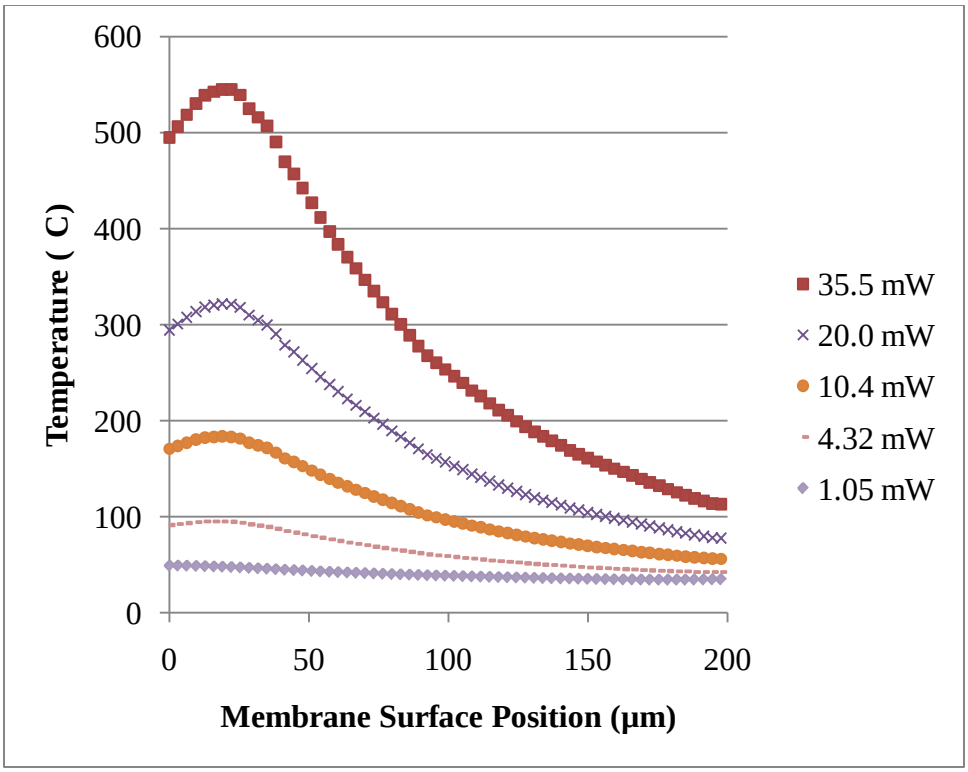

FIGURE 3.15 – Temperature Line Traces Extracted from a Thermally Isolated 100 µm Microhotplate Simulation with Heat Loss by Convection

The temperature ranges demonstrated across the microhotplate in Figure 3.15 are now reasonable, with a temperature peak at 35.5 mW of 545°C, compared to the 519°C peak of the fabricated device in Figure 2.9 at the same power consumption. An absolute percent error is determined for each data point by the formula

$$\frac{\qquad\qquad}{\qquad\qquad}$$

and an average is found by adding the percent error at each data point and dividing by the number of data points. This average error across the microhotplate at a power consumption of 35.5 mW is found to be 18% (see Appendix). In addition, the distribution of the hot area, shown in Figure 3.16, has begun to contract to the microheater area.

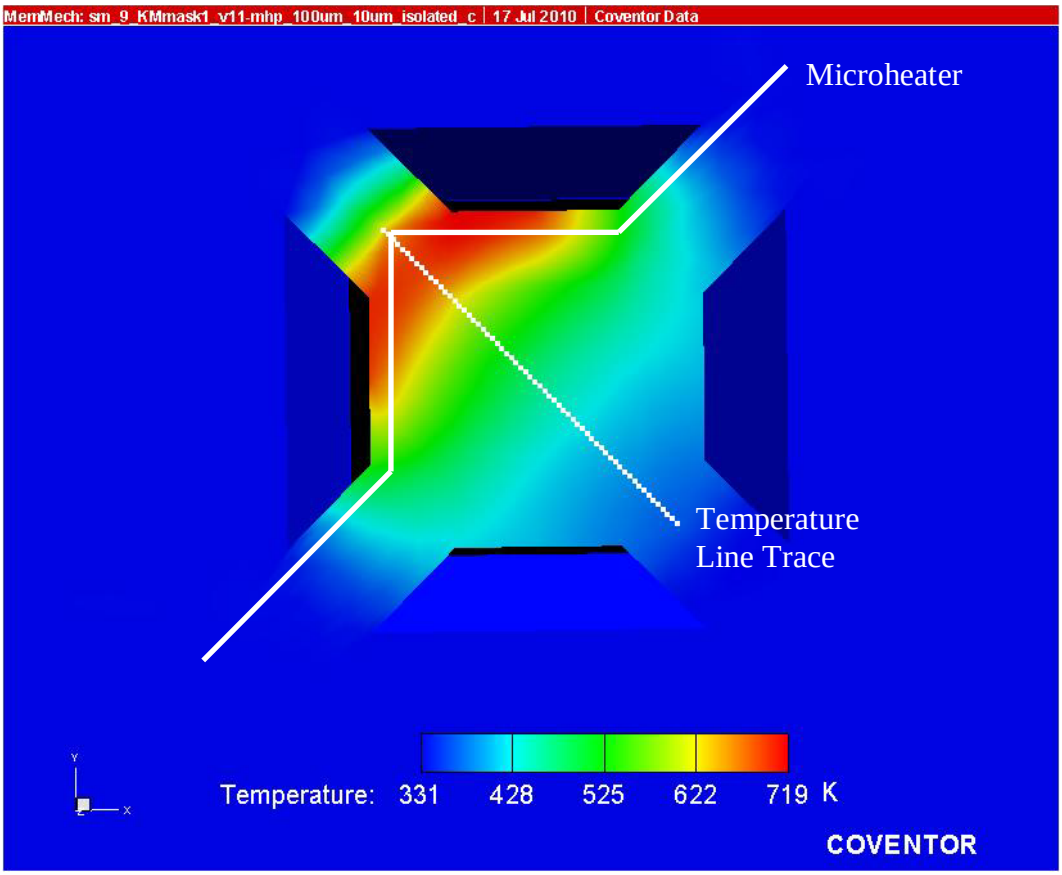

FIGURE 3.16 – Temperature Plot of a Simulated Thermally Isolated 100 µm Microhotplate with 9 mA of Current through One Microheater and Convection Effects

A new set of microhotplate simulations have been developed in an attempt to eliminate the meshing effect shown in Figure 3.12. Only the microhotplate area is included in the model to reduce the calculation time for a finer mesh. The boundary conditions, including convection heat losses, are identical, though the current density must be changed to reflect the cross-sectional area of the microheater trace rather than that of the contact pads. Figures 3.17 and 3.18 show the temperature profile results from the 100 µm and 200 µm unreleased microhotplate simulations when a fine mesh is applied.

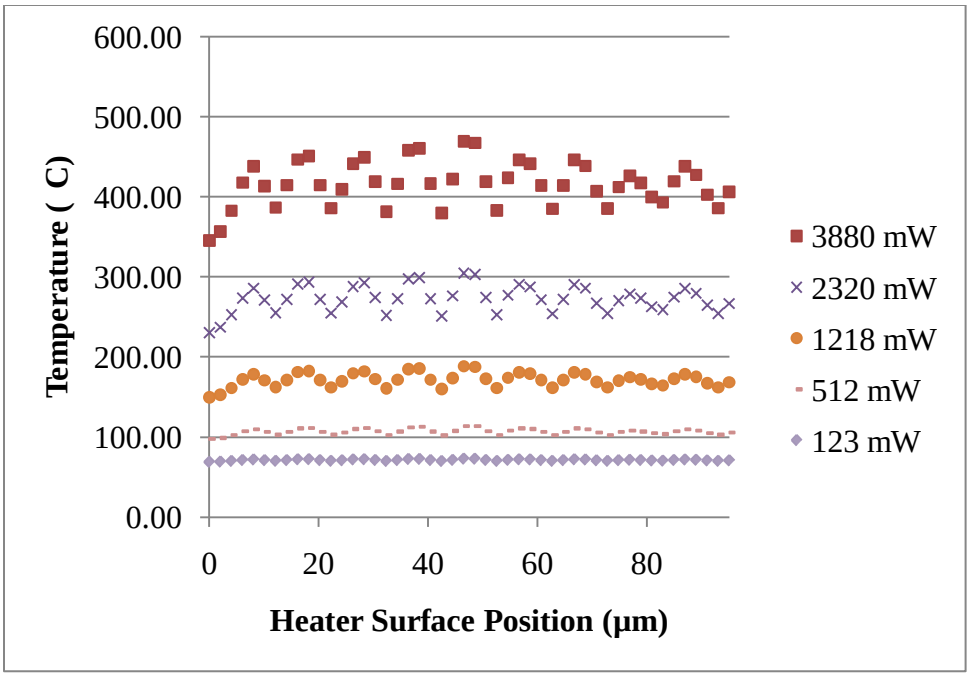

FIGURE 3.17 – Temperature Line Traces Extracted from an Unreleased 100 µm Microhotplate Simulation using a Fine Mesh

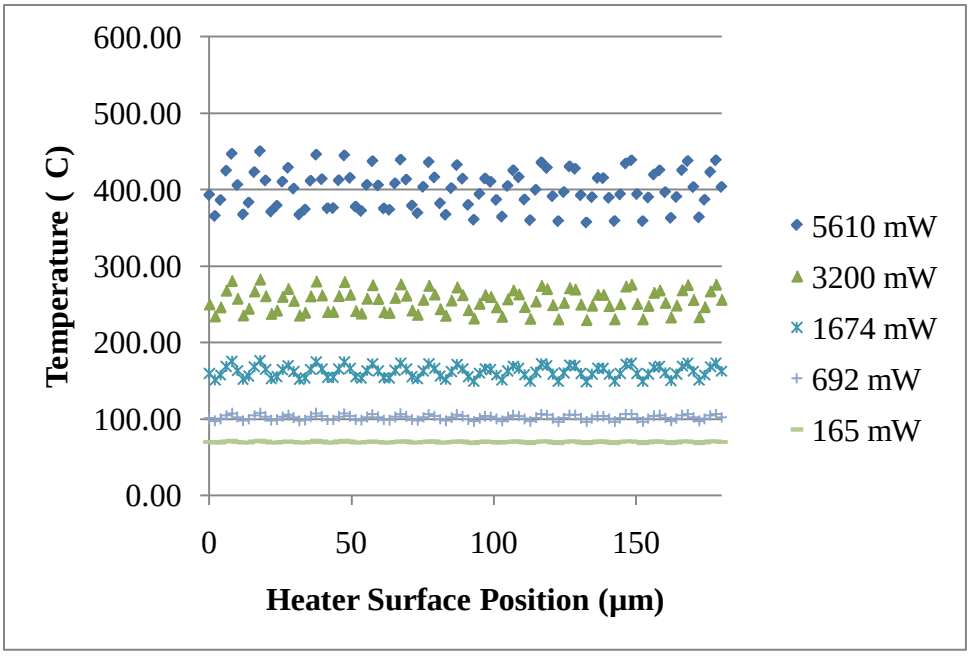

FIGURE 3.18 – Temperature Line Traces Extracted from an Unreleased 200 µm Microhotplate Simulation using a Fine Mesh

Immediately apparent is that the simulation now models the variations in temperature within the microhotplate geometry, shown by the spiking effect. Also apparent is the significant improvement in temperature exhibited by these simulations over the previous iteration. The 100 µm microhotplate microheater now reaches an average temperature of 410°C at 3.9 W, while the 200 µm microhotplate reaches 400°C on average at 5.6 W. Again compared to the tested device results of 340°C and 360°C, the finer mesh simulations show a much closer approximation, reaching within 20% of the experimental averages, though now the average temperatures of the simulations are higher than the experimental results. Figure 3.19 shows the temperature distribution of the unreleased 100 µm fine mesh simulation; the 200 µm distribution is similar.

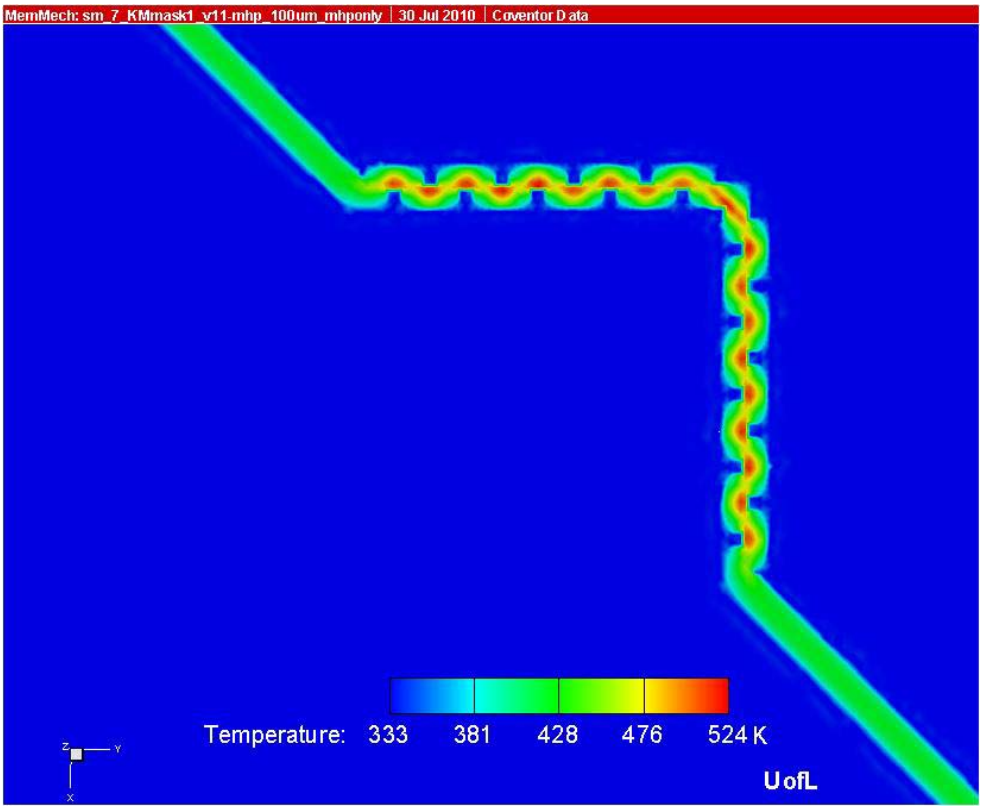

FIGURE 3.19 – Temperature Plot of a Finely Meshed Simulated Unreleased 100 µm Microhotplate with 70 mA of Current through One Microheater

Additionally, the current loss is not expressed in the finely meshed simulations; current magnitudes ntering and exiting the model at the specified boundaries are reported to be approximately equal, in most cases differing by one to two percent of the inlet current. See Table A.11 in appendix.

The same mesh improvement is applied to the thermally isolated microhotplate, with results shown in Figure 3.20.

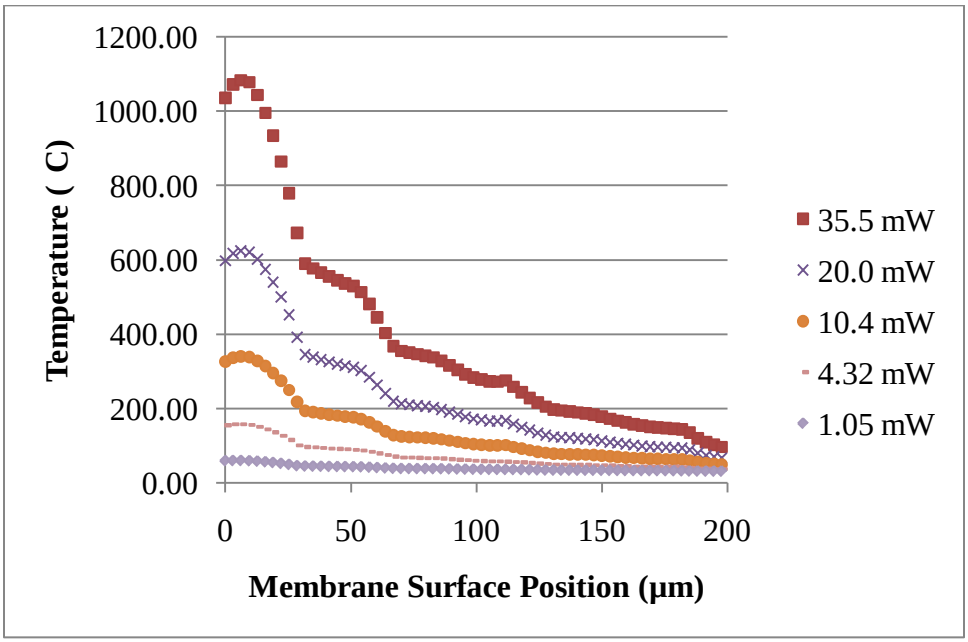

FIGURE 3.20 – Temperature Line Traces Extracted from a Finely Meshed Thermally Isolated 100 µm Microhotplate Simulation with Heat Loss by Convection

In the finely meshed thermally isolated simulation, the software begins to display a closer trend to the experimental results, where the platinum of the electrodes is found to be hotter than the underlying oxide; this can be seen in Figure 3.21.

Unfortunately, the temperature is once again much hotter than experimentally observed, even with the maximum convection coefficient case of 550 $W/m^2/K$ applied. One possible explanation for the high temperatures is that the resistance of the

microheaters may be slightly higher than necessary due to the fact that a portion of the platinum trace was removed from the simulation to decrease the model size and calculation time. In addition, though the silicon is no longer in contact with the microhotplate in the tested device, the silicon wafer was not completely etched through as is modeled in the simulation, and there may be some heat losses that were not considered.

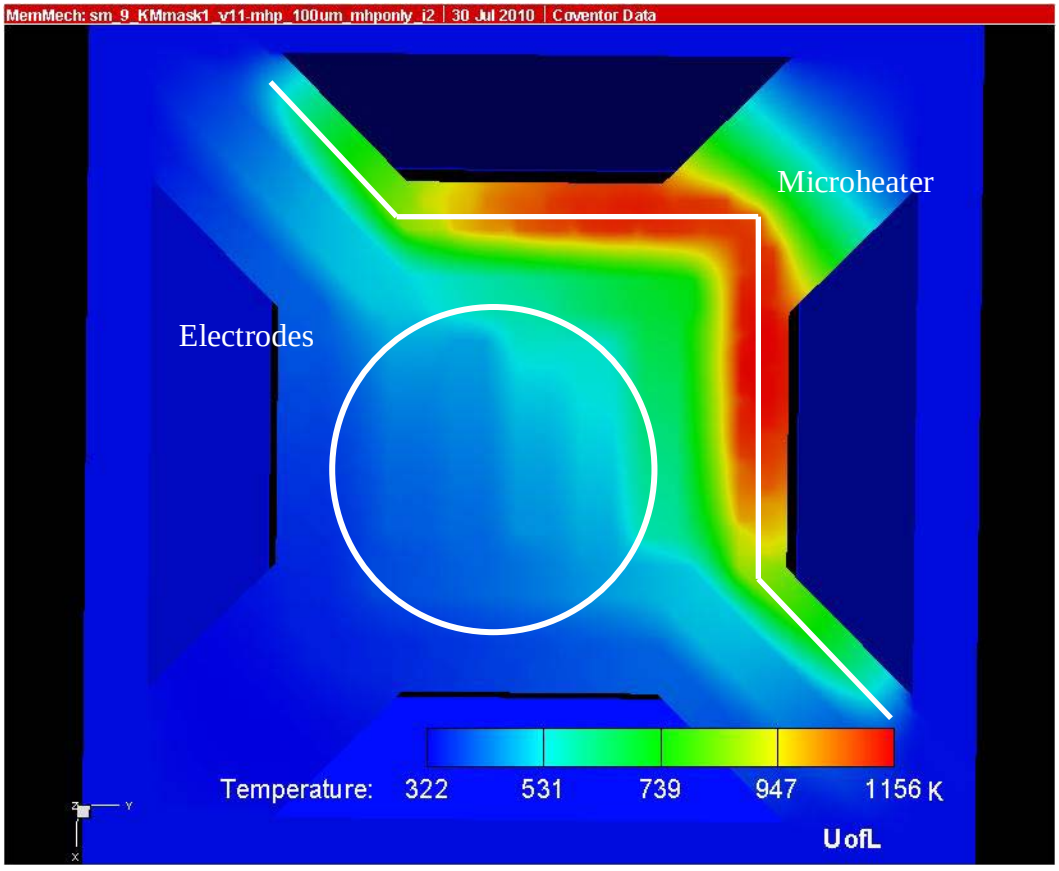

FIGURE 3.21 – Temperature Plot of a Finely Meshed Simulated Thermally Isolated 100 µm Microhotplate with 9 mA of Current through One Microheater and Convection Effects

Summary of Simulation Results

Simulations were performed on 100 µm unreleased, 200 µm unreleased, and 100 µm thermally isolated microhotplates to compare with experimentally observed results.

Initial simulations resulted in an average microheater temperature of 130°C and 210°C for the 100 µm and 200 µm unreleased microhotplates at 3.9 W and 5.6 W, or 40% and 60% of the experimentally observed average temperatures. Fine meshing eliminated current loss and improved the temperature distributions of the unreleased microhotplates, bringing the average temperatures to 410°C and 400°C, or within 20% of the experimental average temperatures. In all unreleased microhotplate simulations, heating of the thermal oxide membrane was negligible, as expected from the tested device results.

Initial simulations of the 100 µm thermally isolated microhotplate resulted in very high temperatures, peaking at nearly 1400°C for the 35.5 mW power consumption. The addition of a maximum convection coefficient case of 550 $W/m^2/K$ reduced the temperatures to within 18% of the experimentally observed temperatures across the microhotplate membrane. Finer meshing improved the temperature distribution and allowed the simulation to model heating of the platinum electrodes, but increased the microhotplate temperature.

IV. SIMULATION AND OPTIMIZATION OF MICROHOTPLATES USING SILICON CARBIDE MICROHEATERS

The motivation for using silicon carbide (SiC) is noted in the introduction of this work. Silicon carbide has attracted attention for use in microelectronic devices in past years because of its desirable material properties. These properties, including resistance to thermal oxidation, wide band gap, high thermal conductivity, high mechanical strength, resistance to corrosion and erosion, and resistance to high temperatures, make silicon carbide useful for applications in harsh, chemically active, or high-temperature environments. Normal silicon-based devices are not capable of operating for long periods in these environments.

The goal of the following simulations is to develop and optimize a SiC-based microhotplate platform for a gas sensor, making use of the desirable material properties inherent in silicon carbide. Specifically, it is desired to replace the platinum microheaters with microheaters formed of nitrogen-doped silicon carbide. As a semiconductor, silicon carbide possesses a much higher resistivity than most metals, including platinum, allowing for much shorter microheaters, which in turn allows the microhotplate size to be reduced. Table 4.1 gives a comparison between the room-temperature resistivity of platinum and doped silicon carbide.

TABLE 4.1

COMPARISON OF ROOM TEMPERATURE ELECTRICAL RESISTIVITY AND THERMAL CONDUCTIVITY OF DOPED SIC TO PLATINUM

Heating Element Material	**Electrical Resistivity at 25°C**	**Thermal Conductivity at 25°C**
Platinum	1.05×10^{-5} Ω·cm	0.716 W/cm/K
Doped 3C-SiC (10^{18} atoms/cm^3)	2.31×10^{-2} Ω·cm	4.9 W/cm/K

As Table 4.1 shows, the resistivity of heavily-doped SiC is about three orders of magnitude greater than that of platinum. In general, the thickness of PECVD-deposited SiC can reach one or two microns, while a metal such as platinum can only be sputtered to a thickness of about 200 nanometers due to high film residual stress; as reported in Chapter II, the platinum/titanium traces fabricated in this work were 150 nm thick.

Referring to equation (3-1) for a rectangular resistor, where resistance is proportional to resistivity and length and inversely proportional to cross-sectional area, it becomes apparent that, for microheaters of equal width, platinum heating elements still must be at least 100 times longer than doped SiC heating elements to reach the same resistance.

From equation (3-2), recall that heat generated by a resistor is equivalent to the power dissipated, which is proportional to the resistance of the microheater. Therefore, a relatively high resistance is desirable, and a microheater made of doped silicon carbide will reach the resistance of a platinum microheater in a much more compact volume.

These assertions can be easily proven using a one-dimensional analytical calculation. Considering rectangular bar resistors of length L, width w, and thickness t, under boundary conditions such that each end of the length of the bar (L = 0, L = L) is

held at a constant temperature of 300 Kelvin, equation (3-3) may be solved to find temperature, T, as a function of distance, x, along the resistor [33]:

- — — (4-1)

The heat generated per unit volume, Q, can be calculated using equations (3-1) and (3-2) combined, where the volume, denoted Vol, is taken as the product of length, width, and thickness:

—— (4-2)

Then, Figure 4.1 shows the expected temperatures reached in resistors of each material having lengths of 1000 µm, widths of 10 µm, and thicknesses of 0.2 µm, when 100 µA is applied to each. The silicon carbide resistor reaches 450 K at the center, while negligible heating occurs in the platinum resistor; this is the result of the much higher resistance of silicon carbide in the same volume.

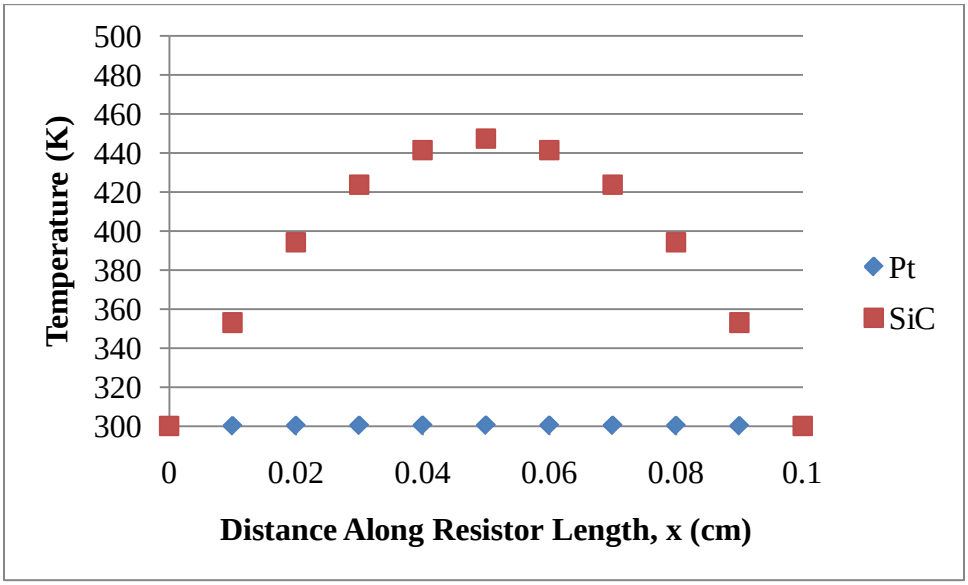

FIGURE 4.1 – One-dimensional Analytical Solution of Heat Equation for Identical 2000 μm^3 Rectangular Resistors with 100 µA Applied

When the properties from Table 3.1 are used, simple CoventorWare simulations of these resistors, as shown in Figure 4.2, result in nearly identical results as the analytical solution displayed in Table 4.2.

TABLE 4.2

ANALYTICAL AND SIMULATED ONE-DIMENSIONAL TEMPERATURE PROFILES OF PLATINUM AND SILICON CARBIDE RESISTORS

	Analytical solution from (4-1)		**CoventorWare results**	
x (cm)	**Pt**	**SiC**	**Pt**	**SiC**
0	300.0	300.0	300.0	300.0
0.01	300.2	353.0	300.2	353.0
0.02	300.3	394.3	300.3	394.3
0.03	300.4	423.8	300.4	423.8
0.04	300.4	441.4	300.4	441.4
0.05	300.5	447.3	300.5	447.3
0.06	300.4	441.4	300.4	441.4
0.07	300.4	423.8	300.4	423.8
0.08	300.3	394.3	300.3	394.3
0.09	300.2	353.0	300.2	353.0
0.1	300.0	300.0	300.0	300.0

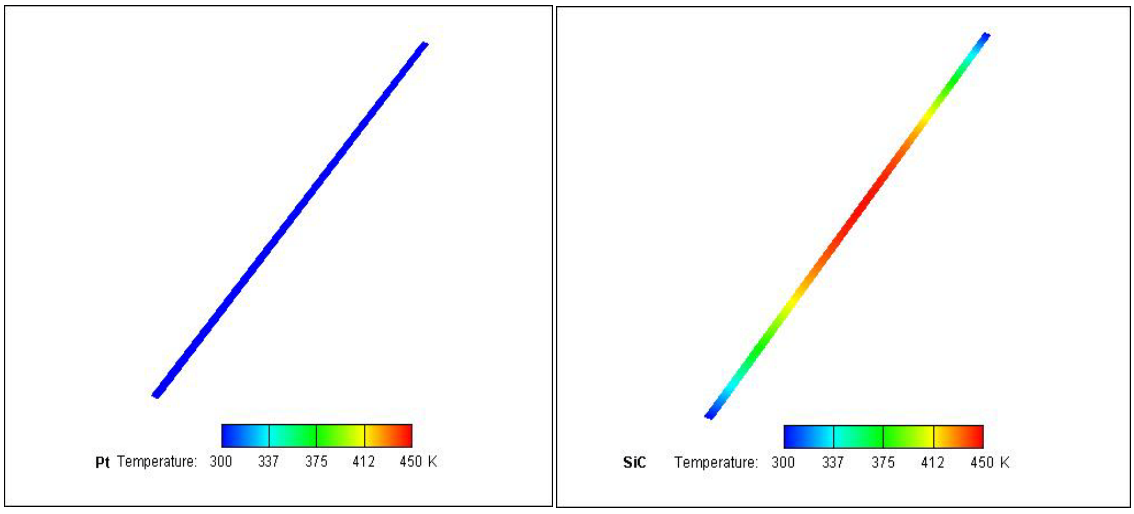

FIGURE 4.2 – Simulated Temperature Profiles of Simple Platinum and Silicon Carbide 2000 μm^3 Resistors with 100 µA Applied

The procedure for simulating microhotplates using silicon carbide is identical to the procedure outlined in Chapter III, but specifying different materials in the process definition, along with different layouts. Table 4.3 shows the process definition for a coplanar-configured microhotplate, which is explained below.

TABLE 4.3

SIMULATION PROCESS DEFINITION FOR A COPLANAR-CONFIGURED MICROHOTPLATE USING SILICON CARBIDE TRACES

Step Name	**Material**	**Thickness (μm)**	**Mask Name**	**Photoresist type**
Substrate	Si	50	SubstrateMask	
Thermal Oxidation	SiO_2	1		
Wet Etch		Last layer	MembraneMask	+
PECVD	SiC	1		
Dry Etch		Last layer	HeaterMask	+
Sputtering	Pt	0.2		
"Etch" (Liftoff)		Last layer	SensorMask	+
Anisotropic Wet Etch – Frontside	Si only	50	SubstrateMask	-

Figure 4.3 illustrates the four-microheater arrangement designed to provide a uniform temperature distribution across the sensor area of the microhotplate. Each microheater is composed of silicon carbide, while the central interdigitated electrode structure is still composed of low-resistivity metal. Figure 4.4 shows the dimensions of the resulting three-dimensional model created from the process definition in Table 4.3 combined with the layout in Figure 4.3.

Process definitions and layouts are each interchangeable. Comparisons are drawn by creating different iterations of microhotplate models and subjecting the meshed models to similar tests. In this way, an optimum microhotplate configuration may be designed.

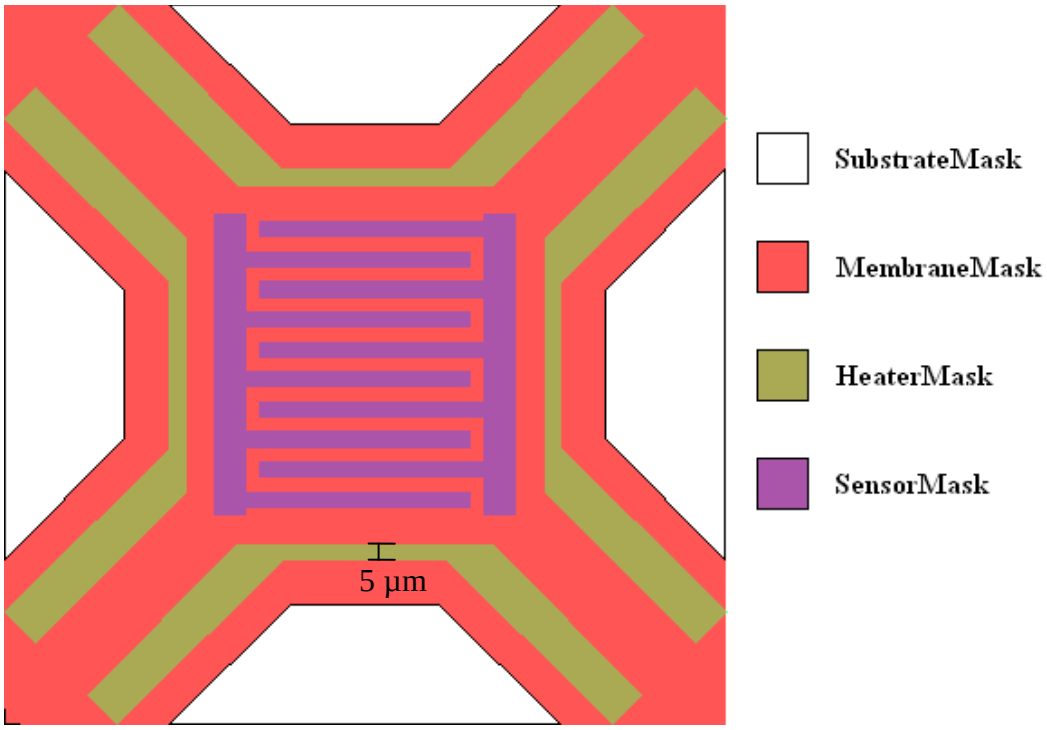

FIGURE 4.3 – Layout of a 100 µm Isolated Microhotplate with 4.5-kΩ Silicon Carbide Microheaters

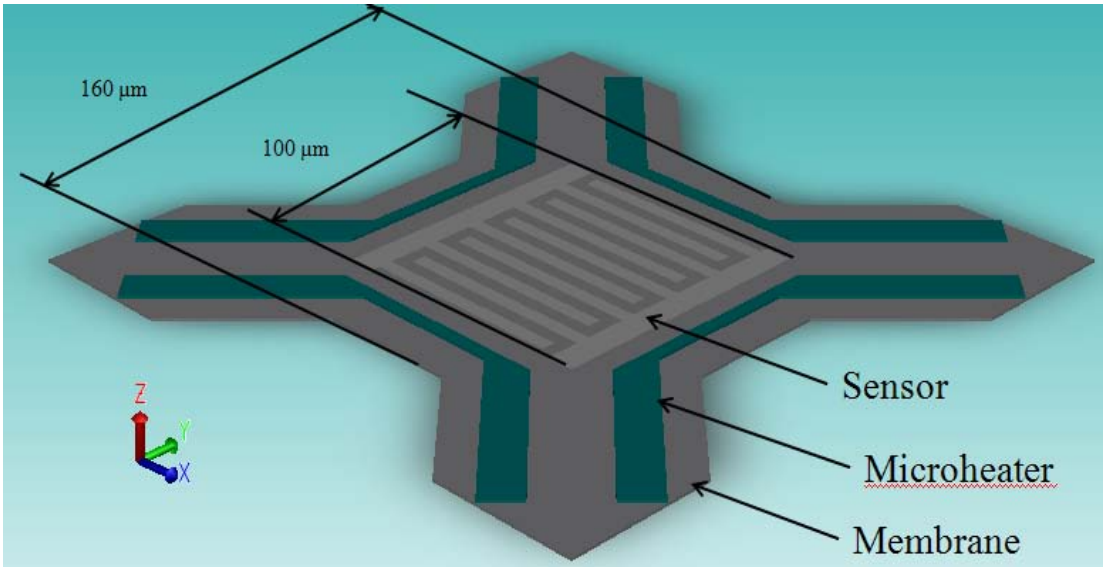

FIGURE 4.4 – Dimensions of Coplanar-configured 100 µm Isolated Microhotplate Model with Silicon Carbide Microheaters

One significant design comparison is between that of the "coplanar" microhotplate configuration and the "stacked" microhotplate configuration. This refers to the relative locations of the microheaters and electrodes for gas sensing. In a coplanar configuration, as in Figures 4.3 and 4.4, the microheaters and sensors are deposited on the same plane, while in a stacked configuration, an extra insulating layer separates the sensing element from the microheaters.

The results of a comparison of one microhotplate of each configuration, both using silicon carbide, are presented here. The coplanar microhotplate is identical to that outlined in Figures 4.3 and 4.4. The stacked microhotplate has a similar design, but a 1 µm layer of PECVD silicon dioxide separates the microheaters from the sensing element, and the thermally isolated area (not including the four support legs) has been reduced by a factor of 1.78. The sensor area and the resistance of each microheater were held constant. Figure 4.5 shows the dimensions of the stacked-configuration microhotplate model, with the insulating layer of CVD silicon dioxide hidden.

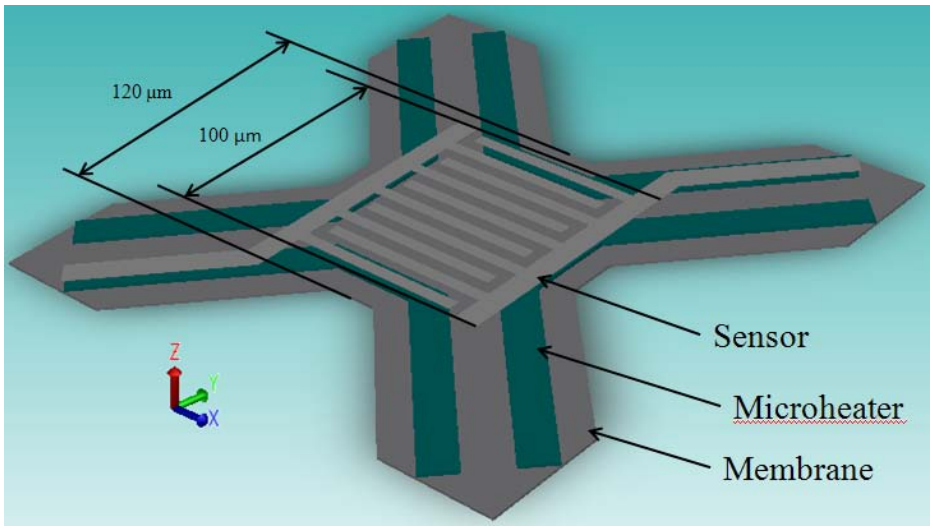

FIGURE 4.5 – Dimensions of Stacked-configured 100 µm Isolated Microhotplate Model with Silicon Carbide Microheaters

For sensing elements occupying a given area on the surface of the wafer, the advantage of a coplanar-type microhotplate is in the ease of fabrication, particularly if the heating and sensing elements are composed of the same material. However, a larger area surrounding the sensing element must be thermally isolated from the substrate in order to allow the heating elements to fit beside the sensor. Conversely, an advantage of the stacked microhotplate configuration is that the heating elements can be placed directly underneath the sensor, allowing the thermally isolated area to be smaller.

Figure 4.6 shows an analysis of the coplanar-configured microhotplate when a potential of eight volts is applied across the microheaters, for a total power consumption of 60 mW. The ends of the support legs are fixed at a temperature of 300 K; the "X" and "Y" label the data points extracted across the microhotplate surface, and the temperatures read at those points are plotted in Figure 4.7.

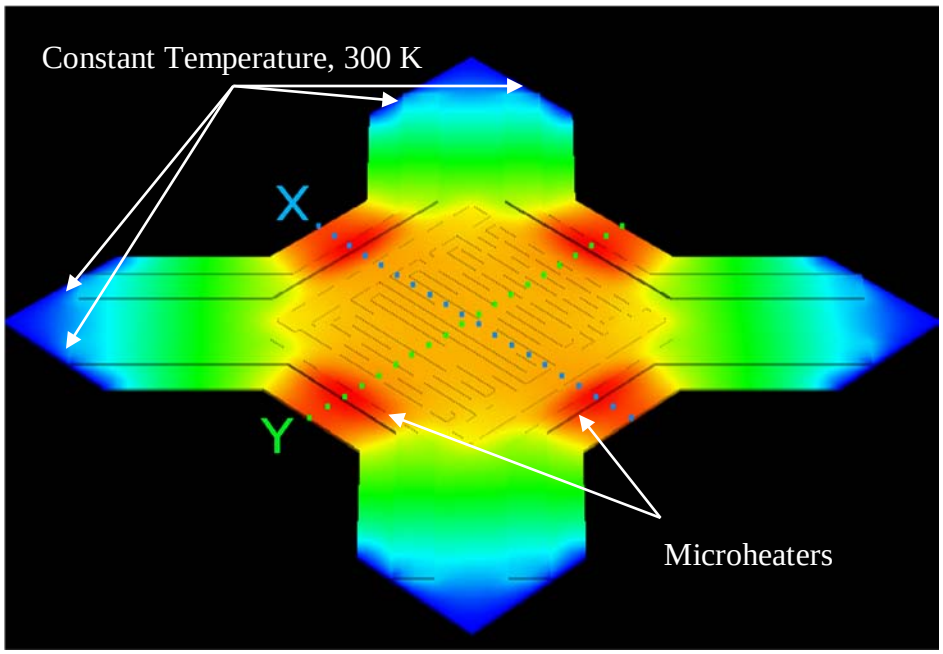

FIGURE 4.6 – Temperature Plot of a Simulated Coplanar Microhotplate with SiC Microheaters Using 60 mW of Power

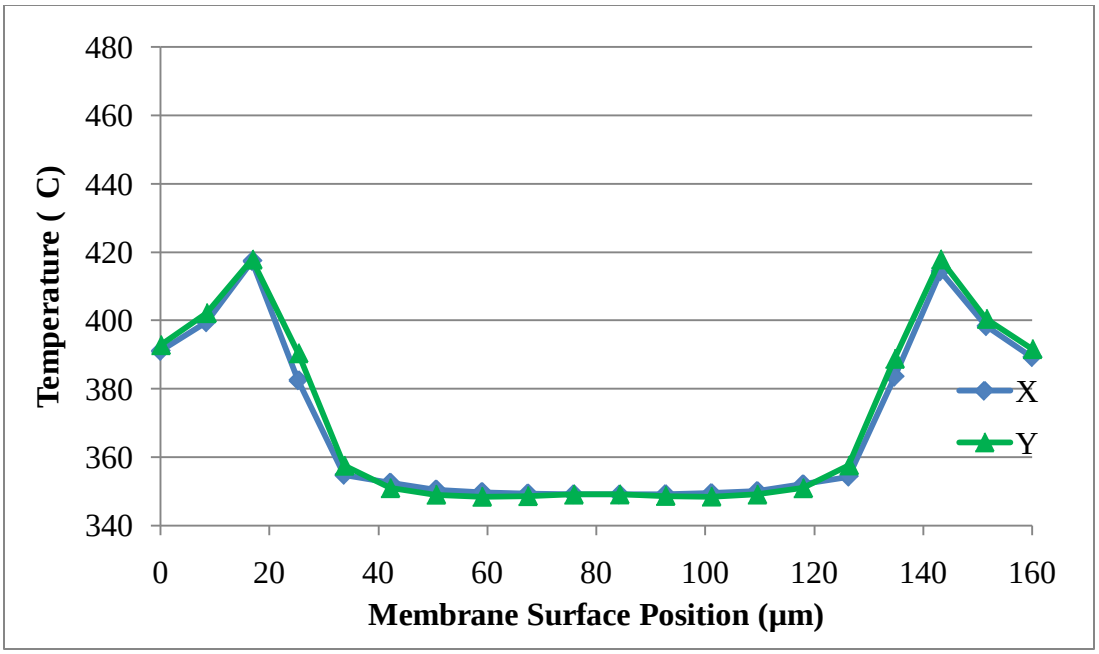

FIGURE 4.7 – Temperature Profile across Coplanar Microhotplate with SiC Microheaters Using 60 mW of Power

The sensor area of the coplanar microhotplate, which is between the 30 and 130 µm marks of the membrane surface position plot in Figure 4.7, reaches an average temperature of 350°C under these conditions in the simulation. Though the temperature may not be proven accurate without a fabricated and tested device, the temperature distribution in Figure 4.6 indicates an even temperature profile, with a temperature variation of less than 10°C across the sensor area, although hot spots are observed directly over the microheaters.

The same boundary conditions are applied to the stacked-configuration microhotplate. Compare Figure 4.8 to Figure 4.6; data is extracted from the "X" and "Y" lines as previously, and temperature readings are plotted in Figure 4.9.

As seen in Figure 4.9, the stacked-configuration microhotplate, having a smaller area to heat, reaches a significantly higher average temperature of 450°C in the

simulation. As with the coplanar-configured microhotplate, the temperature variation across the sensor area, between 10 µm and 110 µm, is less than 10°C.

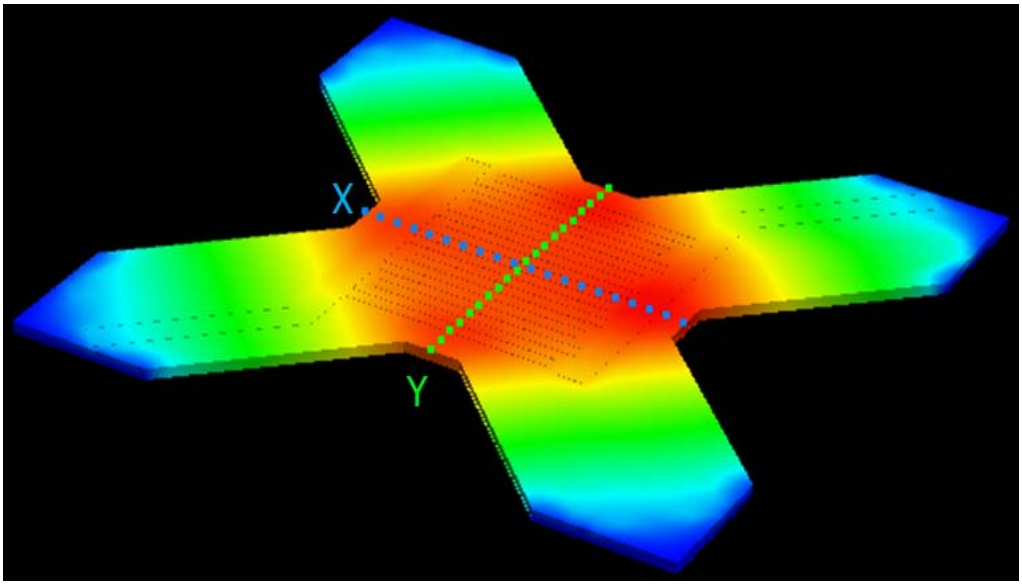

FIGURE 4.8 – Temperature Plot of a Simulated Stacked Microhotplate with SiC Microheaters Using 60 mW of Power

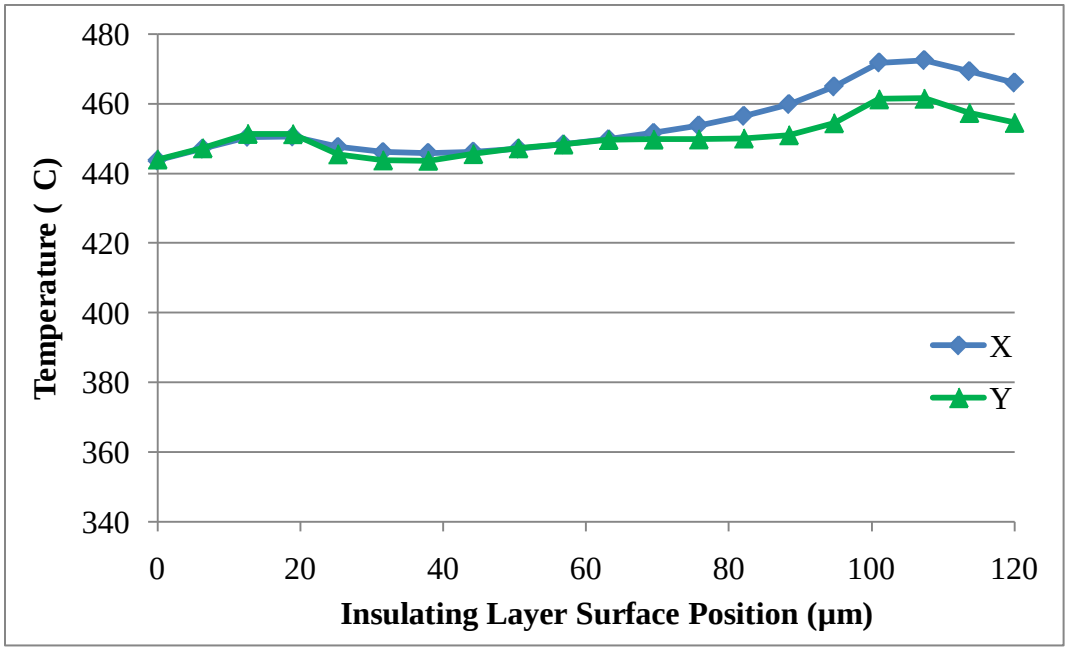

FIGURE 4.9 – Temperature Profile across Stacked Microhotplate with SiC Microheaters Using 60 mW of Power

Though the absolute temperature cannot be confirmed without experimentation and consideration of the effects of convective heat loss, these simulations provide evidence that the reduced membrane size of the stacked microhotplate configuration significantly increases the microhotplate temperature attainable for a given power consumption. In addition, the symmetric microheater structure surrounding the sensor area of the microhotplate helps to achieve a uniform temperature distribution.

Summary of SiC Simulation Results

The higher resistivity of doped silicon carbide than that of platinum reduces the size requirement of the microhotplate microheaters. Coplanar and stacked configurations of microhotplates were compared, using a constant sensor area of 100 µm by 100 µm and four rectangular bar microheaters. At a power consumption of 60 mW, the coplanar microhotplate sensor area was shown to reach an average of 350°C, while the stacked microhotplate sensor area reached an average of 450°C. It was concluded that the stacked microhotplate configuration of these microhotplate simulations allows the thermally isolated area to be reduced, which increases the temperature attainable for a given power consumption.

V. CONCLUSIONS

Fabricated 150 nm thick platinum microheaters on unreleased silicon dioxide membranes with sensor areas of 10,000 μm^2 and 40,000 μm^2 each required a power consumption of over 1 W to reach a temperature above 100°C. Power usages of 3.9 W and 5.6 W resulted in an average microheater temperatures of 340°C and 360°C across the 100 µm and 200 µm microheaters respectively. Coarsely meshed simulations using the same resistances reached average microheater temperatures of 130°C and 210°C, or 40% and 60% of those experimentally observed. Fine meshing improved the averages to within 20%. Heating of the unreleased microhotplate membranes was minimal.

A test on a thermally isolated microhotplate membrane showed temperatures of over 300°C at 35.5 mW of power. Initial simulation temperatures reached 1400°C; when a convection coefficient of 550 $W/m^2/K$ was applied, an 18% average error compared to fabricated results was found. Fine meshing improved the temperature distribution, but increased temperature, possibly due to additional heat losses not previously considered.

Simulations of 10,000 μm^2 sensor area thermally isolated microhotplates using 10^{18} $atoms/cm^3$ nitrogen doped silicon carbide microheaters reached average temperatures of 350°C and 450°C with less than 10°C variation for coplanar and stacked configurations when 60 mW of power is distributed across four symmetric bar microheaters.

VI. RECOMMENDATIONS

To further this study, experimentally fabricated devices using silicon carbide microheaters would be invaluable to compare to the simulations in Chapter IV, in an attempt to prove the theoretical conclusions resulting from the simulations. Additional iterations of both simulated and fabricated devices would improve the power consumption of these devices, especially when considering geometries not shown in this work. Smaller isolated membranes may reduce power consumption, though the influence of the size of the microhotplate on the gas sensor sensitivity must be considered.

Mechanical effects were not considered in microhotplate design. Films of silicon dioxide formed using thermal oxidation have internal stress; silicon dioxide deposited by chemical vapor deposition may improve the stability of the microhotplate membranes. Also, fabricated devices using other insulating or membrane materials than silicon dioxide should prove to have relevant results. A layer of high thermal conductivity material can be used as a temperature distributor for the gas sensor.

As in reference [30], testing of the fabricated devices need not be restricted to one method. Usage of different methods of temperature analysis, including melt crayon particles, thermocouples, and on-chip temperature sensors, may provide a more accurate temperature average than solely relying on infrared microscopy.

APPENDIX

TEMPERATURE DATA

TABLE A.1

OBSERVED TEMPERATURE DATA FROM FABRICATED 308-Ω MICROHEATER ON 100 μm UNRELEASED MICROHOTPLATE

Position		Temperature (°C) observed at:										
Pixel#	Pos. (μm)	5038 mW	3880 mW	2997 mW	2320 mW	1708 mW	1218 mW	820 mW	512 mW	281 mW	123 mW	30.4 mW
0	0	424.94	313.74	232.25	186.20	147.19	113.09	85.88	72.78	65.12	61.89	61.97
1	2	465.69	329.23	233.82	188.76	148.08	113.09	87.09	73.15	64.46	61.50	61.11
2	5	465.69	329.23	232.25	186.20	148.08	113.09	88.29	73.88	64.73	61.50	60.71
3	7	436.58	329.23	235.39	182.36	144.52	114.31	89.09	74.61	66.30	62.37	60.05
4	10	465.69	302.12	233.82	186.20	143.63	115.54	89.09	75.16	68.01	62.86	59.72
5	12	471.51	309.86	230.68	186.20	144.52	114.31	89.89	74.61	67.35	62.66	60.45
6	14	448.23	317.61	229.12	182.36	143.63	113.70	90.30	74.06	66.43	62.28	61.24
7	17	448.23	333.10	229.12	182.36	143.63	112.47	90.30	74.43	65.78	61.69	61.64
8	19	442.40	364.09	236.95	186.20	145.41	113.70	89.89	74.61	65.91	62.28	61.51
9	21	442.40	364.09	241.66	188.76	148.97	115.54	89.09	74.43	66.57	62.37	60.78
10	24	459.87	383.45	243.23	192.61	153.42	116.15	89.09	74.61	65.78	61.98	60.71
11	26	483.15	395.07	241.66	193.89	155.20	116.76	89.49	74.80	64.86	61.59	60.91
12	29	500.62	344.72	236.95	192.61	150.75	114.92	90.70	75.16	65.25	61.59	60.91
13	31	471.51	340.85	235.39	188.76	144.52	114.92	91.10	75.53	67.09	62.86	60.18
14	33	494.79	329.23	233.82	186.20	144.52	113.70	89.89	75.34	67.88	63.05	59.85
15	36	494.79	336.97	230.68	182.36	142.74	111.86	88.69	74.25	67.09	62.66	60.58
16	38	459.87	329.23	235.39	184.92	145.41	113.70	89.49	73.70	66.17	62.18	61.24
17	40	483.15	356.34	240.09	187.48	148.97	115.54	91.10	74.25	65.78	61.98	62.24
18	43	430.76	336.97	246.36	191.32	150.75	117.99	91.90	75.71	66.57	62.47	62.04
19	45	459.87	344.72	249.50	195.17	153.42	119.21	91.50	75.71	66.83	62.96	61.24
20	48	745.10	398.95	247.93	197.73	156.09	118.60	91.10	75.53	66.04	62.18	60.98
21	50	745.10	379.58	246.36	195.17	154.31	117.37	90.70	75.16	65.38	61.89	61.18
22	52	436.58	383.45	238.52	192.61	151.64	116.76	91.50	75.53	65.38	61.79	60.71
23	55	419.12	344.72	235.39	186.20	146.30	115.54	91.50	75.89	67.09	62.47	59.72
24	57	448.23	313.74	229.12	182.36	141.85	112.47	89.89	74.80	67.49	63.05	59.98
25	59	459.87	313.74	221.28	175.96	138.29	108.80	87.89	73.52	66.57	62.37	60.58
26	62	454.05	336.97	222.85	175.96	140.07	108.80	87.49	72.42	65.38	62.08	61.18
27	64	465.69	352.47	227.55	178.52	142.74	110.64	88.29	72.97	64.86	61.69	62.10
28	67	483.15	406.69	236.95	184.92	145.41	113.70	90.30	73.33	66.04	62.28	61.84
29	69	494.79	437.68	244.79	191.32	150.75	117.37	91.10	74.25	66.17	62.66	60.71
30	71	494.79	329.23	244.79	195.17	154.31	117.37	91.10	75.16	66.17	62.18	60.25
31	74	477.33	344.72	240.09	193.89	153.42	116.15	91.10	75.16	65.25	61.89	60.84
32	76	483.15	348.59	232.25	187.48	147.19	113.70	91.10	75.53	66.04	61.59	60.45
33	78	459.87	329.23	225.98	179.80	140.96	113.09	89.89	75.89	67.22	62.76	59.98
34	81	430.76	302.12	222.85	177.24	139.18	113.70	89.09	74.98	68.40	63.35	59.72
35	83	442.40	317.61	216.57	173.40	136.51	111.86	89.09	74.61	67.09	62.66	61.11
36	86	424.94	298.24	215.01	169.56	135.62	109.41	89.49	73.88	65.65	62.18	61.97
37	88	424.94	302.12	216.57	172.12	136.51	109.41	89.49	74.06	65.25	61.89	62.37
38	90	436.58	317.61	224.41	175.96	140.07	110.02	89.09	74.43	65.52	61.89	61.71
39	93	454.05	336.97	236.95	183.64	146.30	113.70	89.89	74.80	66.30	62.37	60.51
40	95	523.90	278.88	233.82	186.20	148.08	114.92	90.70	75.16	66.30	62.37	60.05
Avg		474.49	340.56	233.86	185.52	146.17	114.07	89.80	74.58	66.18	62.25	60.90

TABLE A.2

OBSERVED TEMPERATURE DATA FROM FABRICATED 411-Ω MICROHEATER ON 200 μm UNRELEASED MICROHOTPLATE

Position		Temperature (°C) observed at:									
Pixel#	Pos. (μm)	5610 mW	4203 mW	3200 mW	2359 mW	1674 mW	1120 mW	692 mW	378 mW	165 mW	40.8 mW
0	0	272.47	196.34	146.81	129.07	98.23	82.73	72.62	65.17	61.62	60.07
1	2	309.62	209.24	159.53	136.24	102.93	85.51	74.43	65.73	61.98	59.37
2	4	322.01	223.76	172.26	142.39	108.29	88.69	75.64	66.56	62.69	58.81
3	6	346.78	233.43	179.33	147.51	111.64	90.28	75.04	66.84	63.05	59.79
4	8	346.78	244.72	182.16	149.56	114.99	91.47	74.83	66.84	62.57	60.35
5	10	359.16	252.79	189.23	152.64	118.34	92.66	75.24	67.11	62.57	60.21
6	12	388.06	252.79	194.89	151.61	119.01	92.27	75.64	67.39	62.45	60.21
7	14	375.68	249.56	194.89	149.56	117.00	91.47	76.04	67.81	62.69	60.50
8	16	342.65	241.50	186.40	148.54	113.65	90.68	75.24	66.84	62.57	60.78
9	18	330.26	236.66	179.33	147.51	111.64	89.88	75.64	66.42	62.45	60.92
10	20	334.39	236.66	183.57	147.51	111.64	89.49	75.64	66.42	62.33	60.35
11	22	326.14	236.66	183.57	148.54	111.64	89.88	76.65	66.84	62.93	59.51
12	24	371.55	238.27	187.82	147.51	113.65	91.07	76.65	66.97	63.17	59.23
13	26	367.42	239.89	184.99	148.54	114.32	91.87	75.64	67.11	63.41	60.07
14	28	371.55	246.34	186.40	154.69	117.67	92.66	75.24	66.84	63.17	61.20
15	30	392.19	254.40	193.47	157.76	120.35	93.46	75.04	67.11	62.81	61.20
16	32	363.29	256.01	199.13	154.69	120.35	92.66	75.64	67.53	62.81	60.50
17	34	363.29	251.18	199.13	152.64	118.34	91.87	75.64	67.39	62.93	60.50
18	36	342.65	243.11	189.23	150.59	115.66	91.47	75.64	66.97	62.33	61.06
19	38	342.65	239.89	186.40	150.59	114.32	90.68	75.84	66.70	62.10	61.06
20	40	330.26	241.50	186.40	148.54	113.65	91.07	76.24	65.87	62.22	60.07
21	42	342.65	241.50	189.23	149.56	114.32	91.47	77.05	66.28	62.69	59.37
22	44	396.32	244.72	193.47	150.59	115.66	92.66	76.24	67.11	63.05	58.95
23	45	388.06	243.11	192.06	151.61	116.33	92.27	75.64	67.11	63.29	60.07
24	47	379.80	247.95	187.82	153.66	119.01	93.06	75.24	67.11	62.69	60.92
25	49	371.55	254.40	192.06	155.71	121.02	93.06	75.04	67.11	62.45	61.20
26	51	375.68	256.01	199.13	155.71	121.70	93.46	75.64	67.39	62.45	60.92
27	53	367.42	254.40	200.54	154.69	120.35	93.46	76.45	67.81	62.33	60.64
28	55	392.19	247.95	190.64	151.61	117.67	92.66	76.24	66.97	62.69	60.92
29	57	371.55	246.34	186.40	152.64	117.00	92.66	76.65	66.56	62.33	60.78
30	59	367.42	247.95	190.64	150.59	117.00	92.66	77.05	66.70	62.57	60.21
31	61	350.91	246.34	193.47	149.56	117.00	93.06	77.66	66.84	62.81	59.23
32	63	359.16	246.34	197.71	148.54	117.00	91.87	76.45	67.25	63.05	59.37
33	65	367.42	244.72	192.06	147.51	115.66	91.47	74.83	66.97	62.93	60.21
34	67	367.42	244.72	187.82	150.59	117.00	91.07	74.23	66.56	62.81	61.34
35	69	388.06	249.56	192.06	151.61	118.34	91.07	74.03	66.97	62.45	61.48
36	71	375.68	251.18	197.71	150.59	119.01	91.47	74.83	67.11	61.74	60.50
37	73	383.93	249.56	201.96	150.59	119.01	92.27	76.04	67.67	61.62	60.07
38	75	367.42	244.72	194.89	150.59	117.00	92.27	76.24	67.25	61.98	60.64
39	77	363.29	246.34	193.47	153.66	117.67	93.06	76.85	67.11	61.98	60.92
40	79	359.16	247.95	196.30	154.69	118.34	93.06	77.25	66.97	62.93	59.93
41	81	359.16	249.56	197.71	153.66	118.34	93.06	77.45	67.39	63.17	59.37

42	83	371.55	247.95	199.13	150.59	117.67	92.27	76.24	67.53	63.29	59.93
43	85	359.16	243.11	189.23	147.51	115.66	91.07	74.23	67.11	62.81	60.64
44	87	429.34	243.11	186.40	147.51	115.66	90.28	73.62	66.42	62.22	61.20
45	89	396.32	246.34	189.23	147.51	117.67	89.88	73.22	66.00	61.98	61.20
46	91	437.60	256.01	197.71	155.71	120.35	94.25	76.85	67.39	62.81	60.50
47	93	408.70	251.18	197.71	150.59	117.67	92.66	76.04	67.25	63.05	60.21
48	95	367.42	241.50	186.40	149.56	112.98	90.28	75.04	66.14	62.33	61.06
49	97	346.78	231.82	176.50	147.51	109.63	88.29	74.23	65.59	62.10	60.92
50	99	326.14	230.21	176.50	144.44	107.62	87.10	74.43	65.45	62.10	60.35
51	101	326.14	226.98	173.67	143.41	107.62	87.90	75.24	66.00	62.10	59.51
52	103	342.65	231.82	180.75	143.41	109.63	89.49	76.04	66.70	62.81	59.23
53	105	350.91	236.66	183.57	148.54	112.31	91.07	75.44	66.97	62.33	59.65
54	107	375.68	244.72	184.99	153.66	117.00	93.06	75.84	67.39	62.93	60.64
55	109	388.06	257.63	193.47	156.74	121.02	94.25	76.04	67.53	62.69	60.92
56	111	416.96	260.85	200.54	157.76	121.70	94.25	76.45	67.25	62.93	60.35
57	113	404.57	256.01	200.54	153.66	119.68	93.06	76.45	67.39	62.93	60.50
58	115	350.91	244.72	190.64	149.56	114.99	91.07	75.64	66.97	62.57	60.92
59	117	326.14	238.27	182.16	147.51	112.31	89.88	75.24	66.70	62.45	61.06
60	119	346.78	235.05	180.75	147.51	111.64	89.49	75.64	66.28	62.33	60.07
61	121	342.65	236.66	182.16	148.54	111.64	89.88	76.24	66.56	62.33	59.37
62	123	355.03	239.89	187.82	148.54	113.65	91.47	76.65	67.25	63.05	59.23
63	125	379.80	241.50	189.23	148.54	114.99	91.87	75.64	67.25	62.93	60.35
64	127	392.19	247.95	187.82	154.69	118.34	93.06	75.84	67.25	62.81	60.78
65	129	383.93	257.63	194.89	157.76	121.70	93.86	75.64	67.39	62.45	60.92
66	131	375.68	260.85	200.54	151.61	122.37	93.86	76.24	67.39	62.45	60.50
67	133	371.55	256.01	200.54	148.54	119.68	93.06	76.04	67.53	62.57	60.64
68	135	379.80	249.56	194.89	151.61	116.33	91.47	75.84	66.84	62.69	60.92
69	136	359.16	241.50	184.99	149.56	114.32	91.07	75.84	66.70	62.22	60.78
70	138	363.29	243.11	186.40	149.56	114.32	91.07	76.45	66.14	62.33	59.93
71	140	342.65	241.50	187.82	149.56	114.32	91.47	77.25	66.42	62.69	59.51
72	142	346.78	246.34	193.47	150.59	115.66	92.27	76.65	67.53	63.05	59.23
73	144	334.39	247.95	192.06	152.64	116.33	92.66	75.84	67.25	63.05	59.93
74	146	375.68	256.01	187.82	153.66	119.01	93.46	75.24	67.25	62.10	61.20
75	148	404.57	259.24	193.47	154.69	120.35	93.06	75.04	66.70	62.57	61.06
76	150	408.70	249.56	199.13	153.66	121.02	92.66	75.64	67.11	62.69	60.64
77	152	412.83	246.34	201.96	153.66	119.68	92.66	76.04	67.67	62.69	60.64
78	154	383.93	246.34	194.89	155.71	117.00	92.27	76.04	67.11	62.45	60.21
79	156	371.55	239.89	187.82	156.74	115.66	91.47	76.24	66.97	62.33	60.64
80	158	375.68	247.95	189.23	148.54	114.99	91.07	76.65	66.56	62.45	60.21
81	160	367.42	247.95	192.06	148.54	114.99	91.87	76.65	67.11	62.69	59.65
82	162	363.29	247.95	194.89	151.61	116.33	92.27	76.85	67.53	62.93	58.95
83	164	363.29	244.72	192.06	150.59	117.00	92.66	75.84	67.25	63.05	59.93
84	166	355.03	247.95	187.82	153.66	119.68	93.46	75.44	66.84	62.81	60.64
85	168	371.55	252.79	192.06	154.69	121.70	93.06	75.04	66.70	62.57	60.78
86	170	379.80	252.79	200.54	154.69	119.68	91.87	74.83	66.97	62.45	61.20
87	172	375.68	247.95	200.54	151.61	117.00	90.68	75.04	67.25	62.33	60.64
88	174	379.80	239.89	189.23	146.49	114.99	90.28	75.44	66.84	62.45	60.92
89	176	350.91	239.89	187.82	149.56	116.33	92.66	75.44	66.70	62.45	60.92
90	178	350.91	246.34	193.47	153.66	118.34	93.86	77.45	67.25	62.45	60.50
91	180	363.29	251.18	200.54	153.66	120.35	94.25	77.86	67.53	62.93	59.65
Avg		365.71	244.88	189.89	150.59	116.11	91.67	75.76	66.93	62.60	60.35

TABLE A.3

OBSERVED TEMPERATURE DATA FROM FABRICATED 100 μm THERMALLY ISOLATED MICROHOTPLATE

Position		Temperature (°C) observed at:									
Pixel#	Pos. (μm)	35.5 mW	27.0 mW	20.0 mW	14.8 mW	10.4 mW	6.90 mW	4.32 mW	2.38 mW	1.05 mW	0.261 mW
0	0	387.34	301.65	208.51	156.37	114.65	84.93	70.75	64.33	61.50	60.18
1	3	459.34	362.81	248.59	187.84	139.00	102.47	80.46	68.31	62.92	60.58
2	6	518.63	405.97	266.01	196.66	144.88	106.16	82.40	69.20	63.18	60.79
3	10	518.63	402.38	257.30	192.88	143.20	105.70	81.67	69.49	63.43	60.58
4	13	400.04	298.05	218.96	161.40	120.53	91.86	73.90	65.51	61.89	60.28
5	16	349.22	272.87	192.82	142.52	106.25	82.16	69.29	63.45	61.05	60.18
6	19	328.04	258.48	180.63	133.71	100.37	78.93	67.83	63.00	60.92	60.18
7	22	319.57	251.29	175.40	129.93	97.01	76.63	66.62	62.56	60.79	59.97
8	26	323.81	251.29	171.91	127.41	96.17	76.16	66.62	62.56	60.79	60.28
9	29	315.34	244.10	171.91	127.41	95.33	75.70	66.38	62.56	60.92	60.07
10	32	336.51	262.08	185.85	138.74	104.57	81.24	69.53	64.18	61.50	60.28
11	35	357.69	280.07	198.05	150.07	114.65	89.09	74.39	66.25	62.40	60.48
12	38	383.10	298.05	199.80	150.07	113.81	89.09	74.39	66.54	62.27	60.68
13	42	387.34	301.65	201.54	152.59	115.49	90.01	74.63	66.84	62.53	60.68
14	45	370.40	308.85	203.28	153.85	118.85	92.32	76.33	67.43	62.92	60.38
15	48	400.04	312.44	199.80	152.59	117.17	91.86	76.09	67.58	62.66	60.68
16	51	395.81	312.44	199.80	152.59	117.17	91.86	76.33	67.43	62.79	60.48
17	54	353.45	283.67	192.82	147.56	113.81	90.01	75.12	67.13	62.98	60.28
18	57	340.75	269.28	178.88	134.96	103.73	83.55	71.23	65.07	62.34	60.18
19	61	315.34	247.69	164.94	123.63	95.33	77.09	67.59	63.45	61.50	60.18
20	64	298.40	236.90	159.71	119.86	91.97	75.24	66.86	62.86	61.11	60.18
21	67	294.16	233.30	157.97	118.60	91.97	75.24	67.11	63.00	61.24	60.07
22	70	289.93	222.51	161.46	122.37	96.17	78.47	69.05	63.89	61.37	60.18
23	73	298.40	240.50	163.20	126.15	99.53	81.24	70.75	65.07	61.63	60.48
24	77	306.87	236.90	164.94	126.15	99.53	81.70	71.23	65.22	61.89	60.79
25	80	319.57	262.08	161.46	123.63	98.69	80.78	70.99	65.22	61.95	60.38
26	83	315.34	247.69	157.97	122.37	97.01	80.32	70.50	65.07	62.14	60.38
27	86	289.93	229.71	152.74	118.60	94.49	78.47	69.53	64.63	62.21	60.07
28	89	268.75	208.12	144.03	111.04	87.77	74.32	66.86	63.15	61.57	60.07
29	93	243.34	193.73	138.80	104.75	83.57	71.09	65.16	62.27	60.99	60.07
30	96	260.28	208.12	133.58	102.23	81.89	70.16	64.44	61.97	60.86	60.07
31	99	234.87	186.54	131.83	100.97	81.89	70.63	64.92	62.27	60.73	60.18
32	102	251.81	200.93	135.32	104.75	85.25	72.93	66.13	62.86	60.99	60.38
33	105	247.57	197.33	137.06	107.27	87.77	74.78	67.59	63.74	61.18	60.48
34	109	256.04	204.53	135.32	106.01	87.77	74.78	68.08	63.74	61.50	60.48
35	112	256.04	204.53	131.83	103.49	86.93	74.78	67.83	63.74	61.89	60.28
36	115	251.81	186.54	128.35	102.23	85.25	73.39	67.35	63.89	61.69	60.07
37	118	230.63	182.94	121.38	97.19	81.89	72.01	66.62	63.30	61.69	60.18
38	121	205.22	164.96	110.92	88.38	76.01	68.32	64.19	62.12	61.18	59.97
39	125	179.81	139.77	102.21	82.08	71.81	66.01	62.74	61.38	60.53	59.87

40	128	179.81	139.77	96.98	79.57	70.13	65.09	62.49	61.24	60.47	60.07
41	131	171.34	136.18	98.72	82.08	71.81	66.01	63.22	61.53	60.47	60.07
42	134	179.81	143.37	103.95	87.12	75.17	68.32	64.19	62.12	60.60	60.18
43	137	200.98	157.76	110.92	90.90	77.69	70.16	65.16	62.71	60.86	60.58
44	141	200.98	157.76	110.92	90.90	78.53	70.63	65.65	62.86	61.18	60.38
45	144	209.45	168.55	110.92	90.90	77.69	70.16	65.65	63.00	61.37	60.18
46	147	200.98	161.36	107.44	88.38	76.85	69.70	65.41	62.71	61.31	60.07
47	150	175.57	143.37	102.21	85.86	75.17	68.32	64.68	62.42	61.44	59.87
48	153	175.57	139.77	96.98	80.83	70.97	66.01	63.22	61.68	61.11	59.87
49	156	162.87	125.39	91.75	77.05	68.45	64.16	62.49	61.24	60.53	59.97
50	160	154.40	121.79	90.01	75.79	68.45	64.16	62.25	61.09	60.53	60.07
51	163	154.40	125.39	90.01	75.79	68.45	64.16	62.25	61.09	60.47	60.07
52	166	145.93	118.19	88.27	75.79	68.45	64.16	62.25	61.09	60.41	59.97
53	169	150.16	118.19	88.27	74.53	67.61	63.70	62.01	60.94	60.41	59.97
54	172	158.63	125.39	88.27	74.53	67.61	63.70	61.77	60.94	60.53	59.97
55	176	154.40	128.98	90.01	75.79	67.61	63.70	62.49	60.94	60.92	59.97
56	179	154.40	125.39	93.50	77.05	69.29	65.09	63.22	61.24	61.11	59.97
57	182	167.10	136.18	93.50	78.31	70.97	66.01	63.95	61.68	60.99	60.07
58	185	162.87	132.58	91.75	78.31	70.97	66.01	63.46	61.68	60.79	60.07
59	188	162.87	125.39	90.01	78.31	70.13	65.09	62.98	61.68	60.92	59.97
60	192	145.93	121.79	88.27	74.53	67.61	63.70	62.25	61.24	60.53	59.87
61	195	145.93	114.59	84.78	72.01	65.93	62.78	61.52	60.65	60.34	59.97
62	198	150.16	118.19	84.78	70.75	65.93	62.78	61.28	60.65	60.21	59.97

TABLE A.4

TEMPERATURE DATA FROM 100 µm UNRELEASED MICROHOTPLATE SIMULATION

	Temperature (°C) observed at:										
Pos. (µm)	5038 mW	3880 mW	2997 mW	2320 mW	1708 mW	1218 mW	820 mW	512 mW	281 mW	123 mW	30.4 mW
0	130.42	114.23	101.84	92.33	83.77	76.90	71.34	67.02	63.79	61.57	60.28
2	143.48	124.29	109.61	98.34	88.19	80.06	73.47	68.35	64.52	61.89	60.35
4	150.83	129.95	113.99	101.72	90.68	81.84	74.66	69.10	64.93	62.07	60.40
6	157.42	135.03	117.91	104.76	92.92	83.43	75.74	69.77	65.30	62.23	60.44
8	164.38	140.40	122.05	107.96	95.28	85.11	76.87	70.47	65.69	62.40	60.48
10	169.85	144.61	125.31	110.48	97.13	86.43	77.76	71.03	65.99	62.53	60.51
12	173.10	147.11	127.24	111.97	98.23	87.22	78.29	71.36	66.17	62.61	60.53
14	178.95	151.62	130.72	114.66	100.21	88.63	79.24	71.95	66.50	62.75	60.57
16	182.66	154.48	132.93	116.37	101.47	89.53	79.85	72.33	66.71	62.84	60.59
18	180.26	152.63	131.50	115.27	100.66	88.95	79.46	72.09	66.57	62.78	60.58
20	170.55	145.15	125.72	110.80	97.37	86.60	77.88	71.10	66.03	62.55	60.52
22	166.40	141.95	123.25	108.89	95.96	85.60	77.20	70.68	65.80	62.44	60.49
24	174.22	147.98	127.91	112.49	98.61	87.49	78.47	71.47	66.24	62.64	60.54
26	179.40	151.96	130.99	114.87	100.37	88.74	79.32	72.00	66.53	62.76	60.57
28	177.82	150.74	130.04	114.14	99.83	88.36	79.06	71.84	66.44	62.72	60.56
30	170.75	145.30	125.84	110.89	97.44	86.65	77.91	71.12	66.04	62.55	60.52
32	168.86	143.84	124.71	110.02	96.79	86.19	77.60	70.93	65.94	62.50	60.51

34	171.30	145.72	126.17	111.14	97.62	86.78	78.00	71.18	66.07	62.56	60.52
36	171.60	145.95	126.34	111.28	97.72	86.85	78.05	71.21	66.09	62.57	60.52
38	169.65	144.45	125.18	110.39	97.06	86.38	77.73	71.01	65.98	62.52	60.51
40	167.04	142.44	123.63	109.19	96.18	85.75	77.30	70.74	65.84	62.46	60.50
42	166.99	142.41	123.60	109.16	96.16	85.74	77.30	70.74	65.83	62.46	60.50
44	166.88	142.32	123.54	109.11	96.12	85.71	77.28	70.73	65.83	62.46	60.50
46	163.03	139.35	121.25	107.34	94.82	84.78	76.65	70.34	65.61	62.36	60.47
49	157.83	135.34	118.15	104.94	93.06	83.53	75.80	69.81	65.32	62.24	60.44
51	152.56	131.28	115.02	102.52	91.27	82.25	74.95	69.27	65.03	62.11	60.41
53	147.28	127.21	111.87	100.09	89.48	80.98	74.09	68.74	64.73	61.98	60.38
55	142.43	123.48	108.99	97.86	87.84	79.81	73.30	68.24	64.46	61.86	60.35
57	140.76	122.20	108.00	97.09	87.27	79.40	73.03	68.07	64.37	61.82	60.34
59	139.88	121.52	107.47	96.69	86.97	79.19	72.88	67.98	64.32	61.80	60.33
61	139.10	120.92	107.01	96.33	86.71	79.00	72.76	67.90	64.28	61.78	60.33
63	138.58	120.51	106.70	96.09	86.53	78.87	72.67	67.85	64.25	61.77	60.32
65	138.34	120.33	106.55	95.97	86.45	78.82	72.63	67.83	64.23	61.76	60.32
67	139.98	121.59	107.53	96.73	87.01	79.21	72.90	67.99	64.32	61.80	60.33
69	140.71	122.16	107.97	97.07	87.26	79.39	73.02	68.07	64.37	61.82	60.34
71	140.43	121.94	107.80	96.94	87.16	79.32	72.97	68.04	64.35	61.81	60.34
73	140.31	121.85	107.73	96.88	87.12	79.29	72.95	68.03	64.34	61.81	60.34
75	143.12	124.01	109.40	98.18	88.07	79.97	73.41	68.31	64.50	61.88	60.35
77	141.11	122.46	108.20	97.25	87.39	79.49	73.08	68.11	64.39	61.83	60.34
79	141.82	123.01	108.63	97.58	87.63	79.66	73.20	68.18	64.43	61.85	60.34
81	143.25	124.11	109.48	98.24	88.12	80.00	73.43	68.33	64.51	61.88	60.35
83	143.54	124.33	109.65	98.37	88.21	80.07	73.48	68.36	64.52	61.89	60.35
85	145.21	125.62	110.64	99.14	88.78	80.48	73.75	68.53	64.62	61.93	60.36
87	149.34	128.80	113.10	101.04	90.18	81.47	74.42	68.94	64.85	62.03	60.39
89	153.46	131.98	115.55	102.93	91.57	82.47	75.09	69.36	65.08	62.13	60.41
91	154.36	132.67	116.08	103.35	91.88	82.69	75.24	69.45	65.13	62.15	60.42
93	151.52	130.48	114.40	102.04	90.92	82.00	74.78	69.17	64.97	62.08	60.40
95	147.94	127.72	112.27	100.39	89.70	81.14	74.19	68.80	64.77	62.00	60.38
Avg	156.01	133.95	117.07	104.11	92.44	83.09	75.51	69.62	65.22	62.19	60.43

TABLE A.5

TEMPERATURE DATA FROM 200 μm UNRELEASED MICROHOTPLATE SIMULATION

	Temperature (°C) observed at:									
Pos. (μm)	5610 mW	4203 mW	3200 mW	2359 mW	1674 mW	1120 mW	692 mW	378 mW	165 mW	40.8 mW
0	182.80	151.78	130.00	111.49	96.48	84.38	75.01	68.13	63.47	60.74
2	203.39	167.18	141.74	120.14	102.62	88.49	77.54	69.52	64.08	60.89
4	213.14	174.46	147.30	124.23	105.52	90.43	78.74	70.17	64.36	60.96
6	219.43	179.16	150.89	126.87	107.39	91.68	79.52	70.60	64.55	61.01
8	223.53	182.23	153.23	128.59	108.61	92.50	80.02	70.87	64.67	61.04
10	217.36	177.62	149.71	126.01	106.78	91.27	79.27	70.46	64.49	61.00
12	212.40	173.91	146.88	123.92	105.30	90.28	78.65	70.12	64.34	60.96
14	205.94	169.08	143.20	121.21	103.38	88.99	77.86	69.69	64.15	60.91

16	203.28	167.09	141.68	120.09	102.58	88.46	77.53	69.51	64.07	60.89
18	203.01	166.89	141.53	119.98	102.50	88.41	77.50	69.49	64.06	60.89
20	180.73	150.23	128.82	110.62	95.86	83.96	74.75	67.99	63.41	60.73
22	179.91	149.62	128.35	110.28	95.62	83.80	74.65	67.93	63.38	60.72
24	181.88	151.09	129.47	111.10	96.21	84.19	74.89	68.07	63.44	60.74
26	187.03	154.95	132.41	113.27	97.74	85.22	75.53	68.41	63.59	60.77
28	197.07	162.45	138.13	117.48	100.73	87.22	76.76	69.09	63.89	60.85
30	200.29	164.86	139.97	118.83	101.69	87.87	77.16	69.31	63.98	60.87
32	206.70	169.65	143.63	121.53	103.60	89.15	77.95	69.74	64.17	60.92
34	211.82	173.47	146.55	123.68	105.13	90.17	78.58	70.08	64.32	60.96
36	219.25	179.03	150.79	126.80	107.34	91.65	79.50	70.58	64.54	61.01
38	233.89	189.98	159.14	132.95	111.70	94.57	81.30	71.57	64.97	61.12
40	228.62	186.04	156.13	130.73	110.13	93.52	80.65	71.21	64.82	61.08
42	222.10	181.16	152.42	127.99	108.19	92.22	79.85	70.78	64.63	61.03
44	214.42	175.42	148.04	124.77	105.90	90.69	78.90	70.26	64.40	60.97
45	206.97	169.85	143.79	121.64	103.68	89.20	77.98	69.76	64.18	60.92
47	202.59	166.58	141.29	119.80	102.38	88.33	77.44	69.46	64.05	60.89
49	197.69	162.91	138.49	117.74	100.92	87.35	76.84	69.13	63.91	60.85
51	199.18	164.02	139.34	118.37	101.36	87.64	77.02	69.23	63.95	60.86
53	202.93	166.83	141.48	119.94	102.48	88.39	77.49	69.48	64.06	60.89
55	206.91	169.80	143.75	121.61	103.66	89.19	77.98	69.75	64.18	60.92
57	212.80	174.21	147.11	124.09	105.42	90.36	78.70	70.15	64.35	60.96
59	205.32	168.61	142.84	120.95	103.19	88.87	77.78	69.65	64.13	60.91
61	202.62	166.59	141.30	119.81	102.38	88.33	77.45	69.46	64.05	60.89
63	201.29	165.60	140.54	119.25	101.99	88.06	77.28	69.37	64.01	60.88
65	199.46	164.23	139.50	118.49	101.44	87.70	77.06	69.25	63.96	60.87
67	209.68	171.87	145.33	122.78	104.49	89.74	78.32	69.94	64.26	60.94
69	207.17	170.00	143.90	121.72	103.74	89.24	78.01	69.77	64.19	60.92
71	203.84	167.51	142.00	120.32	102.75	88.57	77.60	69.55	64.09	60.90
73	200.81	165.25	140.27	119.05	101.85	87.97	77.22	69.34	64.00	60.88
75	198.05	163.18	138.70	117.90	101.03	87.42	76.88	69.16	63.92	60.86
77	205.63	168.84	143.02	121.08	103.28	88.93	77.82	69.67	64.14	60.91
79	206.80	169.72	143.69	121.57	103.63	89.16	77.96	69.75	64.18	60.92
81	213.09	174.42	147.27	124.21	105.50	90.42	78.74	70.17	64.36	60.96
83	225.80	183.93	154.52	129.55	109.29	92.95	80.30	71.02	64.73	61.06
85	240.86	195.19	163.12	135.87	113.78	95.96	82.16	72.04	65.18	61.17
87	238.51	193.43	161.78	134.89	113.08	95.49	81.87	71.88	65.11	61.15
89	227.31	185.06	155.39	130.18	109.74	93.26	80.49	71.13	64.78	61.07
91	216.35	176.87	149.14	125.58	106.48	91.07	79.14	70.39	64.46	60.99
93	207.19	170.02	143.91	121.73	103.75	89.24	78.01	69.77	64.19	60.92
95	193.96	160.12	136.36	116.18	99.81	86.60	76.38	68.88	63.80	60.83
97	198.71	163.68	139.07	118.17	101.22	87.55	76.97	69.20	63.94	60.86
99	194.80	160.75	136.84	116.53	100.06	86.77	76.48	68.94	63.82	60.83
101	190.76	157.73	134.53	114.83	98.85	85.96	75.99	68.67	63.70	60.80
103	191.26	158.10	134.82	115.04	99.00	86.06	76.05	68.70	63.72	60.81
105	191.31	158.14	134.85	115.06	99.02	86.07	76.05	68.70	63.72	60.81
107	196.33	161.89	137.71	117.17	100.51	87.08	76.67	69.04	63.87	60.84
109	190.73	157.71	134.52	114.82	98.84	85.96	75.98	68.66	63.70	60.80
111	187.34	155.17	132.59	113.40	97.83	85.28	75.56	68.43	63.60	60.78
113	196.26	161.84	137.67	117.14	100.49	87.06	76.66	69.04	63.87	60.84
115	201.51	165.77	140.67	119.35	102.05	88.11	77.31	69.39	64.02	60.88

117	224.20	182.73	153.62	128.88	108.82	92.64	80.11	70.92	64.69	61.05
119	235.97	191.53	160.33	133.82	112.32	94.98	81.56	71.71	65.03	61.13
121	236.19	191.69	160.45	133.91	112.39	95.03	81.58	71.72	65.04	61.13
123	231.99	188.56	158.06	132.15	111.14	94.19	81.07	71.44	64.92	61.10
125	229.96	187.04	156.90	131.29	110.53	93.78	80.82	71.30	64.86	61.09
127	222.09	181.15	152.41	127.99	108.19	92.21	79.85	70.77	64.63	61.03
129	209.79	171.96	145.39	122.83	104.52	89.76	78.33	69.95	64.26	60.94
131	198.38	163.43	138.88	118.03	101.12	87.49	76.93	69.18	63.93	60.86
133	196.08	161.71	137.57	117.07	100.44	87.03	76.64	69.02	63.86	60.84
135	193.82	160.02	136.28	116.12	99.76	86.58	76.36	68.87	63.79	60.82
136	198.82	163.76	139.13	118.22	101.25	87.57	76.98	69.21	63.94	60.86
138	200.58	165.08	140.14	118.96	101.78	87.92	77.20	69.33	63.99	60.87
140	195.52	161.29	137.25	116.83	100.27	86.92	76.57	68.99	63.84	60.84
142	187.22	155.08	132.52	113.34	97.80	85.26	75.55	68.43	63.60	60.78
144	193.16	159.52	135.90	115.84	99.57	86.44	76.28	68.83	63.77	60.82
146	200.78	165.22	140.25	119.04	101.84	87.96	77.22	69.34	64.00	60.87
148	202.91	166.82	141.47	119.94	102.47	88.39	77.48	69.48	64.06	60.89
150	197.41	162.70	138.33	117.62	100.83	87.29	76.81	69.11	63.90	60.85
152	193.44	159.73	136.06	115.96	99.65	86.50	76.32	68.85	63.78	60.82
154	193.35	159.67	136.02	115.92	99.62	86.48	76.31	68.84	63.78	60.82
156	196.29	161.86	137.69	117.15	100.50	87.07	76.67	69.04	63.87	60.84
158	198.37	163.42	138.88	118.03	101.12	87.48	76.92	69.18	63.93	60.86
160	197.31	162.62	138.27	117.58	100.80	87.27	76.79	69.11	63.90	60.85
162	201.63	165.86	140.74	119.40	102.09	88.13	77.33	69.40	64.02	60.88
164	206.49	169.49	143.51	121.44	103.54	89.10	77.92	69.72	64.17	60.92
166	214.19	175.25	147.90	124.67	105.83	90.64	78.87	70.24	64.39	60.97
168	222.18	181.22	152.46	128.03	108.21	92.23	79.86	70.78	64.63	61.03
170	226.86	184.72	155.13	129.99	109.61	93.17	80.44	71.10	64.77	61.06
172	236.59	192.00	160.68	134.08	112.51	95.11	81.63	71.75	65.05	61.14
174	246.62	199.50	166.40	138.29	115.49	97.11	82.87	72.43	65.35	61.21
176	254.23	205.18	170.74	141.49	117.76	98.63	83.81	72.94	65.57	61.26
178	258.84	208.63	173.37	143.42	119.13	99.55	84.38	73.25	65.71	61.30
180	261.49	210.62	174.89	144.54	119.93	100.08	84.70	73.43	65.79	61.32
Avg	208.51	171.00	144.66	122.29	104.14	89.51	78.17	69.86	64.23	60.93

TABLE A.6

TEMPERATURE DATA FROM 100 μm THERMALLY ISOLATED MICROHOTPLATE SIMULATION

	Temperature (°C) observed at:									
Pos. (μm)	35.5 mW	27.0 mW	20.0 mW	14.8 mW	10.4 mW	6.90 mW	4.32 mW	2.38 mW	1.05 mW	0.261 mW
0	1184.35	915.28	693.81	530.06	390.98	278.71	196.62	135.49	93.12	68.11
3	1219.20	941.79	713.46	544.63	401.25	285.49	200.86	137.83	94.15	68.37
6	1252.09	966.81	732.00	558.38	410.93	291.89	204.86	140.04	95.12	68.61
10	1281.23	988.97	748.43	570.57	419.51	297.56	208.40	142.00	95.98	68.83
13	1308.78	1009.93	763.96	582.09	427.62	302.92	211.75	143.86	96.80	69.03
16	1325.42	1022.59	773.34	589.05	432.52	306.16	213.78	144.98	97.29	69.15

19	1340.63	1034.16	781.92	595.41	437.00	309.12	215.63	146.00	97.74	69.26
22	1350.29	1041.51	787.36	599.45	439.85	311.00	216.80	146.65	98.03	69.33
25	1351.34	1042.30	787.95	599.88	440.15	311.21	216.93	146.72	98.06	69.34
29	1351.98	1042.79	788.32	600.15	440.34	311.33	217.01	146.76	98.08	69.35
32	1311.67	1012.13	765.59	583.30	428.47	303.49	212.11	144.05	96.88	69.05
35	1299.25	1002.68	758.59	578.10	424.82	301.07	210.60	143.22	96.52	68.96
38	1286.83	993.23	751.59	572.91	421.16	298.65	209.08	142.38	96.15	68.87
41	1274.41	983.78	744.58	567.72	417.50	296.24	207.57	141.54	95.78	68.78
45	1262.06	974.39	737.62	562.55	413.86	293.83	206.07	140.71	95.42	68.69
48	1242.63	959.61	726.67	554.43	408.14	290.05	203.71	139.41	94.84	68.54
51	1221.68	943.67	714.85	545.67	401.97	285.97	201.16	138.00	94.22	68.39
54	1202.19	928.85	703.87	537.52	396.24	282.18	198.79	136.69	93.64	68.25
57	1181.44	913.06	692.17	528.84	390.12	278.14	196.27	135.29	93.03	68.09
61	1163.51	899.42	682.06	521.34	384.85	274.65	194.09	134.09	92.50	67.96
64	1143.53	884.22	670.80	512.99	378.96	270.76	191.66	132.74	91.91	67.81
67	1125.58	870.57	660.68	505.48	373.68	267.27	189.47	131.53	91.38	67.68
70	1108.32	857.43	650.95	498.27	368.59	263.91	187.37	130.37	90.87	67.56
73	1090.16	843.62	640.71	490.67	363.25	260.38	185.16	129.15	90.33	67.42
77	1073.46	830.92	631.29	483.69	358.33	257.13	183.13	128.03	89.84	67.30
80	1054.20	816.27	620.44	475.64	352.66	253.38	180.79	126.73	89.27	67.16
83	1036.29	802.64	610.34	468.15	347.38	249.89	178.61	125.53	88.74	67.03
86	1017.72	788.51	599.87	460.38	341.91	246.28	176.35	124.28	88.19	66.89
89	999.78	774.87	589.76	452.88	336.63	242.79	174.17	123.07	87.66	66.76
93	983.88	762.78	580.79	446.23	331.95	239.69	172.24	122.00	87.19	66.64
96	972.85	754.38	574.58	441.62	328.70	237.55	170.90	121.26	86.86	66.56
99	962.52	746.52	568.75	437.30	325.66	235.53	169.64	120.57	86.55	66.48
102	950.76	737.58	562.12	432.38	322.20	233.25	168.21	119.78	86.21	66.40
105	941.07	730.21	556.66	428.33	319.34	231.36	167.03	119.12	85.92	66.33
109	928.83	720.90	549.76	423.22	315.74	228.98	165.54	118.30	85.56	66.24
112	920.34	714.44	544.97	419.66	313.24	227.32	164.51	117.73	85.31	66.17
115	908.30	705.28	538.18	414.63	309.69	224.98	163.04	116.92	84.95	66.09
118	899.13	698.30	533.01	410.79	306.99	223.20	161.93	116.30	84.68	66.02
121	889.36	690.87	527.50	406.71	304.12	221.29	160.74	115.65	84.39	65.95
124	878.56	682.66	521.42	402.19	300.94	219.19	159.43	114.92	84.07	65.87
128	869.71	675.93	516.43	398.49	298.33	217.47	158.35	114.32	83.81	65.80
131	862.56	670.48	512.40	395.50	296.22	216.08	157.48	113.84	83.60	65.75
134	855.12	664.82	508.20	392.39	294.03	214.63	156.58	113.34	83.38	65.70
137	847.47	659.00	503.89	389.19	291.78	213.14	155.65	112.83	83.15	65.64
140	839.22	652.73	499.24	385.74	289.35	211.54	154.64	112.27	82.91	65.58
144	830.41	646.02	494.27	382.06	286.76	209.82	153.57	111.68	82.65	65.51
147	823.76	640.97	490.52	379.28	284.80	208.53	152.76	111.23	82.45	65.46
150	817.11	635.91	486.77	376.50	282.84	207.23	151.95	110.79	82.25	65.42
153	809.97	630.48	482.75	373.51	280.74	205.84	151.08	110.31	82.04	65.36
156	802.68	624.93	478.64	370.46	278.59	204.42	150.20	109.81	81.83	65.31
160	795.32	619.33	474.49	367.39	276.42	202.99	149.30	109.32	81.61	65.26
163	788.71	614.30	470.76	364.62	274.48	201.71	148.50	108.88	81.41	65.21
166	780.90	608.36	466.35	361.35	272.18	200.18	147.55	108.35	81.18	65.15
169	773.08	602.41	461.95	358.09	269.88	198.66	146.60	107.82	80.95	65.09
172	763.36	595.02	456.47	354.02	267.01	196.77	145.42	107.17	80.66	65.02
176	754.06	587.94	451.22	350.13	264.27	194.96	144.28	106.54	80.39	64.95
179	743.69	580.06	445.38	345.80	261.22	192.94	143.02	105.85	80.08	64.88

182	732.21	571.33	438.91	341.00	257.84	190.71	141.63	105.08	79.74	64.79
185	720.23	562.21	432.15	335.99	254.31	188.38	140.17	104.27	79.39	64.70
188	707.96	552.88	425.24	330.86	250.70	185.99	138.68	103.44	79.02	64.61
191	695.59	543.47	418.26	325.69	247.06	183.58	137.17	102.61	78.66	64.52
195	682.99	533.88	411.16	320.42	243.35	181.13	135.64	101.76	78.28	64.43
198	678.42	530.40	408.58	318.50	242.00	180.24	135.08	101.46	78.15	64.40

TABLE A.7

TEMPERATURE DATA FROM 100 μm THERMALLY ISOLATED MICROHOTPLATE SIMULATION WITH CONVECTION

	Temperature (°C) observed at:									
Pos. (μm)	35.5 mW	27.0 mW	20.0 mW	14.8 mW	10.4 mW	6.90 mW	4.32 mW	2.38 mW	1.05 mW	0.261 mW
0	495.18	385.18	294.64	227.70	170.84	124.94	91.39	66.39	49.07	38.85
3	506.37	393.60	300.80	232.17	173.89	126.84	92.44	66.82	49.06	38.58
6	518.79	402.94	307.58	237.07	177.19	128.85	93.50	67.18	48.94	38.17
10	530.59	411.77	313.98	241.67	180.25	130.67	94.42	67.43	48.72	37.68
13	539.16	418.16	318.57	244.94	182.40	131.91	95.00	67.51	48.45	37.21
16	542.72	420.78	320.41	246.19	183.16	132.28	95.08	67.37	48.17	36.84
19	545.11	422.51	321.60	246.98	183.61	132.46	95.05	67.20	47.89	36.50
22	544.97	422.32	321.38	246.73	183.34	132.16	94.75	66.88	47.57	36.17
25	539.43	418.05	318.15	244.28	181.54	130.89	93.86	66.28	47.17	35.89
29	525.21	407.21	310.10	238.29	177.31	128.07	92.08	65.27	46.69	35.73
32	516.03	400.19	304.85	234.36	174.49	126.15	90.82	64.50	46.26	35.49
35	506.85	393.17	299.61	230.43	171.67	124.23	89.55	63.73	45.83	35.26
38	490.25	380.54	290.24	223.47	166.77	120.99	87.52	62.59	45.32	35.12
41	469.70	364.92	278.68	214.91	160.76	117.04	85.07	61.27	44.77	35.03
45	457.10	355.34	271.59	209.66	157.06	114.60	83.55	60.43	44.41	34.96
48	442.40	344.16	263.31	203.53	152.75	111.76	81.79	59.47	44.01	34.88
51	426.90	332.37	254.57	197.05	148.19	108.75	79.91	58.44	43.55	34.77
54	411.56	320.71	245.94	190.64	143.69	105.78	78.06	57.42	43.11	34.67
57	397.13	309.73	237.81	184.62	139.45	102.99	76.33	56.47	42.71	34.59
60	383.88	299.66	230.34	179.09	135.56	100.42	74.73	55.60	42.34	34.51
64	370.63	289.59	222.89	173.57	131.68	97.87	73.15	54.74	41.98	34.45
67	358.71	280.54	216.19	168.62	128.21	95.59	71.74	53.98	41.67	34.40
70	346.78	271.46	209.47	163.64	124.71	93.28	70.30	53.19	41.33	34.33
73	335.03	262.53	202.86	158.74	121.27	91.02	68.90	52.43	41.02	34.28
76	323.55	253.80	196.39	153.94	117.89	88.79	67.51	51.66	40.68	34.20
80	311.29	244.48	189.49	148.83	114.30	86.42	66.04	50.86	40.34	34.13
83	300.42	236.22	183.39	144.32	111.14	84.35	64.77	50.18	40.07	34.11
86	289.28	227.76	177.12	139.68	107.88	82.21	63.45	49.47	39.78	34.07
89	277.96	219.15	170.75	134.96	104.56	80.03	62.09	48.72	39.46	34.00
92	267.60	211.27	164.90	130.62	101.50	78.00	60.81	48.01	39.14	33.91
96	260.51	205.87	160.90	127.65	99.41	76.61	59.94	47.52	38.92	33.84
99	253.56	200.57	156.97	124.72	97.34	75.23	59.07	47.03	38.69	33.76
102	246.36	195.10	152.91	121.71	95.21	73.82	58.19	46.54	38.47	33.70
105	239.38	189.77	148.95	118.76	93.13	72.43	57.30	46.03	38.22	33.61

108	231.57	183.83	144.54	115.48	90.81	70.89	56.32	45.48	37.96	33.52
112	225.65	179.31	141.18	112.98	89.03	69.70	55.56	45.04	37.74	33.43
115	218.12	173.58	136.93	109.82	86.80	68.22	54.63	44.51	37.49	33.36
118	211.33	168.40	133.07	106.95	84.76	66.85	53.75	44.00	37.24	33.25
121	205.63	164.07	129.85	104.56	83.07	65.73	53.05	43.60	37.06	33.20
124	199.39	159.32	126.33	101.95	81.23	64.51	52.29	43.18	36.87	33.15
128	193.72	154.99	123.12	99.55	79.54	63.38	51.56	42.77	36.67	33.07
131	188.51	151.01	120.15	97.33	77.95	62.31	50.87	42.35	36.44	32.96
134	183.85	147.46	117.50	95.35	76.54	61.36	50.25	41.98	36.25	32.87
137	179.10	143.83	114.80	93.34	75.11	60.40	49.64	41.62	36.07	32.79
140	174.30	140.17	112.09	91.32	73.69	59.45	49.04	41.29	35.91	32.74
144	169.35	136.40	109.29	89.24	72.22	58.47	48.42	40.94	35.75	32.69
147	165.25	133.27	106.95	87.49	70.97	57.62	47.87	40.61	35.57	32.60
150	161.22	130.20	104.67	85.79	69.75	56.81	47.34	40.30	35.41	32.53
153	157.42	127.30	102.51	84.18	68.61	56.05	46.86	40.01	35.27	32.47
156	153.62	124.41	100.36	82.58	67.48	55.29	46.38	39.74	35.14	32.42
159	150.22	121.82	98.44	81.15	66.47	54.62	45.95	39.50	35.03	32.39
163	146.76	119.18	96.48	79.70	65.44	53.93	45.52	39.25	34.91	32.35
166	143.11	116.41	94.43	78.18	64.37	53.23	45.08	39.02	34.81	32.33
169	139.46	113.63	92.37	76.65	63.30	52.53	44.65	38.78	34.71	32.31
172	135.99	111.00	90.44	75.23	62.31	51.89	44.26	38.59	34.65	32.33
175	132.27	108.19	88.36	73.70	61.26	51.21	43.86	38.38	34.59	32.35
179	128.86	105.61	86.47	72.32	60.31	50.60	43.51	38.23	34.57	32.41
182	125.50	103.08	84.63	70.99	59.41	50.05	43.21	38.12	34.59	32.51
185	122.36	100.73	82.92	69.75	58.57	49.54	42.94	38.03	34.62	32.61
188	119.25	98.40	81.24	68.55	57.77	49.07	42.70	37.97	34.68	32.74
191	116.33	96.22	79.67	67.44	57.04	48.65	42.52	37.95	34.79	32.92
195	113.63	94.21	78.24	66.42	56.39	48.29	42.36	37.95	34.90	33.09
198	112.96	93.72	77.89	66.18	56.24	48.21	42.34	37.97	34.94	33.15

TABLE A.8

TEMPERATURE DATA FROM FINELY MESHED 100 μm UNRELEASED MICROHOTPLATE SIMULATION

	Temperature (°C) observed at:										
Pos. (μm)	5038 mW	3880 mW	2997 mW	2320 mW	1708 mW	1218 mW	820 mW	512 mW	281 mW	123 mW	30.4 mW
0	430.14	345.64	280.81	230.56	185.52	149.49	120.10	97.50	80.54	68.90	62.08
2	444.35	356.60	289.29	237.11	190.34	152.93	122.41	98.95	81.33	69.25	62.17
4	478.11	382.66	309.44	252.67	201.80	161.11	127.91	102.38	83.22	70.08	62.37
6	523.61	417.77	336.59	273.65	217.24	172.12	135.31	107.01	85.76	71.19	62.65
8	550.22	438.32	352.47	285.92	226.27	178.57	139.64	109.71	87.25	71.84	62.81
10	517.89	413.36	333.18	271.01	215.30	170.74	134.38	106.42	85.44	71.05	62.61
12	483.11	386.52	312.42	254.98	203.50	162.32	128.72	102.89	83.50	70.20	62.40
14	519.58	414.67	334.19	271.79	215.88	171.15	134.66	106.60	85.54	71.09	62.62
16	561.00	446.63	358.90	290.89	229.93	181.18	141.40	110.81	87.85	72.10	62.87
18	566.53	450.91	362.21	293.44	231.81	182.52	142.30	111.37	88.16	72.24	62.91
20	519.39	414.52	334.07	271.70	215.81	171.10	134.62	106.58	85.53	71.09	62.62

22	482.35	385.93	311.97	254.63	203.24	162.14	128.60	102.81	83.46	70.18	62.40
24	512.82	409.45	330.15	268.68	213.58	169.51	133.56	105.91	85.16	70.93	62.58
26	554.25	441.43	354.88	287.78	227.64	179.54	140.30	110.12	87.48	71.94	62.83
28	564.68	449.47	361.10	292.58	231.18	182.07	141.99	111.18	88.06	72.19	62.90
30	525.18	418.99	337.53	274.37	217.77	172.50	135.57	107.17	85.85	71.23	62.66
32	476.66	381.54	308.57	252.00	201.31	160.76	127.67	102.23	83.14	70.04	62.36
34	521.72	416.32	335.46	272.78	216.60	171.67	135.00	106.81	85.66	71.14	62.64
36	575.71	457.99	367.68	297.67	234.93	184.74	143.79	112.31	88.67	72.46	62.96
38	579.13	460.63	369.72	299.25	236.09	185.57	144.35	112.65	88.87	72.55	62.98
40	521.96	416.50	335.60	272.89	216.68	171.72	135.04	106.84	85.67	71.15	62.64
42	474.54	379.90	307.31	251.03	200.59	160.24	127.33	102.02	83.02	69.99	62.35
44	529.54	422.35	340.13	276.38	219.25	173.56	136.28	107.61	86.09	71.33	62.68
46	590.47	469.38	376.49	304.47	239.93	188.31	146.19	113.81	89.50	72.82	63.05
49	588.00	467.47	375.02	303.33	239.10	187.71	145.79	113.55	89.36	72.76	63.04
51	525.54	419.27	337.75	274.54	217.90	172.59	135.63	107.20	85.87	71.24	62.66
53	478.28	382.79	309.54	252.75	201.86	161.15	127.93	102.40	83.23	70.08	62.37
55	531.28	423.70	341.17	277.19	219.85	173.98	136.56	107.79	86.19	71.38	62.69
57	560.49	446.24	358.60	290.65	229.76	181.05	141.31	110.76	87.82	72.09	62.87
59	553.91	441.16	354.67	287.62	227.52	179.46	140.24	110.09	87.46	71.93	62.83
61	518.92	414.16	333.79	271.49	215.65	170.99	134.55	106.53	85.50	71.07	62.62
63	481.08	384.96	311.21	254.04	202.81	161.83	128.39	102.68	83.39	70.15	62.39
65	519.32	414.46	334.03	271.67	215.78	171.08	134.61	106.57	85.52	71.08	62.62
67	560.17	446.00	358.41	290.51	229.65	180.98	141.26	110.72	87.81	72.08	62.87
69	550.42	438.47	352.59	286.01	226.34	178.62	139.67	109.73	87.26	71.84	62.81
71	509.45	406.85	328.14	267.12	212.44	168.70	133.01	105.57	84.97	70.84	62.56
73	481.40	385.20	311.40	254.19	202.92	161.91	128.44	102.71	83.40	70.16	62.39
75	516.47	412.27	332.33	270.36	214.82	170.40	134.15	106.28	85.36	71.01	62.60
77	534.51	426.19	343.09	278.67	220.94	174.76	137.08	108.11	86.37	71.46	62.71
79	522.97	417.28	336.21	273.35	217.02	171.97	135.21	106.94	85.73	71.17	62.64
81	500.19	399.70	322.62	262.85	209.29	166.45	131.50	104.62	84.45	70.62	62.51
83	491.56	393.04	317.47	258.87	206.36	164.37	130.10	103.75	83.97	70.40	62.45
85	525.72	419.41	337.85	274.62	217.96	172.64	135.66	107.22	85.88	71.24	62.66
87	549.73	437.94	352.18	285.69	226.11	178.45	139.56	109.66	87.22	71.83	62.81
89	536.09	427.41	344.04	279.40	221.48	175.15	137.34	108.28	86.46	71.49	62.72
91	503.84	402.52	324.79	264.53	210.53	167.34	132.09	105.00	84.66	70.71	62.53
93	482.22	385.83	311.89	254.57	203.19	162.10	128.58	102.80	83.45	70.18	62.40
95	508.37	406.01	327.50	266.62	212.07	168.43	132.83	105.46	84.91	70.82	62.56
Avg	521.52	416.16	335.34	272.68	216.53	171.62	134.97	106.79	85.65	71.14	62.64

TABLE A.9

TEMPERATURE DATA FROM FINELY MESHED 200 μm UNRELEASED MICROHOTPLATE SIMULATION

	Temperature (°C) observed at:									
Pos. (μm)	5610 mW	4203 mW	3200 mW	2359 mW	1674 mW	1120 mW	692 mW	378 mW	165 mW	40.8 mW
0	392.95	309.68	250.19	200.02	159.41	126.29	100.91	82.33	69.67	62.27
2	365.41	289.02	234.45	188.43	151.18	120.79	97.52	80.47	68.86	62.07

4	386.20	304.61	246.33	197.18	157.39	124.94	100.08	81.87	69.47	62.22
6	424.47	333.32	268.20	213.28	168.83	132.58	104.80	84.46	70.60	62.50
8	446.57	349.89	280.83	222.58	175.43	136.98	107.52	85.95	71.25	62.66
10	405.86	319.36	257.57	205.45	163.27	128.86	102.50	83.20	70.05	62.36
12	367.58	290.65	235.69	189.34	151.82	121.23	97.78	80.62	68.92	62.08
14	382.90	302.14	244.45	195.79	156.40	124.28	99.67	81.65	69.38	62.20
16	422.73	332.01	267.21	212.55	168.31	132.23	104.58	84.34	70.55	62.49
18	449.97	352.44	282.77	224.01	176.45	137.66	107.94	86.18	71.36	62.68
20	411.80	323.81	260.96	207.95	165.04	130.05	103.24	83.60	70.23	62.41
22	371.25	293.40	237.79	190.88	152.92	121.96	98.24	80.86	69.03	62.11
24	378.69	298.98	242.04	194.02	155.15	123.44	99.15	81.37	69.25	62.16
26	410.26	322.66	260.08	207.30	164.58	129.74	103.05	83.50	70.18	62.39
28	428.36	336.23	270.43	214.92	169.99	133.35	105.28	84.72	70.72	62.53
30	401.16	315.83	254.88	203.47	161.86	127.92	101.92	82.88	69.91	62.33
32	367.30	290.43	235.53	189.22	151.74	121.17	97.75	80.60	68.92	62.08
34	373.76	295.28	239.23	191.94	153.67	122.46	98.55	81.03	69.11	62.13
36	411.44	323.54	260.76	207.80	164.93	129.98	103.19	83.58	70.22	62.40
38	445.43	349.03	280.18	222.10	175.09	136.75	107.38	85.87	71.22	62.65
40	413.44	325.04	261.90	208.64	165.53	130.37	103.44	83.71	70.28	62.42
42	375.54	296.62	240.24	192.69	154.20	122.81	98.76	81.15	69.16	62.14
44	375.67	296.71	240.31	192.74	154.24	122.84	98.78	81.16	69.16	62.14
45	412.09	324.03	261.13	208.07	165.13	130.11	103.27	83.62	70.24	62.41
47	444.49	348.33	279.64	221.70	174.81	136.57	107.27	85.81	71.19	62.64
49	415.18	326.35	262.89	209.37	166.05	130.72	103.65	83.83	70.33	62.43
51	377.72	298.25	241.49	193.61	154.86	123.25	99.03	81.30	69.22	62.16
53	371.92	293.90	238.17	191.17	153.12	122.09	98.32	80.91	69.05	62.12
55	406.02	319.47	257.66	205.51	163.31	128.89	102.52	83.21	70.06	62.36
57	436.96	342.68	275.34	218.53	172.56	135.07	106.34	85.30	70.97	62.59
59	405.33	318.96	257.26	205.22	163.11	128.76	102.44	83.16	70.04	62.36
61	375.30	296.44	240.11	192.59	154.13	122.77	98.74	81.14	69.15	62.14
63	373.44	295.04	239.04	191.81	153.58	122.40	98.51	81.01	69.10	62.13
65	408.01	320.97	258.79	206.35	163.91	129.29	102.77	83.34	70.12	62.38
67	438.94	344.16	276.47	219.37	173.15	135.46	106.58	85.43	71.03	62.60
69	412.93	324.66	261.61	208.42	165.38	130.27	103.37	83.68	70.26	62.41
71	379.06	299.26	242.26	194.17	155.26	123.52	99.20	81.39	69.26	62.17
73	369.07	291.77	236.55	189.97	152.27	121.52	97.97	80.72	68.97	62.09
75	403.50	317.59	256.22	204.45	162.56	128.39	102.21	83.04	69.98	62.35
77	435.72	341.75	274.63	218.01	172.19	134.82	106.18	85.21	70.93	62.58
79	415.73	326.76	263.21	209.60	166.22	130.83	103.72	83.87	70.34	62.43
81	381.99	301.45	243.93	195.40	156.13	124.10	99.56	81.59	69.35	62.19
83	366.97	290.19	235.34	189.08	151.64	121.10	97.71	80.57	68.91	62.08
85	401.82	316.32	255.26	203.75	162.06	128.06	102.00	82.93	69.93	62.33
87	431.87	338.86	272.43	216.39	171.04	134.05	105.71	84.96	70.82	62.55
89	414.09	325.53	262.27	208.91	165.73	130.50	103.52	83.76	70.30	62.42
91	379.87	299.86	242.72	194.51	155.50	123.68	99.30	81.45	69.29	62.17
93	360.48	285.32	231.64	186.35	149.70	119.81	96.91	80.14	68.71	62.03
95	394.19	310.61	250.90	200.54	159.78	126.54	101.06	82.41	69.71	62.28
97	414.42	325.77	262.46	209.05	165.82	130.57	103.56	83.78	70.31	62.43
99	409.99	322.45	259.93	207.18	164.50	129.69	103.01	83.48	70.18	62.39
101	386.40	304.76	246.44	197.26	157.45	124.98	100.10	81.89	69.48	62.22
103	364.58	288.39	233.98	188.08	150.93	120.63	97.41	80.41	68.84	62.06

105	404.58	318.40	256.84	204.91	162.88	128.61	102.34	83.11	70.02	62.35
107	425.13	333.80	268.58	213.55	169.02	132.71	104.88	84.50	70.62	62.50
109	415.92	326.90	263.32	209.68	166.27	130.87	103.74	83.88	70.35	62.44
111	386.96	305.18	246.77	197.49	157.62	125.09	100.17	81.92	69.50	62.23
113	359.95	284.92	231.33	186.13	149.54	119.70	96.84	80.10	68.70	62.03
115	399.55	314.62	253.96	202.79	161.38	127.60	101.72	82.77	69.87	62.32
117	435.47	341.56	274.49	217.91	172.12	134.77	106.15	85.20	70.93	62.58
119	428.02	335.97	270.23	214.77	169.89	133.28	105.23	84.69	70.71	62.52
121	391.26	308.41	249.23	199.30	158.90	125.95	100.70	82.21	69.62	62.26
123	358.65	283.95	230.59	185.58	149.15	119.45	96.68	80.01	68.66	62.02
125	396.58	312.40	252.26	201.54	160.49	127.01	101.36	82.57	69.78	62.30
127	430.26	337.66	271.51	215.72	170.56	133.73	105.51	84.85	70.77	62.54
129	427.03	335.23	269.66	214.35	169.59	133.08	105.11	84.63	70.68	62.52
131	392.56	309.38	249.97	199.85	159.29	126.21	100.86	82.30	69.66	62.27
133	356.93	282.66	229.61	184.86	148.64	119.10	96.47	79.90	68.61	62.01
135	390.01	307.47	248.51	198.78	158.53	125.70	100.55	82.13	69.59	62.25
136	415.16	326.33	262.88	209.36	166.04	130.72	103.65	83.83	70.33	62.43
138	414.80	326.06	262.68	209.21	165.94	130.65	103.61	83.80	70.32	62.43
140	389.16	306.83	248.02	198.42	158.27	125.53	100.44	82.07	69.56	62.24
142	358.80	284.06	230.67	185.64	149.20	119.48	96.70	80.02	68.66	62.02
144	393.62	310.18	250.57	200.30	159.61	126.42	100.99	82.37	69.69	62.27
146	434.04	340.49	273.67	217.30	171.69	134.48	105.98	85.10	70.88	62.57
148	438.07	343.51	275.97	219.00	172.89	135.29	106.47	85.37	71.00	62.60
150	393.99	310.46	250.79	200.45	159.72	126.50	101.04	82.40	69.70	62.28
152	358.66	283.95	230.59	185.58	149.16	119.45	96.68	80.01	68.66	62.02
154	389.54	307.11	248.24	198.58	158.39	125.61	100.49	82.10	69.57	62.24
156	419.54	329.62	265.39	211.20	167.35	131.59	104.19	84.12	70.46	62.46
158	424.99	333.71	268.50	213.50	168.98	132.68	104.86	84.49	70.62	62.50
160	396.53	312.36	252.24	201.52	160.48	127.00	101.35	82.57	69.78	62.29
162	362.94	287.16	233.04	187.39	150.44	120.30	97.21	80.30	68.79	62.05
164	390.21	307.62	248.62	198.86	158.59	125.74	100.57	82.14	69.59	62.25
166	425.37	333.99	268.72	213.66	169.10	132.75	104.91	84.52	70.63	62.50
168	437.13	342.81	275.43	218.61	172.61	135.10	106.36	85.31	70.98	62.59
170	403.19	317.36	256.04	204.33	162.47	128.33	102.17	83.02	69.97	62.34
172	363.60	287.66	233.42	187.67	150.64	120.43	97.29	80.35	68.81	62.06
174	386.58	304.90	246.55	197.34	157.50	125.02	100.13	81.90	69.48	62.22
176	422.83	332.08	267.26	212.59	168.34	132.25	104.59	84.34	70.55	62.49
178	438.17	343.59	276.03	219.04	172.92	135.31	106.49	85.38	71.01	62.60
180	403.37	317.49	256.15	204.40	162.52	128.37	102.20	83.03	69.98	62.34
Avg	400.61	315.42	254.57	203.24	161.70	127.81	101.86	82.84	69.90	62.32

TABLE A.10

TEMPERATURE DATA FROM FINELY MESHED 100 μm THERMALLY ISOLATED MICROHOTPLATE SIMULATION WITH CONVECTION

	Temperature (°C) observed at:									
Pos. (μm)	35.5 mW	27.0 mW	20.0 mW	14.8 mW	10.4 mW	6.90 mW	4.32 mW	2.38 mW	1.05 mW	0.261 mW
0	1036.29	795.28	597.62	451.59	326.42	229.86	155.18	98.80	59.97	37.03
3	1072.42	822.73	617.95	466.66	336.98	233.13	157.20	99.89	60.42	37.10
6	1082.94	830.73	623.87	471.05	340.06	234.26	157.90	100.25	60.56	37.11
10	1077.78	826.79	620.94	468.85	338.50	230.55	155.54	98.91	59.92	36.88
13	1043.57	800.74	601.59	454.45	328.33	223.48	151.06	96.40	58.76	36.51
16	995.24	763.95	574.26	434.12	314.00	212.83	144.34	92.63	57.03	35.99
19	934.55	717.76	539.97	408.61	296.02	200.35	136.47	88.25	55.04	35.42
22	864.33	664.33	500.30	379.12	275.25	185.45	127.09	83.04	52.71	34.78
25	779.23	599.59	452.26	343.42	250.12	166.92	115.46	76.61	49.85	34.05
29	672.02	518.04	391.76	298.46	218.50	143.20	100.58	68.41	46.25	33.16
32	590.35	455.93	345.69	264.24	194.43	136.96	96.67	66.25	45.31	32.93
35	576.84	445.66	338.07	258.58	190.45	134.85	95.35	65.53	44.99	32.86
38	565.85	437.30	331.87	253.98	187.21	132.65	93.97	64.77	44.67	32.79
41	554.97	429.03	325.73	249.42	184.01	130.38	92.55	63.99	44.33	32.71
45	544.72	421.23	319.95	245.13	181.00	128.41	91.32	63.32	44.04	32.65
48	536.37	414.88	315.25	241.63	178.54	126.75	90.28	62.75	43.79	32.59
51	529.47	409.64	311.35	238.74	176.51	125.33	89.39	62.26	43.57	32.53
54	513.00	397.11	302.06	231.83	171.64	122.49	87.60	61.27	43.14	32.42
57	481.47	373.12	284.26	218.61	162.34	116.33	83.74	59.13	42.19	32.18
60	444.79	345.22	263.56	203.23	151.52	109.28	79.32	56.70	41.13	31.92
64	403.06	313.49	240.04	185.76	139.25	101.69	74.57	54.10	40.00	31.67
67	367.41	286.39	219.94	170.85	128.77	95.36	70.62	51.94	39.08	31.48
70	354.78	276.79	212.83	165.57	125.07	91.82	68.41	50.74	38.57	31.38
73	350.25	273.35	210.28	163.68	123.74	90.89	67.83	50.43	38.44	31.36
76	346.00	270.12	207.89	161.91	122.50	90.03	67.30	50.14	38.33	31.35
80	341.90	267.01	205.58	160.20	121.30	89.22	66.80	49.88	38.22	31.33
83	337.85	263.93	203.30	158.51	120.12	88.41	66.30	49.61	38.11	31.32
86	327.74	256.24	197.60	154.27	117.14	86.97	65.40	49.12	37.91	31.28
89	315.84	247.19	190.89	149.29	113.63	84.65	63.94	48.31	37.55	31.19
92	303.93	238.14	184.17	144.30	110.13	82.06	62.31	47.41	37.14	31.08
96	292.52	229.46	177.74	139.52	106.77	79.79	60.89	46.63	36.80	31.00
99	283.22	222.39	172.49	135.63	104.04	77.85	59.68	45.96	36.51	30.93
102	277.87	218.32	169.47	133.39	102.46	76.41	58.78	45.46	36.29	30.87
105	273.04	214.64	166.74	131.36	101.03	75.53	58.22	45.15	36.15	30.84
108	272.23	214.03	166.29	131.02	100.79	74.68	57.68	44.85	36.02	30.80
112	275.66	216.64	168.23	132.46	101.81	73.84	57.16	44.56	35.89	30.77
115	258.55	203.62	158.56	125.27	96.74	73.03	56.65	44.28	35.77	30.73
118	243.42	192.10	150.01	118.92	92.27	71.19	55.49	43.64	35.48	30.65
121	228.65	180.87	141.68	112.72	87.91	68.38	53.72	42.65	35.03	30.53
124	215.90	171.18	134.49	107.39	84.16	65.79	52.10	41.76	34.64	30.43
128	205.10	162.97	128.41	102.88	81.00	63.57	50.71	41.01	34.32	30.37
131	197.48	157.18	124.12	99.70	78.77	61.85	49.65	40.44	34.09	30.34
134	194.73	155.09	122.57	98.55	77.96	60.82	49.01	40.09	33.95	30.32

137	192.28	153.22	121.19	97.52	77.24	60.33	48.70	39.92	33.88	30.31
140	189.85	151.38	119.82	96.51	76.53	59.88	48.42	39.77	33.82	30.30
144	187.44	149.54	118.46	95.50	75.82	59.44	48.15	39.63	33.76	30.29
147	183.89	146.85	116.46	94.01	74.77	58.99	47.87	39.48	33.70	30.28
150	177.84	142.24	113.04	91.47	72.98	58.10	47.31	39.16	33.55	30.24
153	172.25	137.99	109.89	89.13	71.34	56.86	46.52	38.71	33.34	30.16
156	167.45	134.33	107.18	87.11	69.91	55.69	45.78	38.29	33.14	30.09
159	162.72	130.73	104.49	85.11	68.49	54.71	45.15	37.94	32.97	30.04
163	158.23	127.30	101.94	83.20	67.14	53.94	44.66	37.66	32.84	30.00
166	154.17	124.21	99.64	81.49	65.93	53.46	44.36	37.49	32.76	29.96
169	151.15	121.91	97.93	80.21	65.02	53.02	44.08	37.32	32.67	29.93
172	149.32	120.51	96.89	79.43	64.47	52.59	43.80	37.16	32.59	29.89
175	147.53	119.15	95.87	78.67	63.94	52.17	43.53	37.01	32.51	29.86
179	145.78	117.81	94.88	77.93	63.41	51.50	43.10	36.76	32.40	29.82
182	143.81	116.32	93.77	77.11	62.83	49.45	41.80	36.03	32.06	29.71
185	135.17	109.74	88.88	73.47	60.26	47.24	40.41	35.26	31.72	29.62
188	119.39	97.73	79.97	66.85	55.60	45.44	39.30	34.66	31.47	29.59
191	109.27	90.05	74.28	62.63	52.65	43.96	38.39	34.19	31.30	29.59
195	102.09	84.60	70.26	59.67	50.59	42.86	37.74	33.88	31.22	29.65
198	96.74	80.56	67.29	57.49	49.09	41.97	37.23	33.66	31.20	29.75

TABLE A.11

CURRENT MAGNITUDE QUERIES AT SIMULATION INLET AND OUTLET BOUNDARIES

Microhotplate Simulation	**Current Specified (mA)**	**Inlet Current (pA)**	**Outlet Current (pA)**	**Difference (pA)**	**Percent Difference (%)**
Unreleased	10	-1.47E+11	3.59E+09	-1.43E+11	97.6
100 µm	20	-2.93E+11	7.18E+09	-2.86E+11	97.5
Coarse mesh	30	-4.40E+11	1.08E+10	-4.29E+11	97.5
	40	-5.87E+11	1.44E+10	-5.73E+11	97.5
	50	-7.34E+11	1.79E+10	-7.16E+11	97.6
	60	-8.80E+11	2.15E+10	-8.59E+11	97.6
	70	-1.03E+12	2.51E+10	-1.00E+12	97.6
	80	-1.17E+12	2.87E+10	-1.14E+12	97.5
	90	-1.32E+12	3.23E+10	-1.29E+12	97.6
	100	-1.47E+12	3.59E+10	-1.43E+12	97.6
	110	-1.61E+12	3.95E+10	-1.57E+12	97.5
Unreleased	10	-8.30E+10	9.43E+09	-7.36E+10	88.6
200 µm	20	-1.66E+11	1.88E+10	-1.47E+11	88.7
Coarse mesh	30	-2.49E+11	2.83E+10	-2.21E+11	88.6
	40	-3.32E+11	3.77E+10	-2.94E+11	88.6
	50	-4.15E+11	4.71E+10	-3.68E+11	88.7
	60	-4.98E+11	5.66E+10	-4.41E+11	88.6
	70	-5.81E+11	6.60E+10	-5.15E+11	88.6
	80	-6.64E+11	7.54E+10	-5.89E+11	88.6
	90	-7.47E+11	8.48E+10	-6.62E+11	88.6
	100	-8.30E+11	9.43E+10	-7.36E+11	88.6
Isolated	1	-6.64E+09	8.85E+08	-5.76E+09	86.7

100 µm	2	-1.33E+10	1.77E+09	-1.15E+10	86.7
Coarse mesh	3	-2.00E+10	2.65E+09	-1.74E+10	86.8
	4	-2.66E+10	3.54E+09	-2.31E+10	86.7
	5	-3.33E+10	4.42E+09	-2.89E+10	86.7
	6	-4.00E+10	5.31E+09	-3.47E+10	86.7
	7	-4.66E+10	6.19E+09	-4.04E+10	86.7
	8	-5.33E+10	7.08E+09	-4.62E+10	86.7
	9	-6.00E+10	7.96E+09	-5.20E+10	86.7
	10	-6.66E+10	8.85E+09	-5.78E+10	86.7
Unreleased	10	-8.96E+09	8.82E+09	-1.40E+08	1.56
100 µm	20	-1.79E+10	1.76E+10	-3.00E+08	1.68
Fine mesh	30	-2.69E+10	2.65E+10	-4.00E+08	1.49
	40	-3.58E+10	3.53E+10	-5.00E+08	1.40
	50	-4.48E+10	4.41E+10	-7.00E+08	1.56
	60	-5.38E+10	5.29E+10	-9.00E+08	1.67
	70	-6.27E+10	6.17E+10	-1.00E+09	1.59
	80	-7.17E+10	7.06E+10	-1.10E+09	1.53
	90	-8.06E+10	7.94E+10	-1.20E+09	1.49
	100	-8.96E+10	8.82E+10	-1.40E+09	1.56
	110	-9.85E+10	9.70E+10	-1.50E+09	1.52
Unreleased	10	-8.82E+09	8.82E+09	0.00E+00	0.00
200 µm	20	-1.76E+10	1.76E+10	0.00E+00	0.00
Fine mesh	30	-2.64E+10	2.64E+10	0.00E+00	0.00
	40	-3.53E+10	3.52E+10	-1.00E+08	0.28
	50	-4.41E+10	4.41E+10	0.00E+00	0.00
	60	-5.29E+10	5.29E+10	0.00E+00	0.00
	70	-6.17E+10	6.17E+10	0.00E+00	0.00
	80	-7.06E+10	7.06E+10	0.00E+00	0.00
	90	-7.94E+10	7.93E+10	-1.00E+08	0.13
	100	-8.82E+10	8.81E+10	-1.00E+08	0.11
Isolated	1	-8.94E+08	8.82E+08	-1.20E+07	1.34
100 µm	2	-1.79E+09	1.76E+09	-3.00E+07	1.68
Fine mesh	3	-2.68E+09	2.65E+09	-3.00E+07	1.12
	4	-3.58E+09	3.53E+09	-5.00E+07	1.40
	5	-4.47E+09	4.41E+09	-6.00E+07	1.34
	6	-5.37E+09	5.29E+09	-8.00E+07	1.49
	7	-6.26E+09	6.17E+09	-9.00E+07	1.44
	8	-7.16E+09	7.06E+09	-1.00E+08	1.40
	9	-8.05E+09	7.94E+09	-1.10E+08	1.37
	10	-8.95E+09	8.82E+09	-1.30E+08	1.45

REFERENCES

[1] Semancik, S., Cavicchi, R. E., Wheeler, M. C., Tiffany, J. E., Poirier, G. E., Walton, R. M., Suehle, J. S., Panchapakesan, and B., DeVoe, D. L. 2001. Microhotplate platforms for chemical sensor research. *Sensors and Actuators B* 77:579-591.

[2] Raman, B., Meier, D. C., Evju, J. K., and Semancik, S. 2009. Designing and optimizing microsensor arrays for recognizing chemical hazards in complex environments. *Sensors and Actuators B* 137:617-629.

[3] Triantafyllopoulou, R. and Tsamis, C. 2008. Detection of CO and NO using low power metal oxide sensors. *Physica Status Solidi A* 205 11:2643-2646.

[4] Ahn, J., Kim, Y., and Wang, G. 2009. Electrochemical properties of SnO_2 nanowires prepared by a simple heat treatment of Sn-Ag alloys. *Journal of Alloys and Compounds* 483:422-424.

[5] Xu, J., Wang, D., Qin, L., Yu, W., and Pan, Q. 2009. SnO_2 nanorods and hollow spheres: Controlled synthesis and gas sensing properties. *Sensors and Actuators B* 137:490-495.

[6] Köck, A., Tischner, A., Maier, T., Kast, M., Edtmaier, C., Gspan, C., and Kothleitner, G. 2009. Atmospheric pressure fabrication of SnO_2-nanowires for highly sensitive CO and CH_4 detection. *Sensors and Actuators B* 138:160-167.

[7] Sberveglieri, G., Baratto, C., Comini, E., Faglia, G., Ferroni, M., Pardo, M., Ponzoni, A., and Vomiero, A. 2009. Semiconducting tin oxide nanowires and thin films for Chemical Warfare Agents detection. *Thin Solid Films* 517:6156-6160.

[8] Tischner, A., Köck, A., Maier, T., Edtmaier, C., Gspan, C., and Kothleitner, G. 2009. Tin oxide nanocrystalline films and nanowires for gas sensing applications. *Microelectronic Engineering* 86:1258-1261.

[9] Kumar, V., Sen, S., Muth, K. P., Gaur, N. K., Gupta, S. K., and Yakhmi, J. V. 2009. Copper doped SnO_2 nanowires as highly sensitive H_2S gas sensor. *Sensors and Actuators B* 138:587-590.

[10] Feng, H. T., Zhuo, R. F., Chen, J. T., Yan, D., Feng, J. J., Li, H. J., Cheng, S., and Yan, P. X. 2009. Axial periodical nanostructures of Sb-doped SnO_2 grown by chemical vapor deposition. *Physica E* 41:1640-1644.

[11] Cao, Y., Pan, W., Zong, Y., and Jia, D. 2009. Preparation and gas-sensing properties of pure and Nd-doped ZnO nanorods by low-heating solid-state chemical reaction. *Sensors and Actuators B* 138:480-484.

[12] Fan, Z. and Lu, J. G. 2006. Chemical Sensing With ZnO Nanowire Field-Effect Transistor. *IEEE Transactions on Nanotechnology* 5:393-396.

[13] Hari, P., Baumer, M., Tennyson, W. D., and Bumm, L. A. 2008. ZnO nanorod growth by chemical bath method. *Journal of Non-Crystalline Solids* 354:2843-2848.

[14] Zhang, H., Feng, J., Wang, J., and Zhang, M. 2007. Preparation of ZnO nanorods through wet chemical method. *Materials Letters* 61:5202-5205.

[15] Cheng, C., Liu, B., Yang, H., Zhou, W., Sun, L., Chen, R., Yu, S. F., Zhang, J., Gong, H., Sun, H., and Fan, H. J. 2009. Hierarchical Assembly of ZnO Nanostructures on SnO_2 Backbone Nanowires: Low-Temperature Hydrothermal Preparation and Optical Properties. *American Chemical Society Nano* 3:3069-3076.

[16] Choi, S., Park, J. Y., and Kim, S. S. 2009. Synthesis of SnO_2-ZnO core-shell nanofibers via a novel two-step process and their gas sensing properties. *Nanotechnology* 20:465603.

[17] Kim, H. W., Kebede, M. A., and Kim, H. S. 2009. ZnO sputter coating on SnO_2 nanowires: Effects of thin coating and subsequent thermal annealing. *Optical Materials* 31:1853-1856.

[18] Song, X. and Liu, L. 2009. Characterization of electrospun ZnO-SnO_2 nanofibers for ethanol sensor. *Sensors and Actuators A* 154:175-179.

[19] Xiang, Q., Meng, G., Zhang, Y., Xu, J., Xu, P., Pan, Q., and Yu, W. 2010. Ag nanoparticle embedded-Zno nanorods synthesized via a photochemical method and its gas-sensing properties. *Sensors and Actuators B* 143:635-640.

[20] Zong, Y., Cao, Y., Jia, D., Bao, S., and Lu, Y. 2010. Facile synthesis of Ag/ZnO nanorods using Ag/C cables as templates and their gas-sensing properties. *Materials Letters* 64:243-245.

[21] Liao, L., Zhang, Z., Yan, B., Zheng, Z., Bao, Q. L., Wu, T., Li, C. M., Shen, Z. X., Zhang, J. X., Gong, H., Li, J. C., and Yu, T. 2009. Multifunctional CuO nanowire devices: p-type field effect transistors and CO gas sensors. *Nanotechnology* 20:085203.

[22] Mu, Y., Yang, J., Han, S., Hou, H., and Fan, Y. 2010. Syntheses and gas-sensing properties of CuO nanostructures by using $[Cu(pbbt)Cl_2]_2 \cdot CH_3OH$ as a precursor. *Materials Letters* 64:1287-1290.

[23] Hoa, N. D., An, S. Y., Dung, N. Q., Quy, N. V., and Kim, D. 2010. Synthesis of p-type semiconducting cupric oxide thin films and their application to hydrogen detection. *Sensors and Actuators B* 146:239-244.

[24] Righettoni, M., Tricoli, A., and Pratsinis, S. E. 2010. Thermally Stable, Silica-Doped ε-WO_3 for Sensing of Acetone in the Human Breath. *Chemistry of Materials* 22:3152-3157.

[25] Heidari, E. K., Zamani, C., Marzbanrad, E., Raissi, B., and Nazarpour, S. 2010. WO_3-based NO_2 sensors fabricated through low frequency AC electrophoretic deposition. *Sensors and Actuators B* 146:165-170.

[26] Tamaki, J., Zhang, Z., Fujimori, K., Akiyama, M., Harada, T., Miura, N., and Yamazoe, N. 1994. Grain-Size Effects in Tungsten Oxide-Based Sensor for Nitrogen Oxides. *Journal of the Electrochemical Society* 141:2207-2210.

[27] Fine, G. F., Cavanagh, L. M., Afonja, A., and Binions, R. 2010. Metal Oxide Semi-Conductor Gas Sensors in Environmental Monitoring. *Sensors* 10:5469-5502.

[28] Chaudhari, G. N., Jagtap, S. V., Gedam, N. N., Pawar, M. J., and Sangawar, V. S. 2009. Sol-gel synthesized semiconducting $LaCo_{0.8}Fe_{0.2}O_3$-based powder for thick film NH_3 gas sensor. *Talanta* 78:1136-1140.

[29] Kahng, Y. H., Lu, W., Tobin, R. G., Loloee, R., and Ghosh, R. N. 2009. The role of oxygen in hydrogen sensing by a platinum-gate silicon carbide gas sensor: An ultrahigh vacuum study. *Journal of Applied Physics* 105:064511.

[30] Wiche, G., Berns, A., Steffes, H., and Obermeier, E. 2005. Thermal analysis of silicon carbide based micro hotplates for metal oxide gas sensors. *Sensors and Actuators A* 123-124:12-17.

[31] Fung, S. K. H., Tang, Z., Chan, P. C. H., Sin, J. K. O., and Cheung, P. W. 1996. Thermal analysis and design of a micro-hotplate for integrated gas-sensor applications. *Sensors and Actuators A* 54:482-487.

[32] Hunter, G. W., Neudeck, P. G., Liu, C. C., Ward, B., Wu, Q. H., Dutta, P., Frank, M., Trimbol, J., Fulkerson, M., Patton, B., Makel, D., and Thomas, V. 2002. Development of Chemical Sensor Arrays for Harsh Environments and Aerospace Applications. *Proceedings of the IEEE International Conference on Sensors (Orlando, FL)*, 24:1126-1133.

[33] Benn, G. 2001. Design of a Silicon Carbide Micro-Hotplate Geometry for High Temperature Chemical Sensing. Master of Science thesis, Massachusetts Institute of Technology.

[34] Chen, L. 2008. Silicon Carbide Pressure Sensors and Infra-red Emitters. Doctor of Philosophy dissertation, Case Western Reserve University.

[35] Hunter, G. W., Neudeck, P. G., Okojie, R. S., Beheim, G. M., Thomas, V., Chen, L., Lukco, D., Liu, C. C., Ward, B., and Makel, D. 2002. Development of SiC Gas Sensor Systems. *Proceedings of the 201st Meeting of the Electrochemical Society (Philadelphia, PA)*.

[36] Graf, M., Jurischka, R., Barrettino, D., and Hierlemann, A. 2005. 3D nonlinear modeling of microhotplates in CMOS technology for use as metal-oxide-based gas sensors. *Journal of Micromechanics and Microengineering* 15:190-200.

[37] Khanna, V. K., Prasad, M., Dwivedi, V. K., Shekhar, C., Pankaj, A. C., and Basu, J. 2007. Design and electro-thermal simulation of a polysilicon microheater on a suspended membrane for use in gas sensing. *Indian Journal of Pure & Applied Physics* 45:332-335.

[38] Messina, M., Franzè, F., Speciale, N., Cozzani, E., and Roncaglia, A. 2009. Thermofluid Analysis of Ultra Low Power Hotplates for a MOX Gas Sensing Device. *IEEE Sensors Journal* 9:504-511.

[39] Williams, K. R. and Muller, R. S. 1996. Etch Rates for Micromachining Processing. *Journal of Microelectromechanical Systems* 5:256-269.

[40] Incropera, Frank P., DeWitt, David P., Bergman, Theodore L., and Lavine, Adrienne S. 2007. *Fundamentals of Heat and Mass Transfer*, 6th ed. New York: John Wiley & Sons, Inc.

[41] Bird, R. Byron, Stewart, Warren E., and Lightfoot, Edwin N. 2007. *Transport Phenomena*, 2nd ed. New York: John Wiley & Sons, Inc.

[42] Solzbacher, F., Doll, T., and Obermeier, E. 2003. A comprehensive analytical and numerical analysis of transient and static micro hotplate characteristics. *Proceedings of the 12th International Conference on Solid State Sensors, Actuators and Microsystems (Boston, MA), Transducers '03*, 1856-1859.

VITA

NAME:	Kane Jonathan Miller
ADDRESS:	Department of Chemical Engineering University of Louisville Louisville, KY 40292
DOB:	St. Louis, MO - May 18, 1987
EDUCATION & TRAINING:	B.S., Chemical Engineering University of Louisville 2005-09 M.Eng., Chemical Engineering University of Louisville 2009-10
PROFESSIONAL SOCIETIES:	American Institute of Chemical Engineers
NATIONAL MEETING PRESENTATIONS:	"Thermal Analysis of Silicon Carbide Microhotplates for Gas Sensors" American Institute of Chemical Engineers 2009 Annual Meeting - November 2009 Nashville, TN